Risø-R-1242(EN)

Lanthanum Manganate Based Cathodes for Solid Oxide Fuel Cells

Mette Juhl Jørgensen

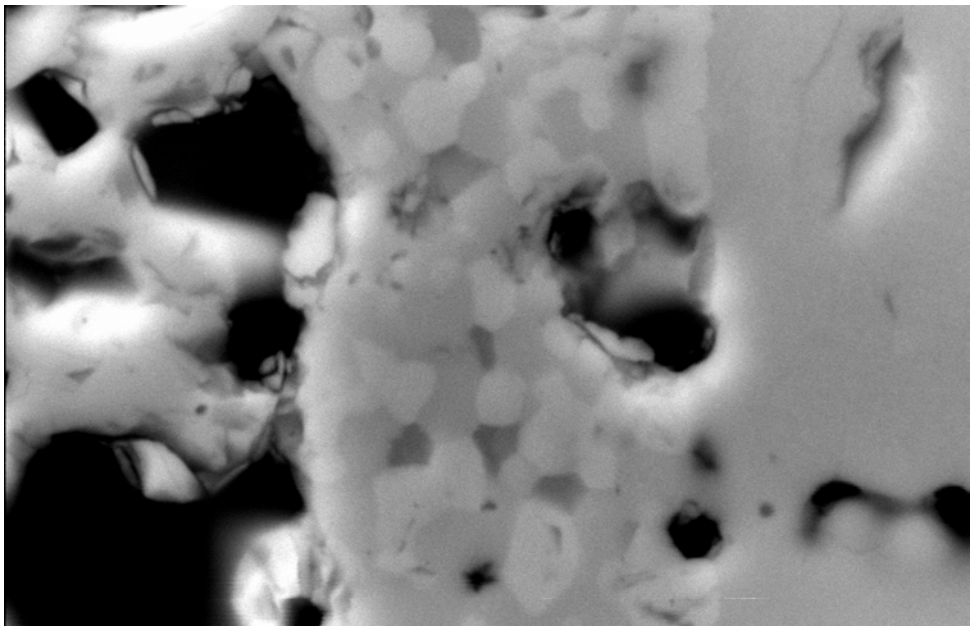

Materials Research Department
Risø National Laboratory, Denmark
July 2001

Thesis submitted for the degree of Doctor of Philosophy at Keele University, UK.

ISBN 87-550-2827-6
ISBN 87-550-2828-4 (internet)
ISSN 0106-2840

Print: Pitney Bowes Management Services Danmark A/S, 2001.

Preface

This thesis is submitted to Keele University, UK for the degree of Doctor of Philosophy. The majority of the work contained in this thesis was performed at The Materials Research Department, Risø National Laboratory, Denmark. The work was funded by the sponsors of the national Danish SOFC program DK-SOFC - the Danish Energy Agency and the Danish utility corporation ELSAM -, by the European Commission within the framework of the programmes Joule II and Joule/Thermie and by Statoil, Norway. The Materials Research Department at Risø Nat. Lab. is acknowledged for financing my course at Keele University and for giving me time off to finish this thesis.

The work contained in this thesis was performed in collaboration with several colleagues, who are co-authors of the papers on which this thesis is based. The electrochemical measurements and analysis are primarily performed by the author of this thesis, while the microstructural analysis are mainly performed by others.

Prof. Kevin Kendall, Keele University[1] is acknowledged for being my supervisor and for inspiring discussions throughout the project period.

Thanks are due to the entire SOFC group at Risø Nat. Lab. for help with the experimental work and for fruitful discussions. Carsten Bagger, Risø Nat. Lab. is thanked for his encouragement throughout my employment at Risø Nat. Lab. Also, I would like to express my sincere thanks to my local supervisor at Risø Nat. Lab. Dr. Mogens Mogensen, whose knowledge and enthusiasm is a daily inspiration.

It is due to mention that the author changed name from Mette Juhl to Mette Juhl Jørgensen during the course (August 1997). Thus, the papers on which this thesis is based are published using different names depending on the year of publication.

[1]From April 2000, Birmingham University, UK.

Abstract

Composite cathodes for solid oxide fuel cells were investigated using electrochemical impedance spectroscopy and scanning electron microscopy. The aim was to study the oxygen reduction process in the electrode in order to minimise the voltage drop in the cathode. The electrodes contained a composite layer made from lanthanum strontium manganate (LSM) and yttria stabilised zirconia (YSZ) and a layer of pure LSM aimed for current collection.

The performance of the composite electrodes was sensitive to microstructure and thickness. Further, the interface between the composite and the current collecting layer proved to affect the performance. In a durability study severe degradation of the composite electrodes was found when passing current through the electrode for 2000 hours at 1000°C. This was ascribed to pore formation along the composite interfaces and densification of the composite and current collector microstructure.

An evaluation of the measurement approach indicated that impedance spectroscopy is a very sensitive method. This affects the reproducibility, as small undesirable variations in for instance the microstructure from electrode to electrode may change the impedance.

At least five processes were found to affect the impedance of LSM/YSZ composite electrodes. Two high frequency processes were ascribed to transport of oxide ions/oxygen intermediates across LSM/YSZ interfaces and through YSZ in the composite. Several competitive elementary reaction steps, which appear as one medium frequency process in the impedance spectra, were observed. A low frequency arc related to gas diffusion limitation in a stagnant gas layer above the composite structure was detected. Finally, an inductive process, assumed to be connected to an activation process involving segregates at the triple phase boundary between electrode, electrolyte and gas phase, was found.

Suggestions for further experiments and for modelling of the oxygen reduction mechanism are given.

List of Contents

Glossary

A	Element in the perovskite structure ABO_3
A_1, A_2	Elements in the doped perovskite structure $(A_1A_2)(B_1B_2)O_3$
A_E	amplitude of the applied potential
A_i	current amplitude
A_{YSZ}	cross-sectional area of a YSZ cylinder
AC	alternating current
AFC	alkaline fuel cell
B	Element in the perovskite structure ABO_3
B_1, B_2	Elements in the doped perovskite structure $(A_1A_2)(B_1B_2)O_3$
C	capacity
C-layer	composite LSM/YSZ cathode layer
CCC-layer	cathode current collecting layer
CG	cerium gadolinium oxide
DC	direct current
E	sinusoidal potential
E_a	activation energy
E_{appl}	applied potential
EDS	energy dispersive spectrometry
EIS	electrochemical impedance spectroscopy
f	frequency
f_{max}	summit frequency
$f_{max,C}$	summit frequency of arc C
FC	fuel cell
i	area-specific current density

I	current
j	imaginary unit
L	induction
L_C	thickness of the composite layer
L_{CCC}	thickness of the sprayed and sintered current collecting layers
L_{elyt}	electrolyte thickness
L'_{TPB}	length of active TPB in one micrometer of the electrode
L^*_{TPB}	area-specific length of TPB
LCM	lanthanum calcium manganate
LnSM	lanthanide strontium manganate
LSCo	lanthanum strontium cobaltite
LSCx	lanthanum strontium chromite with dopants x
LSM	lanthanum strontium manganate
MCFC	molten carbonate fuel cell
n	frequency exponent
OCV	open circuit voltage
p_{O_2}	oxygen partial pressure
P-layer	YSZ particle layer on electrolyte surface
PAFC	phosphoric acid fuel cell
PEMFC	proton exchange membrane fuel cell
PSD	particle size distribution
Q	constant phase element
r	radius of YSZ cylinder
R	resistance
$R_{i,celle}$	area-specific internal cell resistance
$R_{i,stack}$	area-specific internal stack resistance

R_{ion}	the ionic resistance of a YSZ cylinder
R_p	area-specific polarisation resistance
$R_P^{'}$	sum of the polarisation resistances measured on two nominally identical electrodes using a symmetrical two-electrode cell
R_P^{*}	polarisation resistance of one micrometer electrode
$R_{p,spec.}$	line-length specific reaction resistance of the TPB
R_{pol}	polarisation resistance
R_s	series resistance
$R_{YSZ,spec.}$	length specific resistance of YSZ
RLS	rate limiting step
RMS	root mean square
ScYSZ	scandia doped yttria stabilised zirconia
SEM	scanning electron microscopy
SOFC	solid oxide fuel cell
SPFC	solid polymer fuel cell
t	active thickness of the composite electrode
T_m	measuring temperature
T_s	sintering temperature
TEC	thermal expansion coefficient
TPB	triple phase boundary
TZ3YB	yttria stabilised zirconia containing 3 mole % yttria
TZ8Y	yttria stabilised zirconia containing 8 mole % yttria
x	strontium doping level in $(La_{1-x}Sr_x)_yMnO_{3\pm\delta}$
y	A-site stoichiometry in $(La_{1-x}Sr_x)_yMnO_{3\pm\delta}$
Y'	admittance
Y_0	admittance factor

YSZ	yttria stabilised zirconia
z	oxygen partial pressure exponent
ϕ	phase angle
η	overvoltage
σ_{app}	apparent electrolyte conductivity
ω	angular frequency

Chapter 1. Introduction[1]

An introduction to fuel cells in particular solid oxide fuels (SOFCs) is given in this chapter. Further, some of the properties of the SOFC cathode, which is the component investigated in this work, are discussed.

1.1. Fuel Cells

A reappearing problem in the energy field is the conversion of chemical energy in the form of fossil resources and derivatives such as hydrogen and alcohols, into electrical energy. Partly due to industrialisation and technological progress, it has become increasingly important to reduce the losses associated with the applied conversion techniques. Traditional conversion to electrical energy is by gas turbine, steam turbine or reciprocating engine driving a generator, where the Carnot-cycle sets a limit to the efficiency. A fuel cell operating as a sort of continuously replenished battery provides an alternative, whereby electrical energy can be made available with small losses, and no Carnot limit. If the fuel is clean, the effluents are in principle water, heat and CO_2. Fuel cell plants can be modular in design, and the energy release-rate can be adjusted to meet the actual demand, which is a convenient feature for a power source in a technological society.

The discovery of the fuel cell is often ascribed to Sir William Grove (Grove, 1839), demonstrating the reversibility of electrolytic water separation in 1839. However, a similar observation was reported by Sir Humphrey Davy as early as 1802 (Davy, 1802). In 1899 Nernst (Nernst, 1899) contributed by demonstrating that certain oxides attained remarkably high electrical conductivity by doping with other oxides.

[1] The content of section 1.1.-1.6. is partly based on: S. Primdahl and M.J. Jørgensen, *Journal of the Danish Ceramic Society*, **2** (1999a) 13-19 (In Danish).

In the middle of the twentieth century the development accelerated. Several types of fuel cells were developed in the global race for conquering space. In the nineteen eighties, focus on pollution and the demand for higher efficiency in the exploitation of fossil resources initiated a new wave of fuel cell development. Today several types of fuel cells are approaching the consumer market. The primary challenges are cost and durability, to be solved by materials selection and design engineering.

Today five types of fuel cells are commonly known, all named after the electrolyte material. Some of the characteristics of each of these fuel cell types are listed in Table 1.1.

Low temperature fuel cells (AFC, SPFC and PAFC) have a potential for automobile propulsion, where the time of heat-up must be low and the efficiency has to be compared with about 20-30% for a combustion engine.

High temperature fuel cells (MCFC and SOFC) are suited to continuous power/heat production, where the cell temperature can be maintained. These can in combination with a gas turbine reach a total efficiency which is a factor of two higher than a coal-based power plant (Williams, 1998).

In general high temperature fuel cells exhibit higher efficiency and are less sensitive to fuel purity than low temperature fuel cells. At higher temperatures natural gas can be applied directly as a fuel. In some cases this will, however, require some level of catalysed reforming, where higher hydrocarbons are decomposed and part of the CH_4 is converted into H_2, CO and CO_2.

Comparing the two types of high temperature fuel cells, an unfortunate property of the MCFC must be considered. The presence of a molten alkaline salt poses considerable problems with corrosion and creep (transport by wetting metallic surfaces), and the risk of contaminating an internal reforming catalyst.

Table 1.1. Some characteristics of five common types of fuel cells

Name[1]	**Alkaline FC**	**Solid Polymer FC / Proton Exchange Membrane FC**	**Phosphoric Acid FC**	**Molten Carbonate FC**	**Solid Oxide FC**
Abbreviation	**AFC**	**SPFC/PEMFC**	**PAFC**	**MCFC**	**SOFC**
Electrolyte	**KOH**	**Polymer**	**H_3PO_4**	**62% Li_2CO_3 + 38% K_2CO_3**	**$ZrO_2 + Y_2O_3$**
Charge carrier	**OH^-**	**H^+**	**H^+**	**CO_3^{2-}**	**O^{2-}**
Fuel	**Highly pure H_2**	**Pure H_2**	**CO-free H_2**	**H_2, CH_4, CO**	**H_2, CH_4, CO**
Operation Temperature	**80°C**	**80-260°C**	**200°C**	**650°C**	**600-1000°C**
Electrical efficiency[2]	**40%**	**40%**	**40%**	**60%**	**60%**

[1]FC = fuel cell. [2]Higher heating value for Methane.

Based on these characteristics of the various types of fuel cells, the Danish Department of Energy concentrated the public funds for fuel cell research in a national research program dealing with SOFC in the late nineteen eighties. Since 1989 Risø National Laboratory, Haldor Topsøe A/S, IRD A/S (earlier Innovision A/S), The Technical University of Denmark and The University of Odense have been co-operating in the Danish SOFC program DK-SOFC. The overall aim has been to achieve a Danish production of SOFC, alternatively to attain know-how to ensure a Danish participation in production of parts. Simultaneously the participants have been involved in a number of international co-operations with industry and research organisations world-wide.

1.2. Solid Oxide Fuel Cells

1.2.1. Principle of Operation

The operation principle of the solid oxide fuel cell is illustrated in Fig. 1.1. An oxide ion conducting ceramic electrolyte membrane is provided with two electrodes, exposed to air and hydrogen, respectively. The difference in oxygen activity of the two gases at the electrodes provides a driving force for motion of the oxide ions in the electrolyte. Oxide ions formed by splitting of oxygen at the cathode under electron consumption migrate through the electrolyte to the anode. Here they react with hydrogen to form water and release electrons.

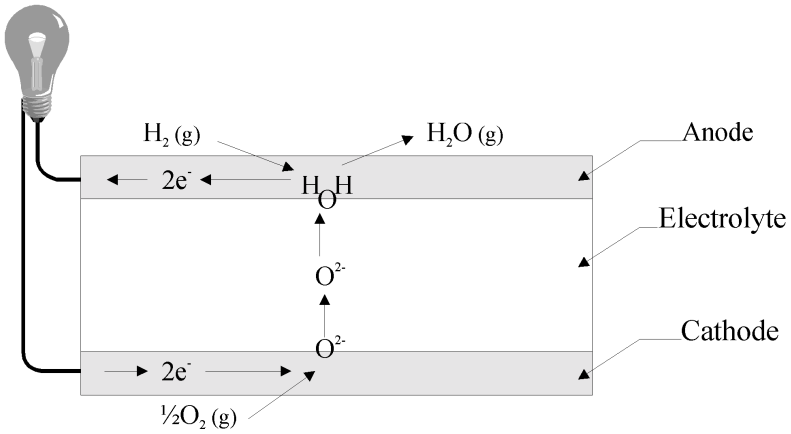

Fig. 1.1 Sketch of solid oxide fuel cell operated on hydrogen and air.

The electrolyte has to be gas impermeable to avoid direct mixing and combustion of the gases. In addition to the electrolyte the electrodes are often based on ceramic materials. The cell produces current as long as the reactants (fresh gases) are provided to the electrodes. An open voltage of about 1 volt is attained when the cell is not loaded, defined by the Nernst potential of the different activity of oxygen on the electrodes. Therefore, the cells must be connected in series in a stack to reach higher voltages necessary for most practical purposes. A stack can in principle comprise any number of

cells depending on the desired effect, and a fuel cell plant can be designed in modules of stacks connected in series and parallel.

An SOFC can be operated as an electrolyser. By applying a voltage higher than the open circuit potential, water can be split into hydrogen on the cathode and oxygen on the anode. In this way pure oxygen can be generated. Unsteady power supplies such as wind turbines can be coupled with an electrolyser to provide storage of energy as hydrogen, which can later be released when the need arises by operating the electrolyser as an SOFC. Furthermore, an SOFC has advantages in 1) the wood and paper industry, where the fuel can be established by gasification of waste products, 2) for operating electrolyser plants requiring direct current with high amps and low voltage, and 3) for cathodic protection against corrosion. In the personal-transport sector the longer start-up time makes the SOFC less appealing than the SPFC, but for larger units such as trains and ships, the SOFC may prove advantageous.

1.2.2. Stack Design

An SOFC stack can be established in different ways. Two examples comprising flat and tubular cells are shown in Fig. 1.2. A common feature of SOFC stacks is that a dense interconnect must be applied to ensure electric connections between the cells and to separate the oxidising and reducing gases between the cells. Apart from this, there are a number of principal differences between the two types of stacks.

Planar cells are characterised by a need for sealing at operation temperature along the cell edges on both electrodes, to avoid direct gas mixing. Additionally, gas manifolds are needed around the stack. A channel structure must be incorporated in the interconnect surface to allow for gas access to the electrodes without significant pressure losses. The major advantages of the planar design are a low component volume and the short current

path perpendicular to the cell plane, with very little in-plane current transport. The latter will potentially lead to low ohmic losses in the stack.

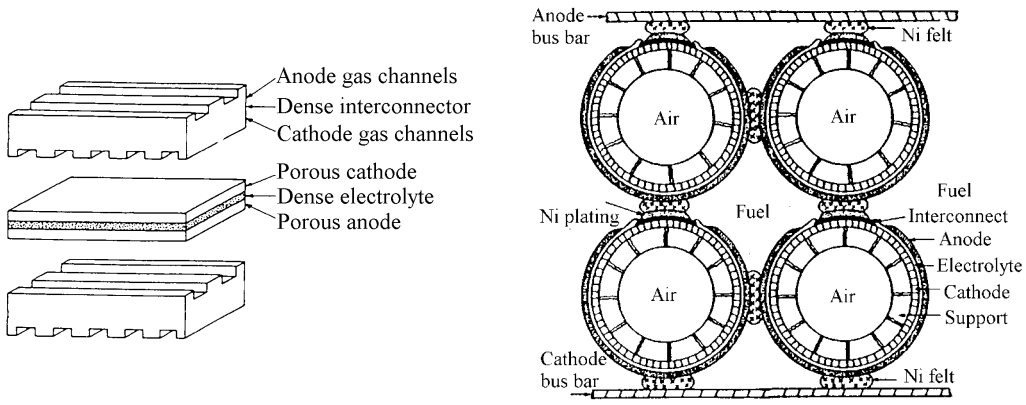

Fig. 1.2. Sketch of two SOFC stack designs. Left: early planar design. Right: early tubular design (Minh and Takahashi,1995).

Tubular cells are operated with one gas inside and the other gas outside the tubes. In the tubular design the gases are readily kept separated up to the point of exhaust from the cells. At the same time the tubes can be extended out of the hot active zone to temperatures where seals and manifolds can be made from conventional materials. The disadvantage of the tubular design is the long in-plane current path in the electrodes, a consequence of only a small part of the cell perimeter being in contact with the next cell. This leads to a critical role of the in-plane conductivity of the electrodes.

If fuel cells are to be operated as electrolysers, the demands for sealing are high. If the SOFC is to be operated in combined electricity/heat devices, a certain level of direct gas mixing and burning can be accepted, provided that it does not happen in direct contact with the cells.

1.2.3. Efficiency, Performance and Economy

The electrical efficiency of a fuel cell can be defined in a number of ways, making comparisons difficult. A good indicator for cell performance is the area-specific internal resistance, $R_{i,cell}$, at given conditions (temperature, current load, gas composition and gas utilisation). $R_{i,cell}$ comprises ionic resistance in the electrolyte in addition to electronic resistance and reaction resistance in the anode and the cathode. A demand for direct comparison of cell results is that the cells are contacted in the same way, as the in-plane electronic resistance in the electrodes can depend significantly on the distance between points of contact during test.

In the same way an area-specific internal stack resistance, $R_{i,stack}$, can be defined. It comprises $R_{i,cell}$, electronic resistance in the interconnects and the contact resistance between electrodes and interconnects. $R_{i,stack}$ can be determined experimentally for stacks with very few cells, to yield a realistic estimate of the expectable resistance obtained by scale-up.

$R_{i,stack}$ is a very important parameter during SOFC development, as an evaluation of the technology will often be based on cost per produced electric effect.

1.3. Materials for SOFC

The selection of materials for SOFC is complicated by the high temperatures of sintering and operation, and the fact that most components are in contact with a number of other materials. Ceramics are primarily selected, based on functionality, compatibility and cost.

1.3.1. Functionality

The primary functional parameters are conductivity, catalytic properties and temperatures of stability and sintering. For instance the electrolyte must exhibit significant ionic conductivity and negligible electronic conductivity. For the interconnect the opposite qualities are favoured. Both materials must be able to sinter to high density to avoid gas mixing. The electrodes must exhibit high electrocatalytic activity for the desired reactions and good conductivity for electrons and preferably also for ions. Furthermore, the anode should preferably be a catalyst for methane reforming. The mixed conductivity is often obtained by using a composite of two materials, each having either dominant electronic or ionic conductivity. Manifolds and glass seals must be able to densify and must exhibit no conductivity.

1.3.2. Compatibility

The compatibility of materials is essential to ensure reliable operation for thousands of hours at high temperature (Badwal and Foger, 1997).

Solid-solid reactions are an explicit problem during sintering of monolithic (materials sintered into one piece) stack components. The allowable sintering temperature is determined considering the formation of reaction products with undesirable properties on the interfaces and minimisation of interdiffusion to maintain the properties of the pure materials.

Certain demands to compatibility of thermal expansion coefficient (TEC) for monolithic stack components and components sharing glass seals are set to maintain physical and electrical contact. Assuming that materials in a monolith are stress free at the maximum sintering temperature, the material exhibiting the higher TEC will experience tensile stress upon cooling. The magnitude of the tension is proportional to the change of temperature and the difference in TEC (Sørensen and Primdahl, 1998).

Stability of materials towards the atmosphere can be a problem as most materials are sensitive to the oxygen partial pressure at higher temperatures. A number of components are exposed to more than one atmosphere during sintering and operation. In principle materials forming more than one phase within the considered oxygen partial pressure range should be avoided. However, this criterion is not sufficient, as some ceramic materials can change their oxygen stoichiometry and molar volume, when the oxygen partial pressure of the atmosphere is changed (Larsen et al., 1998).

1.3.3. Cost

The cost of individual components is primarily governed by component volume, need for processing, required purity of the material and the general availability of the material on the market. It is consequently only natural to aim at making thin components from cheaper materials, or to replace parts of the components by a cheaper material (Tietz, 1998). Savings can also be found by accepting natural contaminants in raw materials where these will not reduce performance.

1.3.4. Choice of Materials

As a consequence of the above demands, the list of available materials for SOFC construction is fairly short. Table 1.2 states the materials used actively at the Risø Nat. Lab. A number of alternative materials are investigated at the Risø Nat. Lab., in the literature and applied by other companies. A common feature of the ceramic SOFC materials is doping of pure oxides to obtain the required properties regarding conductivity and TEC (Larsen et al., 1998). Some materials are only applicable under certain conditions and with certain other materials, and new materials are still searched for.

Table 1.2. List of materials used in SOFC development at Risø Nat. Lab.

Component	Chemical composition	Abbreviation	Comments
Electrolyte	**$(ZrO_2)_{1-x}(Y_2O_3)_x$**	**YSZ**	**classic**
	$(ZrO_2)_{1-x-z}(Y_2O_3)_x(Sc_2O_3)_z$	**ScYSZ**	**better conductivity**
Cathode	**$La_{1-x}Sr_xMn_yO_{3\pm\delta}$/YSZ**	**LSM/YSZ**	**classic**
	$Ln_{1-x}Sr_xMn_yO_{3\pm\delta}$/YSZ	**LnSM/YSZ**	**Cheap, (Ln=lanthanides)**
Anode	**Ni/YSZ cermet**	**Ni/YSZ**	**classic for hydrogen, unfit for methane**
	$Ce_{0.6}Gd_{0.4}O_{1.8}$	**CG**	**for methane and hydrogen, mixed conductor**
Interconnect	**$(La_{1-y}Sr_y)CrO_{3\pm\delta}$ with dopants *x***	**LSC*x***	**classic at high temperature**
	$Cr_{1-x}Fe_x(Y_2O_3)_y$	**Cr-alloy**	**redox stable, moderate temp.**
	$Fe_{1-x}Cr_x$	**Ferritic steel**	**cheap, low temperature (<800°C)**
Sealing	**SiO_2 with additives**	**silicate glass**	**melting required**
Manifold & Housing	**$(MgO)_{1-x}(Al_2O_3)_x$**	**spinel**	**non-conductor**
	Metals		**low temp. <800°C**

1.4. Fabrication Techniques

A broad range of process techniques are available for fabrication of ceramic components. Simple wet ceramic shaping techniques such as slip casting, spray painting, extrusion, viscous processing and tape casting are based on forming the outline of the component by shaping a paste or suspension of ceramic components and organic additives (Onoda and Hench, 1978).

These methods, which all require sintering after shaping, are attractive due to low cost and potential for successful scale-up. A general limitation is, that sintering of two materials in contact requires some extent of reaction at the interface to obtain adhesion.

Furthermore, matching of sintering contraction and TEC is critical to obtain shape-constant components.

Advanced gas phase and plasma techniques such as physical vapour deposition (PVD), chemical and electrochemical vapour deposition (CVD and EVD) and ion beam deposition can form dense and well adhering layers or monoliths and do not require subsequent sintering at higher temperature (Møller, 1998). This advantage has to be balanced against cost, as the processes are time consuming, the vacuum equipment is expensive and the savings on scale-up are limited.

Tubular cells are often based on extrusion of a 1 to 3 mm thick support structure, which is sintered separately. To obtain dense electrolyte and interconnect layers CVD and EVD techniques are typically applied. A shift to the use of wet ceramic processing is considered an economic requirement for commercialisation of tubular SOFC (Singhal, 1997). Kendall and Prica (1994) have manufactured electrolyte tubes using viscous processing and obtained components with high thermal shock resistance. The next challenge is to apply the electrode inside the tube in a controlled manner to ensure high cell efficiency. Kendall and Prica (1994) suggested co-extruding the inner electrode (anode) with the electrolyte, to solve this problem.

Production of planar cells is often based on simple and cost effective wet ceramic processes such as tape casting, which has been developed to produce foils of controlled thickness. The fabrication route could for instance be production of the dense electrolyte by tape casting and subsequent sintering. The electrodes can be produced by tape casting electrode sheets and laminating them with the electrolyte prior to sintering. Alternatively, particle dispersions can be spray painted or screen printed directly onto the electrolyte prior to or after sintering of the electrolyte.

At the current state of development, planar cells are often produced by simple, cheap processes, whereas production of tubular cells require partial use of more costly methods.

1.5. Cell Development

In the following, an example from the development of planar SOFCs at Risø Nat. Lab. is elaborated to illustrate how the materials demands and selection of fabrication methods are interacting.

Planar cells can be designed in several ways. Besides the mentioned materials demands, final stack design and operation temperature must be considered. The operation temperature can be decisive for the allowable thickness of the electrolyte, which must be thin to operate at 700 - 800°C. Most developers initially chose an operation temperature of about 1000°C (SOFC-I, 1989). This choice was based on suppressing the resistance in the electrolyte and the electrodes, as these decrease by increasing temperature. The conductivity of the classical electrolyte material yttria stabilised zirconia, YSZ, at 1000°C is sufficient to form a self-supporting component (Fig. 1.3, left), without the electrolyte resistance being the dominant limitation of the cell performance. Such a supporting electrolyte is typically 100-300 μm thick (Minh and Takahashi, 1995).

The development of electrodes has led to a point where they can be operated at lower temperature, e.g. 800°C. This offers economic advantages, as cheaper materials can be applied as interconnects, manifolds and cell housing. A lowering of the operation temperature causes an increase in the specific resistivity of the electrolyte. To allow for this, the electrolyte contribution must be reduced in combination with the use of improved electrodes. A factor of two improvement is obtainable by co-doping the yttria doped zirconia with scandia. This is, however, not sufficient, so a reduction of the electrolyte

thickness is required. A significant reduction of the electrolyte thickness to e.g. 20-40 μm makes the electrolyte incapable of supporting the cell. Therefore, the cell is constructed by depositing the electrolyte on a porous supporting structure, typically made from one of the electrode materials (Fig. 1.3, right).

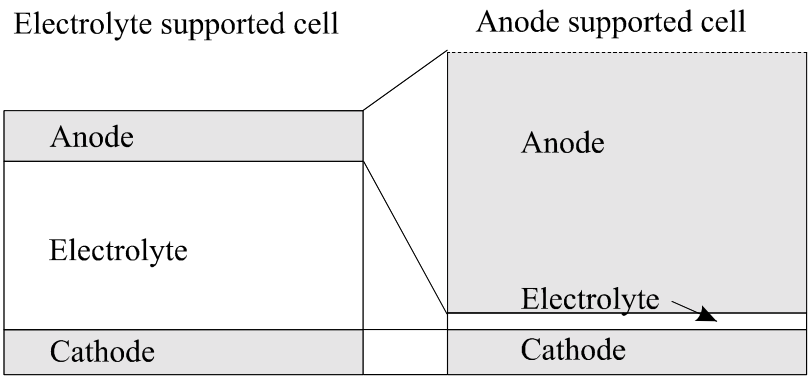

Fig. 1.3. Illustration of two types of planar cells. Left: electrolyte supported cell. Right: anode supported cell.

When selecting the supporting material it is important to consider the reactivity and the significance of sintering temperature on the electrode performance. The supporting structure and the electrolyte are often co-sintered, as it is difficult to sinter an electrolyte to high density on a pre-sintered support. Co-sintering requires thorough control with sintering behaviour of the components to avoid warping and cracks caused by internal stress. The sintering contraction can be manipulated to some extent by addition of organic additives and by changing the powder particle size distribution (Primdahl et al., 1999b). The porosity can be increased by addition of organic fillers, which will burn out on sintering. Densification of the electrolyte typically requires temperatures in excess of 1300°C. Sintering of, for instance, ceria based anodes and lanthanum manganate based cathodes at temperatures in this order may lead to reactivity with the YSZ electrolyte, which may be fatal for the performance. The performance of Ni/YSZ cermet anodes is not

affected by sintering temperatures as high as 1500°C (Primdahl et al., 2000), making this electrode a natural choice for the supporting structure (Fig. 1.3, right). The thickness of a porous supporting structure is typically from 0.5 to 2 mm depending on fabrication methods and materials (Minh and Takahashi, 1995), but can be as low as 200 µm (Primdahl et al., 1999b). Based on cost, only wet ceramic processes, namely tape casting and spraying, are considered for the cell fabrication at Risø Nat. Lab. (Primdahl et al., 1999b).

1.6. Commercialisation

For SOFC to be a commercial product, competitive power generation must be attained. The cost of SOFC power generation is often given in cost/kW for the SOFC stack and for the surrounding equipment (balance of plant). In an EU SOFC-strategy from 1997, a stack cost of 500 ECU/kW is the aim (European Commision, 1997). Typically a lifetime in the order of 40,000 hours is considered with an acceptable degradation rate of less than 1% per 1000 hours (Badwal and Foger, 1997).

Plans for commercialisation of SOFC-technology have been presented. Combined heat and power plants in the MW range based on SOFCs in combination with a gas turbine is the primary aim for Siemens Westinghouse in the US (tubular cells) and Rolls-Royce in the United Kingdom (multi-cell units). Fabrication of commercial units at Siemens Westinghouse is foreseen in the year 2001 (Singhal, 1997). Systems are available at non-commercial prices now. Sulzer Hexis in Switzerland (planar cells) is working on systems for domestic applications with an output of 1 kW electric plus 10 kW heat (Diethelm et al., 1998). The system is based on planar cells in combination with a conventional burner and is also available at a non-commercial price. Market entry is planned for 2001.

1.7. SOFC Cathodes

The SOFC cathode is the subject of this thesis and the properties of this component will, therefore, be discussed in further detail in the following.

The SOFC cathode may give rise to a significant overvoltage drop. The feasibility of SOFC commercialisation may therefore be improved considerably if the losses ascribed to the cathode are minimised. For this purpose it is relevant to study the origin of the losses in this cell component.

1.7.1. Oxygen Reduction

The oxygen reduction process taking place in the SOFC cathode is in principle simple, as illustrated below using Kröger Vink notation (Kröger and Vink, 1956):

$$O_2(g) + 2V_{O,electrolyte}^{\bullet\bullet} \rightarrow 2O_{O,electrolyte}^{x} + 4h_{electrode}^{\bullet} \quad (1.1)$$

$V_O^{\bullet\bullet}$ and O_O^x symbolise an oxide ion vacancy and an oxide ion in the electrolyte crystal lattice, respectively. $h^{\bullet}$ is an electron hole in the electrode crystal lattice. The reaction proceeds through a number of elementary reaction steps. The number and order of these steps has been discussed extensively, but disagreement about the nature of the rate limiting process(es) still exists (this is discussed further in the literature survey in Chapter 7). Some of the possible rate limiting elementary reaction steps are listed below:

- Diffusion of oxygen to the electrode material
- Adsorption of oxygen on the surface of the electrode material
- Dissociation
- Migration of adsorbed oxygen intermediates/oxide ions to the reaction zone
- Charge transfer
- Incorporation of oxide ions into the electrolyte lattice

The listed reaction steps may be combined, for instance dissociative adsorption may occur.

As illustrated by equation (1.1) the oxygen reduction process requires the presence of oxygen and electrons as well as the possibility for generated oxide ions to be transported away from the reaction site into the bulk of the electrolyte. For the simplest case, where the electrode material and the electrolyte material possesses only electronic and ionic conductivity, respectively, these criteria are fulfilled in the vicinity of the triple phase boundary (TPB) between the electrode, electrolyte and air, as illustrated by reaction path I in Fig. 1.4. The species, which have to pass the TPB could be one or more of the following: e^-, O^-, O^{2-}, O_2^- and O_2^{2-}.

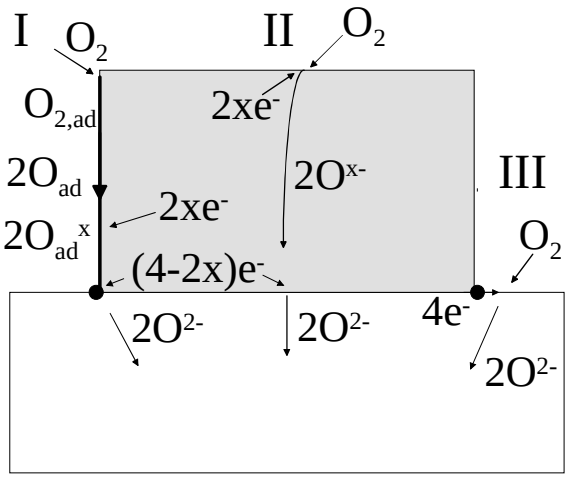

Fig. 1.4. Sketch showing the possible reaction routes for oxygen reduction in an SOFC cathode. The white square illustrates the electrolyte, while the grey square illustrates a grain of the electrode material. The black dot marks the TPB. Three possible reaction routes are illustrated. I. Electronic conducting electrode material. II. Mixed electronic and ionic conducting electrode material. III. Electrolyte material with electronic conductivity in the vicinity of the triple phase boundary.

If the electrode material possesses mixed electronic and ionic conductivity, intermediate oxygen species may be transported through the bulk of the electrode and the

reaction zone may be extended to the interface between the electrode and the electrolyte (reaction path II in Fig. 1.4). Under certain conditions electronic conductivity may be induced in the electrolyte surface close to the TPB (Kleitz et al., 1993), which expands the reaction zone around the TPB (reaction path III in Fig. 1.4).

As illustrated above the TPB is considered to be essential for the oxygen reduction process. The length of the TPB depends on the electrode microstructure. The electrode performance is therefore very sensitive to the electrode composition, particle size distribution and processing as these parameters determine the microstructure. Literature findings about the influence of the microstructure are discussed in Chapter 3.

1.7.2. Electrode-Electrolyte Interactions

When selecting the material at which oxygen should be converted it is important to know if and how the cathode and electrolyte materials interact during oxygen reduction.

Isaacs and Olmer (1982) and Takeda et al. (1987) investigated a number of different metal and ceramic electrode materials in contact with YSZ and found that the electrode material catalyses the oxygen reduction process. This confirmed the work of Fabry and Kleitz (1974), who investigated whether the activation energy of the overpotential related to the oxygen reduction process is independent of the electrode material, the electrolyte material or both. Such independence is reasonable to expect if the rate of the process is limited by, for instance, slow transport of oxide species through the electrolyte or electrode crystal lattice, respectively. The investigation comprised metal point electrodes in contact with calcia or yttria stabilised zirconia. It was found that both the electrode and electrolyte material had qualitative and quantitative influence on the oxygen reduction process. The reason for this behaviour could be that the oxygen surface exchange properties are material specific (Steele, 1994a).

Badwal and Hughes (1991) found that impurities in the electrolyte material tend to migrate from the bulk to the surface. This may alter the electrolyte properties locally, affecting the interfacial resistance between the electrode and the electrolyte in addition to the adhesion of the electrode.

Thus, the measurable electrode activity is the product of the characteristics of the cathode material and its interface with the electrolyte. Therefore, the compatibility of the electrode and the electrolyte material is not only a question of TEC and chemical compatibility; the electrocatalytic interaction must also be considered.

1.7.3. Perovskites

Often materials of the perovskite type ABO_3 where A is a large ion like La^{3+} and Sr^{2+} and B is a small ion e.g. a transition metal ion like Mn^{3+} and Mn^{4+} are used for SOFC cathodes. Takeda et al. (1987) have through investigation of $La_{1-x}Sr_xMO_{3+\delta}$ (M = Cr, Mn, Fe, Co), shown that the electrode activity varies with the B-site dopant. The catalytic activity was found to decrease in the order Co, Mn, Fe, Cr. The differences in activity were ascribed to the varying catalytic properties with respect to dissociation of oxygen.

The best electrocatalyst lanthanum strontium cobaltite, LSCo, has shown severe reactivity towards the classical electrolyte material, YSZ (Minh and Takahashi, 1995). Further, the TEC of LSCo, 19.7×10^{-6} K^{-1} (20% Sr doping; Tai et al., 1995) is excessive to that of YSZ, 10.2×10^{-6} K^{-1} (8 mol% Y_2O_3; Badwal and Foger, 1997). In practise many developers, therefore, use lanthanum strontium manganate, LSM, as this material is more compatible with YSZ and also seems to meet the other requirements for the SOFC cathode material, as discussed in the following.

1.7.4. $LaMnO_3$ based Cathodes

During fabrication LSM may react with the electrolyte material, YSZ. When LSM is sintered in contact with YSZ, MnO_x will diffuse from the LSM phase into the YSZ leaving "free" La_2O_3 or SrO, which immediately reacts with YSZ forming poorly conducting $La_2Zr_2O_7$ or $SrZrO_3$ (Kawada et al., 1992; Roosmalen and Cordfunke, 1992; Poulsen et al., 1992; Clausen et al., 1994; Stochnoil et al., 1995; Mitterdorfer et al., 1996; Mitterdorfer and Gauckler, 1998; Wiik et al., 1999). The formation of $La_2Zr_2O_7$ can be suppressed by using LSM with a few percent A-site substoichiometry, to have enough Mn to saturate the YSZ without forming "free" La_2O_3 or SrO. The oxide ion conductivity decreases when MnO_x is dissolved in the YSZ lattice (roughly a factor of 5 at 800°C for 10 mol% MnO_x addition compared to 2 mol% MnO_x) (Kawada et al., 1992). Further, the activation energy increases from ca. 0.9 eV for undoped YSZ (8 mol% Y_2O_3) to ca. 1.2 eV for YSZ (8 mol% Y_2O_3) with 10 mol% MnO_x (Kawada et al., 1992).

Also the stability of LSM in the potential operation atmosphere is important. The oxygen/manganese (O/Mn) ratio of $La_{1-x}Sr_xMnO_{3\pm\delta}$ varies considerably with p_{O_2}, temperature, degree of strontium doping, and (La + Sr)/Mn-ratio. The O/Mn ratio ranges from 3.18 in pure oxygen at 600°C, to about 2.75 in atmospheres with $p_{O_2} < 10^{-15}$atm. at 1000°C for a Sr doping of 30%. $La_{1-x}Sr_xMnO_3$ is unstable in very reducing atmospheres such as the anode gas at 1000°C. It splits up into La_2O_3, MnO, $SrMnO_3$ and $La_2Mn_2O_4$ when the O/Mn ratio goes below about 2.8, i.e. the decomposition starts in the range 10^{-15} atm. $< p_{O_2} < 10^{-14}$ atm. at 1000°C slightly dependent on the exact composition of the LSM (Tagawa et al., 1997; Zachau-Christiansen et al., 1997; Kuo and Andersen, 1989). Therefore, it is crucial to prevent the fuel gas from getting into contact with the lanthanum manganate cathode.

The lanthanum manganate crystal unit cell volume may change up to 5 % due to stoichiometry changes (Andersen et al, 1994; Roosmalen et al., 1995), and also other

properties of the LSM change with stoichiometry (Mitchell et al., 1996). At high oxygen partial pressures the lattice contains cation vacancies which provides the charge compensation for the Mn^{4+} formed at high p_{O_2}. This means, that the change in molar volume is much less than the change in unit cell volume because the number of unit cells per mole also changes with p_{O_2}.

Selection of the optimal Sr content in $(La_{1-x}Sr_x)_yMnO_{3\pm\delta}$ is a trade off between conductivity, TEC and reactivity. The highest conductivity, the lowest polarisation resistance and the lowest overvoltage above which mixed electronic and ionic conductivity is obtained was found for x = 0.5 (Hammouche et al., 1988; Hammouche et al., 1989). The TEC of YSZ with 8 mol% Y_2O_3 is 10.2×10^{-6} K^{-1} (Badwal and Foger, 1997), and this value should be matched as well as possible by the LSM. The TEC of LSM materials increases with the Sr-content from ca. 11.2×10^{-6} K^{-1} for zero Sr content to ca. 13×10^{-6} K^{-1} for 50% Sr doping (Mackor et al., 1991; Srilomsak et al., 1989), thus a low Sr content is favourable with respect to TEC. x, y in $(La_{1-x}Sr_x)_yMnO_{3\pm\delta}$, the sintering temperature and the yttria content in YSZ are some of the parameters which may affect the formation of $La_2Zr_2O_7$ and $SrZrO_3$ between LSM and YSZ (Ivers-Tiffée et al., 1993; Stoichnoil et al., 1995; Roosmalen et al., 1992). For instance Ivers-Tiffée (1993) found that the amount of $SrZrO_3$ formed between stochiometric LSM and YSZ during heat treatment at 1200°C increases with increasing Sr content in the range of 0.2 – 0.5. For a slightly A-site deficient LSM (y = 0.95) Stoichnoil et al. (1995) found no reaction products between LSM and YSZ for x-values between 0.2 and 0.4 after heat treatment at 1200°C. Thus, the optimum Sr content with respect to reactivity depends strongly on the other parameters chosen, e.g. y and sintering temperature. A reasonable trade off between the influence of the Sr content on conductivity, TEC and reactivity is suggested to be x = 0.15 - 0.30.

1.7.5. Composite LSM/YSZ Cathodes

At realistic SOFC operating conditions the ionic conductivity of an LSM cathode is assumed to be negligible (Mogensen, 1993). Therefore, the oxygen conversion is assumed to primarily take place at the TPB (reaction path I, Fig. 1.4). By adding YSZ to the LSM electrode ionic conductivity within the electrode is obtained, and electrochemically active sites (TPB) are formed within the bulk of the electrode (Kenjo and M. Nishiya, 1992; Østergård et al., 1995). An ideal composite structure requires percolation of LSM, YSZ and pores throughout the electrode structure, demanding careful choice of particle size distribution of the materials involved and controlled processing.

During fabrication, high sintering temperatures should be avoided to prevent formation of secondary phases. However, the sintering temperature has to be high enough to ensure good adhesion between the electrode and the electrolyte. This subject is treated further in Chapter 4.

The in-plane conductivity of a typical composite LSM/YSZ electrode (weight ratio 3/2) of ~ 10 μm is relatively low, which may result in non-perfect current collection. As pure LSM possesses a reasonably high electronic conductivity in the range of 50 - 350 S/cm at temperatures of 700 - 1000°C depending on Sr concentration and temperature (Kertesz et al., 1991; Mackor et al., 1991) it may be used for current collection. Using a bi-layer structure with a composite LSM/YSZ electrode with an LSM current collector, the latter should in principle not affect the electrochemical performance of the composite electrode. However, some contribution from the composite/current collector interface to the TPB is expected, as the current collecting layer covers the surface and fills the voids of the composite, thus contacting a number of YSZ grains. The interaction between the composite and the current collecting layer is addressed further in Chapter 4 and 5.

When investigating the electrochemical properties of LSM/YSZ composite electrodes it should be noted that this system may be dynamic during current flow. It has been reported that the interface between a Pt point electrode and YSZ may change considerably during current loaded experiments (Bay and Jacobsen, 1997a). This may also be the case for the contacts between LSM and YSZ in a composite electrode. Also, kinetic demixing of the electrode and the electrolyte materials when exposed to a potential difference should be considered (Jørgensen et al., 1999c; and references herein). This is treated in more detail in Chapter 5.

The number of elementary processes limiting the performance of LSM/YSZ composite cathodes is uncertain. In the literature several papers addressing this matter exists (see chapter 7). For instance, the author of this thesis has presented a model containing two limiting processes (Juhl et al., 1996 b).

1.7.6. Alternative Materials

Lowering the cost, improving the conductivity and the electrocatalytic activity and minimising the reactivity of the cathode material are some of the motives for investigating alternative cathode materials.

The possibility of substituting lanthanum in LSM with a less pure and cheaper lanthanide material, containing elements such as Ce, Pr and Nd has been tested. With respect to conductivity and TEC Mori et al. (1996) obtained promising results. Preliminary tests of the electrochemical properties of such materials also gave encouraging results (Jørgensen, 2000). However, one of the drawbacks of using lanthanide is that its composition may vary considerably from batch to batch. For instance the Ce content in two Ln batches tested at Risø Nat. Lab. was 9 and 18 atom%, respectively. It may be difficult to obtain reproducible cathode performance using such a material, as the performance has been found to be sensitive to variations in composition and particle size distribution.

In addition to the materials discussed above a broad range of alternative materials with the general formula $(A_1A_2)(B_1B_2)O_3$ with A_1=La, Y, Pr, Nd, Sm, Gd, A_2=Sr, Ba, Ca, Y, B_1=Co, Mn, Fe, Cr and B_2=Fe, Ni, Mn, Co (not all combinations are tested) have been investigated (see for instance Yamamoto et al., 1987; Scotti et al, 1993; Lane et al., 1995; Stevenson et al., 1995; Stevenson et al., 1996; Baker et al., 1997; Ishihara et al., 1998; Huang et al., 1998; Sasaki et al., 1999). For consideration as a cathode material in contact with a YSZ electrolyte none of these materials so far seem to be superior to LSM.

At low operating temperature (450-700°C) a CeO_2 based electrolyte becomes a realistic alternative to the traditional YSZ electrolyte material, as the electronic conductivity of the mixed conducting CeO_2 is low in this temperature range. When using a CeO_2 based electrolyte a broader range of cathode materials than for a YSZ based system may be considered, as reaction products such as $La_2Ce_2O_7$ are not thermodynamically stable (Steele, 1994b). A $La_{0.6}Sr_{0.4}Co_{0.2}Fe_{0.8}O_3$ - $Ce_{0.8}Ga_{0.2}O_{2-x}$ composite cathode has been found to have high electrocatalytic activity in the temperature range 600-750°C (Murray and Barnett, 1999).

1.8. Objective

The electrochemical performance of SOFCs is controlled mainly by the electrode processes. The aim of this work is to improve the understanding of the oxygen reduction process proceeding in the SOFC cathode in order to minimise the total polarisation loss of SOFCs. For this purpose electrochemical characterisation of SOFC cathodes is combined with microstructural analysis.

The system under investigation is a LSM/YSZ composite cathode, which in an optimised form is assumed to be suitable for commercial SOFCs. The mechanism of the oxygen reduction proceeding in SOFC cathodes is far from simple, as parameters such as

composition, processing and test conditions may affect the electrode kinetics. The effect of these parameters is investigated by changing the electrode microstructure by either varying the particle size distribution and electrode thickness or by varying the sintering temperature. A durability study is performed to gain knowledge on the degradation mechanism of the electrodes. Finally, the findings regarding the possible rate limiting processes in the oxygen reduction mechanism are summarised and compared with the literature.

1.9. Thesis Layout

Chapter 2 contains a description of the experimental procedures such as powder processing, sample preparation and measurement techniques. Chapters 3-5 comprise self-contained investigations regarding the influence of microstructure and electrode thickness on the cathode performance (Chapter 3), influence of sintering temperature and microstructure on the cathode performance (Chapter 4) and durability of SOFC cathodes (Chapter 5). An evaluation of the measurement techniques is given in chapter 6. Chapter 7 contains an overview of the trends regarding the rate limiting steps of the oxygen reduction process observed using impedance spectroscopy and of related literature findings. Finally, in Chapter 8 the major achievements in this work are summarised together with the overall conclusions and suggestions for further investigations.

Appendix A contains a paper concerning a model for the impedance of LSM/YSZ cathodes including two rate determining processes (Juhl et al., 1996b). This paper is not enclosed in the main part of this thesis, as the model has proven to be inadequate to describe the impedance of LSM/YSZ cathodes in general. However, the paper provides a good basis for the discussion of the impedance of the LSM/YSZ cathodes presented in chapter 7, and is therefore included as an appendix.

1.10. Basic Parameters

The work has been performed as part of a number of SOFC projects running at Risø Nat. Lab. In these projects the approach has been to investigate electrodes which may be used in a commercial SOFC. Composite LSM/YSZ electrodes were chosen for this purpose. The basic parameters such as materials composition and application technique used in this thesis were defined by the projects.

The cathodes investigated are composite LSM/YSZ electrodes, as this system at present is considered to be the most promising for operation in a commercial SOFC system. The application method is a simple, scaleable spraying technique, which is suitable for commercialisation. Spraying is found to be a well-functioning application technique. The slurry has low viscosity, allowing the electrode particles to distribute well on the electrolyte surface and follow the electrolyte morphology closely.

$(La_{1-x}Sr_x)_yMnO_{3\pm\delta}$ with x = 0.15 - 0.25 and y = 0.9 - 0.95 is investigated. A mixture of fine and coarse (calcined) powder is used, as this has proven to give better performance than fine or coarse powder separately (Østergård et al., 1993).

The electrolyte material used is YSZ with 8 mol% Y_2O_3. The YSZ fraction of the LSM/YSZ composite contains either 3 or 8 mol% Y_2O_3. Despite the better ionic conductivity of YSZ with 8 mol% Y_2O_3 the material containing 3 mol% Y_2O_3 has in some cases proven to lead to better electrode performance (Bagger et al., 1997).

The weight ratio between LSM and YSZ in the composite layer is either 3/2 or 1/1 corresponding to 59 and 49 vol% LSM, respectively. In both compositions percolation of both LSM and YSZ through the electrode structure is in principle obtainable.

To ensure that current is collected from the whole electrode area a bi-layer electrode with a pure LSM layer applied on the composite electrode is used. The thickness

of the composite and the current collecting layers are usually 5 - 10 µm and 25 - 40 µm, respectively.

The basic sintering temperature of the composite layer and the current collecting layer is 1300°C, except in chapter 4, where the influence of sintering temperature on microstructure and performance is investigated.

The exact powder compositions and fabrication parameters are stated where appropriate in the following.

Chapter 2. Experimental Procedures

In this chapter general descriptions of the sample preparation, the electrochemical set-ups and the measurement techniques are given. Details about sample composition and test parameters are stated in each of the succeeding chapters where appropriate.

The majority of the measurements performed are of an electrochemical nature. In addition some structural investigations have been performed using scanning electron microscopy (SEM).

2.1. Electrochemical Test Cells

Two types of electrochemical test cells are prepared. A three-electrode cell (Fig. 2.1) and a two-electrode cell (Fig. 2.2).

The three-electrode test cell can be tested at open circuit voltage (OCV) and under polarised conditions. The three electrodes are the working electrode, which is the electrode under investigation, the counter electrode and the reference electrode. Current is passing through the working electrode and the counter electrode, while the potential difference between the reference electrode and the working electrode is measured using a separate wire at the working electrode (four-wire set-up). Thereby, the overvoltage at the working electrode can be determined as the measured potential difference between reference and working electrode minus the voltage drop related to simple ohmic resistance for instance in the electrolyte.

A three-electrode cell must fulfil certain demands in order to give accurate measurements (Greef et al., 1990). The area of the counter electrode must be large, to ensure that the ohmic loss in this electrode is small. Further, the mutual positioning of the working and the counter electrode must ensure that the current flow through the electrolyte

is uniform. The positioning of the reference electrode must not affect the current flow, as this will affect the equipotential lines in the electrolyte and thereby the measured potential. The area of the reference electrode should be small to ensure that the in-plane current flowing in this electrode is negligible, as such current flow may disturb the determination of the potential. The three-electrode set-up shown in Fig. 2.1.a is designed to fulfil these demands and the feasibility is supported by modeling (Winkler et al., 1998).

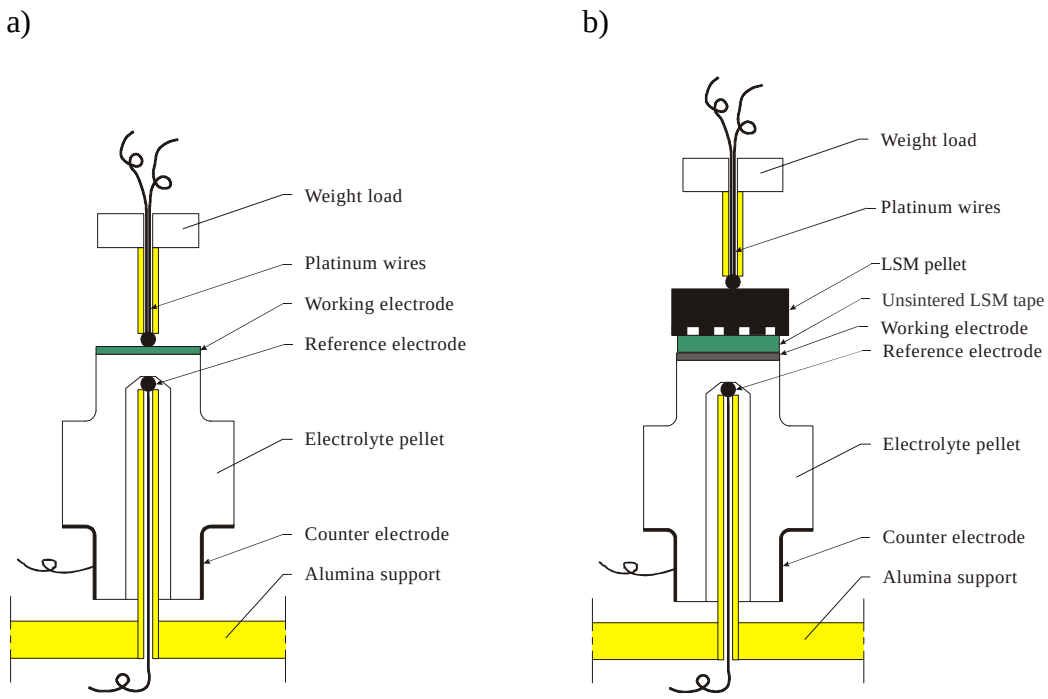

Fig. 2.1. Three-electrode measurement cell developed at Risø Nat. Lab. The cylindrical YSZ electrolyte pellet is mounted on an alumina tube. a) Current is picked up directly from the working electrode using a Pt bead. b) Improved current pick-up is obtained by an unsintered LSM foil in contact with a dense, channeled LSM pellet.

The disadvantages of the three-electrode cell in Fig. 2.1.a are a) the complexity of the electrolyte support geometry, which requires machining; b) rim effects in the electrode structure, which may affect the electrode performance, as masking of the electrode area during application of the electrode is necessary and c) the ohmic drop in the electrolyte is

high compared to the electrode polarisation resistance, which affects the accuracy of the determination of the latter. To compensate for these disadvantages two-electrode cells are tested as a supplement.

Using the symmetrical two-electrode cell shown in Fig. 2.2 two nominally identical electrodes are applied on each side of a YSZ foil and tested simultaneously. The advantage of this cell type is that the tested electrodes resemble cathodes in an operating SOFC better than the electrodes in the three-electrode test. The electrodes can be applied on the same type of substrate as used for a full scale SOFC. Further, the electrodes can be applied without masking the cell area, which prevents rim effects. Finally, the fabrication processes involved with producing symmetrical cells are all simple, wet ceramic processes, and it is therefore fairly easy to produce such cells.

The disadvantage of the two-electrode test cells is that they are only suitable for measurements at open circuit voltage. If the cells should be used for polarised measurements it would be necessary to have a reference electrode in order to compensate for the ohmic drop in the electrolyte and the leads. However, mathematical modelling has shown that three electrode electrochemical cells produced on a relatively thin electrolyte substrate require very accurate alignment of the working and counter electrodes within a fraction of the electrolyte thickness (Winkler et al., 1998). Misalignment may disturb the current distribution in the electrolyte, which may influence the measurement results severely. The requirement for alignment of the electrodes cannot be met in practice using spraying as the application method for the electrodes. Thus, it is not possible to obtain reliable three-electrode measurements with low errors using thin electrolyte YSZ substrates (~ 200 μm) with sprayed electrodes. Therefore, the cells are produced as two-electrode cells and used only for OCV measurements.

The advantages and disadvantages of the two types of measurement cells are discussed in further detail in chapter 6.

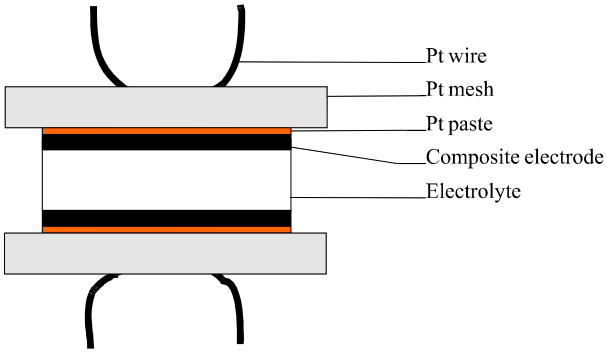

Fig. 2.2. Schematic of a symmetrical two-electrode measurement cell.

2.2. Sample Preparation

The LSM used is $(La_{1-x}Sr_x)_yMnO_{3\pm\delta}$ with x = 0.15 or 0.25 and y = 0.9 or 0.95. It is produced by spray pyrolysis in a rotary furnace at Haldor Topsøe A/S, Denmark (Christiansen and Gordes, 1991) using glycine-nitrate combustion synthesis (Chick et al., 1990). Two YSZ compositions, ZrO_2 with 3 mol% and 8 mol% Y_2O_3, are used. The powders, denoted TZ3YB and TZ8Y, respectively, are commercial products supplied by Tosoh Corporation, Japan.

2.2.1. Electrolyte Substrates

The electrolyte substrates are produced from TZ8Y. The pellets for three-electrode electrochemical test cells are pressed and machined to the cylindrical shape illustrated in Fig. 2.1 before sintering at 1600°C. The area of the working electrode is approx. 0.4 cm^2.

Two-electrode measurements are performed on symmetrical cells, which are produced by application of two nominally identical cathodes on each side of an approximately 180 µm thick TZ8Y foil (Fig. 2.2). For this purpose a 5×5 cm^2 electrolyte foil is produced by tape casting and sintering at 1350°C. After application and sintering of the electrodes electrochemical cells with an area of 0.2-0.5 cm^2 are made from the sample

by breaking or cutting using a diamond tool. Breaking pieces of the sample for test was used for the first generation of symmetrical test cells (Chapter 4). This method was found to be feasible and no problems with for instance delaminations between electrode and electrolyte was found. However, it is more convenient to cut the sample into test cells having a more homogenous area (approximately 0.25 cm^2), as these are easier to handle in practice. To preserve the structure while cutting the pores of the electrodes are filled with water, which is frozen during the cutting procedure. Thereafter, the test cells are cleaned in an ultrasonic bath to remove dust originating from the cutting. The cutting procedure is found to be very efficient in practice.

2.2.2. Cathodes

The cathode consists of two layers. An electrochemical active usually 5 - 10 µm thick composite LSM/YSZ layer, denoted the C-layer, and a layer of pure LSM aimed for current collection, denoted CCC-layer.

For the C-layer a low-viscous ethanol based slurry is produced by ball milling LSM, YSZ (TZ8Y or TZ3YB) and a dispersant. The C-layer is applied by air-borne spraying and dried in air. The C-layer is normally sintered at temperatures between 1100°C and 1300°C with a heating ramp of 100°C/hour and a dwell time of 2 hours at maximum temperature. Different C-layer compositions have been tested. Details about the composition are given in each of the following chapters.

During spraying of the three-electrode cells a teflon tape is wrapped around the top of the pellet to prevent the slurry from contaminating the rim of the pellet. In the case of symmetrical cells no masking is needed, as the rim of the sample, which could be short circuited due to electrode material, is not used in the test.

The CCC-layer consists of two nominally identical LSM sprayings with intermediate drying and sintering. The CCC-layer is normally sintered at the same

temperature as the C-layer using a similar ramp and dwell time. After sintering the CCC-layer thickness is 25 - 40 µm.

2.2.3. Counter and Reference Electrodes and Current Collection

In the three-electrode test the counter electrode consisted of Pt paste painted on the surface indicated in Fig. 2.1.a. The reference electrode was a Pt bead placed at the end of the alumina tube, which served as the sample holder. The distance between the working electrode and the reference electrode was approximately 2 mm.

In the initial measurements (chapter 3) current was collected directly from the working electrode via a Pt bead (Fig. 2.1.a.). This current collection system was found to be inadequate for some electrodes. Therefore, the current collection system was improved by applying an unsintered LSM foil onto the current collecting layer (or directly onto the composite layer, chapter 5). The foil was contacted by a sintered LSM pellet, which was channelled to allow gas access (Fig. 2.1.b.). After binder burnout during approach to test temperature the thickness of the LSM foil was ca. 40 µm.

For the two-electrode test Pt paste was painted on the composite electrodes to improve current collection. The whole electrode area was painted and the edges of the cells are cleaned before test to avoid short circuits. The Pt paste is cured at 1000°C for approximately 1 hour prior to test. During test a Pt mesh is pressed into contact with each side of the test cell (Fig. 2.2.a). To keep the measurement cell in position during test it can be mounted between two LSM pellets, having channels to ensure gas access. In this case the measurement wires are connected to the LSM pellet.

2.3. Electrochemical test

Using both types of test cells four electrochemical cells were placed in a furnace and measurements were performed on one cell at a time. The test atmosphere was air and the test temperature was varied between 600 - 1000°C. The two-electrode cells were tested by electrochemical impedance spectroscopy (EIS) at OCV. For the three-electrode cells EIS was combined with chronoamperometry at OCV and cathodic potentials.

2.3.1. Electrochemical Impedance Spectroscopy

Electrochemical impedance spectroscopy (EIS) is a suitable method for investigating the kinetics of an electrochemical reaction, as the elementary reaction steps limiting the rate of the reaction can in principle be separated.

Electrochemical impedance spectroscopy is an AC method where a sinusoidal potential, E, with varying frequency, f, is applied to the electrode

$$E = A_E \exp(j\omega t) \qquad (2.1)$$

A_E is the amplitude, j is the imaginary unit, ω is the angular frequency ($2\pi f$) and t is the time. In the linear current - overvoltage range (small A_E in equation 2.1) the current response, i, as a function of f is also a sin function

$$i = A_i \exp(j(\omega t - \phi)) \qquad (2.2)$$

A_i is the current amplitude and ϕ is the phase angle. The impedance, Z, equals

$$Z = E/i = (A_E/A_i)\exp(j\phi) \qquad (2.3)$$

The impedance is often plotted in the complex plane with minus the imaginary part along the ordinate axis and the real part along the axis of abscissas (a so-called Nyquist plot). For a simple electrode reaction, illustrated by the equivalent circuit shown in Fig. 2.3.a the impedance response is a perfect semicircle in the imaginary plane (Fig. 2.3.b). In Fig. 2.3 R_s is the series resistance mainly ascribed to the electrolyte (the high frequency intercept with the axis of abscissas), R_{pol} is the electrode polarisation resistance (the

difference between the high and the low frequency intercept with the axis of abscissas) and C is the capacitance. If C is not a perfect capacitor a depressed arc will appear.

In the case of a more complex electrode reaction several elementary processes may limit the reaction rate, and each of these processes may appear in the impedance spectrum as a more or less depressed arc. The arcs may be overlapping and it can be difficult to separate them in practice. In section 2.4. more details about the interpretation of impedance measurements are given.

a) b)

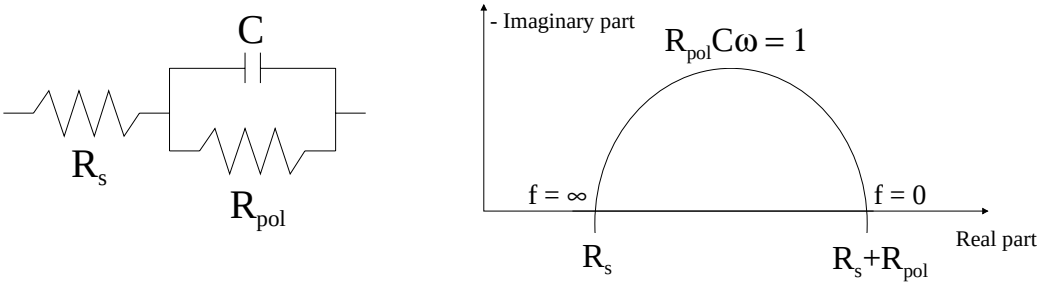

Fig. 2.3. a) Equivalent circuit for a simple electrode reaction. b) The impedance response of the equivalent circuit shown in a). R_s is the series resistance, R_{pol} is the polarisation resistance, C is the capacitance, f is the frequency and ω is the angular frequency.

2.3.2. Chronoamperometry

Chronoamperometry is a DC method, where the applied potential is changed momentarily and kept at constant level for a certain period of time. Simultaneously, the current flow is measured as a function of time.

In this work chronoamperometry is used to stabilise the system at a certain potential in order to obtain current-voltage data under steady state conditions and to ensure that an overlying EIS measurement is performed under stable conditions.

2.3.3. Experimental Details

In general the electrochemical tests were performed at three temperatures for each sample, e.g. 700°C, 850°C and 1000°C. A typical measurement sequence on three-electrode cells involved an impedance measurement at OCV followed by impedance measurements at four different fixed cathodic potentials and finally another impedance measurement was taken at OCV. All impedance measurements were performed after a 10 - 15 minutes chronoamperometry measurement, and the potential was kept constant during the EIS measurement.

Impedance measurements were performed using a frequency response analyser from Solartron Instruments (model 1250, 1260 or 1280[1]). The maximum frequency used in the impedance measurements varied with the used frequency response analyser (20 - 65 kHz). The lowest measuring frequency was 1 - 100 mHz. The amplitude of the potential applied over the cell was 14 mV root mean square (RMS) and 6 - 12 points per decade of frequency were measured going from high to low frequency.

In the chronoamperometry experiments the potential was controlled using a potentiostat. The instruments used were Solartron 1286, 1287, 1280[1] or PAR E&G potentiostat/galvanostat model 273.

2.4. Interpretation of EIS measurements

The electrochemical impedance response obtained on composite cathodes in general comprised a high frequency induction tail, L, ascribed to the measurement leads, an ohmic resistance, R_s, mainly originating from the electrolyte (the high frequency intercept adjusted for induction) and a number of more or less overlapping arcs. The data

[1] S1280 is an electrochemical measurement unit, which operates both as a frequency response analyser and a potentiostat.

was fitted using the computer software EQUIVCRT (Boukamp, 1986), in order to determine the magnitude of R_s and the polarisation resistance, R_{pol}, and to separate the individual arcs in the impedance spectrum. In this work the data were fitted to an equivalent circuit of the type $LR_s(R_1Q_1)(R_2Q_2)(R_3Q_3)$ (Fig. 2.4). R is a resistance. Q is a constant phase element with the admittance $Y' = Y_0(j\omega)^n$, where Y_0 is an admittance factor and n is the frequency exponent. (RQ) is a depressed arc in the impedance spectrum.

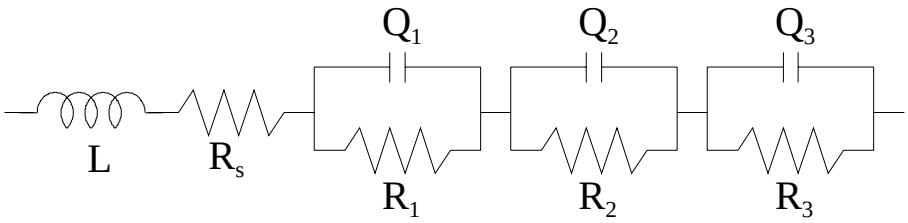

Fig. 2.4. The equivalent circuit used for fitting the data. L is an inductance, R_s is the series resistance, R is a resistance and Q is a constant phase element. $R_{pol} = R_1 + R_2 + R_3$.

The equivalent circuit in Fig. 2.4 has three series connected arcs, which gives the simplest possible description of an impedance spectra containing three limiting processes. When fitting the data one or two of the arcs may turn out to be zero. However, this circuit is not adequate to describe the impedance of all composite electrodes. As found in Chapter 7 more than three processes may contribute to the impedance response. In this work the circuit is used to determine R_{pol} and the magnitude of the individual arcs present in the impedance spectrum, and the circuit has been found to serve this purpose well.

For the symmetric test cell the measured polarisation resistance, R_p', reflects the sum of the polarisation resistances of the two electrodes investigated. Thus, to get the average area-specific polarisation resistance of the two electrodes, R_p, the measured value, R_p', must be divided by two and corrected for area. R_p determined in this way is comparable to the polarisation resistance measured using three-electrode cells. In the

impedance plots presented for symmetrical electrodes in the following the impedance is divided by two and corrected for area, thus the difference between the high and the low frequency intercept equals R_p. Please note, that for simplicity the series resistance is also divided by two in these impedance spectra.

2.5. Microstructural Investigation

When preparing samples for structural analysis it is important to preserve the electrode structure while the sample is cut and polished. Therefore, a vacuum technique for embedding the samples in epoxy prior to cutting has been developed at Risø Nat. Lab. After being embedded the samples were cut perpendicular to the cathode-electrolyte interface, ground and polished. The samples were examined by SEM, a JEOL 840 or JEOL LV5310, and by energy dispersive X-ray spectrometry (EDS), Noran Voyager 3.5. X-ray element mapping was performed on a Philips XL40 SEM with a Noran Vantage EDS system.

Chapter 3. Cathode Thickness and Microstructure[1]

3.1. Introduction

In this chapter the correlation between microstructure, thickness and performance of composite SOFC cathodes consisting of LSM and YSZ is investigated. As discussed in section 1.7.5 the oxygen reduction process is assumed to primarily proceed in the vicinity of the TPB for such electrodes. However, the TPB is only electrochemically active if electrons, oxide ions and gas can percolate freely through LSM, YSZ and pores, respectively, to and from the TPB. The reaction rate of the LSM/YSZ electrode system depends on the microstructure (Mizusaki et al., 1988; Mizusaki et al., 1991; Sasaki et al. 1995; van Heuveln et al., 1993; de Haart et al., 1991; Kenjo and Nishiya, 1992; Østergård et al., 1995), since the microstructure determines the extent of active TPB.

Mizusaki et al. (1988 and 1991) have investigated $La_{0.6}Ca_{0.4}MnO_3$ electrodes painted on a YSZ substrate. Using rather coarse particles (1 - 3 μm) the reaction rate was essentially independent of the electrode thickness and was proportional to the length of TPB (Mizusaki et al., 1988). This implies a close relationship between the electrode morphology and performance (Mizusaki et al., 1991).

The correlation between structure and performance for a $La_{0.85}Sr_{0.15}MnO_3$ cathode screen printed on YSZ was studied at 800°C by Sasaki et al. (1995). They found that the performance correlated to the length of TPB and the electrode thickness. At 800°C a minimum in area specific polarisation resistance, R_p, was found for a cathode thickness of 25 μm. Electrodes manufactured from LSM with a narrow particle size distribution (PSD) had low R_p compared to electrodes manufactured from powder with a wide PSD. A similar effect was observed by van Heuveln et al. (1993) with $La_{0.85}Sr_{0.15}MnO_3$ electrodes on YSZ in

[1]This chapter is based on: M. Juhl, S. Primdahl, C. Manon and M. Mogensen, Performance/Structure Correlation for Composite SOFC Cathodes, *J. Power Sources*, **61** (1996a) 173-181.

oxygen at 920°C. Additionally, they observed that powder with a narrow PSD, calcined at high temperature before electrode manufacture, resulted in a R_p, which exceeded the value for an electrode with a wide PSD.

In contrast, de Haart et al. (1991) found that the polarisation behaviour of a $La_{0.85}Sr_{0.15}MnO_3$ electrode produced by a dip coat process was not significantly dependent on the electrode microstructure and thickness. This in conjunction with the references cited above indicates that the performance of porous LSM electrodes is closely related to the techniques used for powder processing and electrode manufacturing.

Using composite electrodes made from a mixture of electronic and ionic conductive materials, tends to complicate things. Kenjo et al. (1992) investigated composite electrodes of La_xMnO_3 and YSZ with varying weight ratios of the two components. The electrodes were manufactured by painting a turpentine based slurry on an electrolyte disk and isostatically pressing the green electrode. The polarisation behaviour was measured at 900°C in air. It was found that additional reaction sites were created inside composite electrodes. The addition of 50 weight percent YSZ to a $La_{0.85}MnO_3$ electrode decreased the R_p from 0.77 Ωcm^2 to 0.16 Ωcm^2. Electrodes containing a 1:2 weight ratio of $La_{0.85}MnO_3$ and YSZ exhibited decreasing R_p as the electrode thickness was increased.

Østergård et al. (1995) investigated composite electrodes of LSM and YSZ at 1000°C in air. The electrodes were manufactured by the spray coating technique also used in the present work. With a $(La_{0.85}Sr_{0.15})_{0.9}MnO_3$ (nominal composition) electrode an improvement of the R_p from 2.7 Ωcm^2 to 0.65 Ωcm^2 was found by the addition of 20 wt% fine grained YSZ. The structure of the composite electrode was found to be of major importance with respect to performance. Composite electrodes made with a mixture of fine and coarse LSM had lower resistance than electrodes containing only fine or coarse LSM powder. The best result in this work, R_p = 0.5 Ωcm^2, was obtained with a composite electrode containing 40 wt% YSZ (Østergård et al., 1995).

3.2. Experimental

This chapter concerns two series of electrodes. The effect of the C-layer thickness was investigated in series 1. The thickness was varied between 2 and 12 μm. In series 2 the effect of altering the microstructure of the C-layer by applying a layer of YSZ-particles (P-layer) on the electrolyte surface was studied. The purpose of the P-layer was to obtain a more open structure of the C-layer, improve the distribution of YSZ in the C-layer and expand the YSZ surface area. Fig. 3.1 illustrates the design of the electrodes tested, showing the electrodes with no P-layer in a) and the electrodes with a P-layer in b). The electrodes in series 1 and the reference electrodes in series 2 were produced with a different C-layer microstructure. The effect of changing only the microstructure of the C-layer was therefore found by comparing these electrodes.

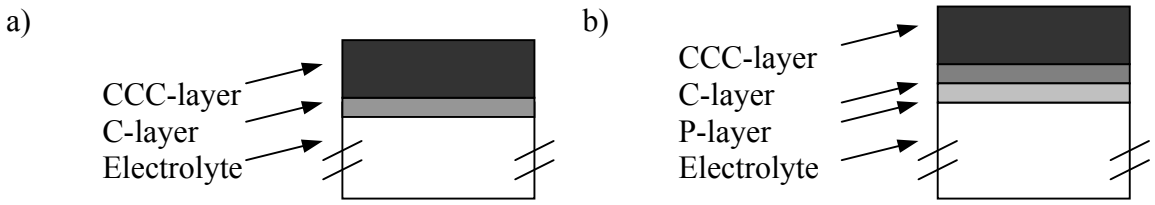

Fig. 3.1. Schematic of the electrode structures studied. The C-layer is the composite LSM/YSZ layer, the CCC-layer is the cathode current collector and the P-layer is a layer of YSZ particles applied on the electrolyte surface. a) Electrode without P-layer (series 1 and reference in series 2). b) Electrode with P-layer (series 2).

3.2.1. Preparation of Powder and Samples

The composition of the LSM used for the C-layer and the CCC-layer was $(La_{0.75}Sr_{0.25})_{0.9}MnO_3$ (nominal composition). The electrodes were applied on YSZ pellets, and tested using the set-up shown in Fig. 2.1.a.

In series 1 the C-layer thickness was varied by changing the spray time. In series 2 the P-layer slurry was applied directly onto electrolyte pellets for two samples, K310-311. The slurry was made as follows: TZ8Y powder was calcined at 1500°C for 4 hours and ball milled

until a mean particle diameter of approximately 23 μm was achieved (measured by light scattering with Malvern Mastersizer equipment). The P-layer was then sprayed onto the electrolyte surface, the C-layer was sprayed on the P-layer and the two layers were cosintered. Two other samples, K319 and K320, were made as references. They were intended to be as identical as possible to K310 and K311 but without the P-layer.

The C-layer consists of equal amounts (by weight) of LSM and TZ3YB. As shown in Table 3.1 the LSM powder used for the C-layer was treated differently for the two series of samples. In series 1 the LSM was a mixture of powder heat treated at 600°C and calcined at 1300°C. The purpose of adding powder calcined at high temperature was to lower the overall sinterability of the powder and introduce larger grains. LSM with high sinterability (heat treated at 600°C) was used in series 2 to ensure adhesion of both the P-layer and the C-layer onto the electrolyte. In both C-layer slurries the YSZ powder was uncalcined.

Table 3.1. Description of C-layer composition for series 1 and 2

Series	Sample	C-layer composition	Remarks
1	**K313-318**	**50 wt% $(La_{0.75}Sr_{0.25})_{0.9}MnO_3$, mixture (1:1) of powder heat treated at 600°C and powder calcined at 1300°C for two hours. 50 wt% uncalcined TZ3YB.**	
2	**K310-311**	**P-layer (TZ8Y particles with an average diameter of 23 μm) followed by C-layer containing 50 wt% $(La_{0.75}Sr_{0.25})_{0.9}MnO_3$ heat treated at 600°C and 50 wt% uncalcined TZ3YB.**	**P-layer and C-layer cosintered.**
	K319-320	**C-layer containing 50 wt% uncalcined $(La_{0.75}Sr_{0.25})_{0.9}MnO_3$ and 50 wt% uncalcined TZ3Y.**	**As K310-311, but no P-layer.**

Fig. 3.2 shows the particle size distributions of the C-layer slurries prior to spraying. The particle size distribution was measured by light scattering and found to be bimodal for both slurries. The slurry used for series 2 contained a large fraction of relatively small particles (mean particle size 0.4 microns). This fraction decreased when part of the powder was calcined at high temperature (series 1).

The C-layer was sintered at 1300°C for 2 hours. Thereafter, the CCC-layer was applied by two sprayings, which were sintered separately at 1300°C for 2 hours.

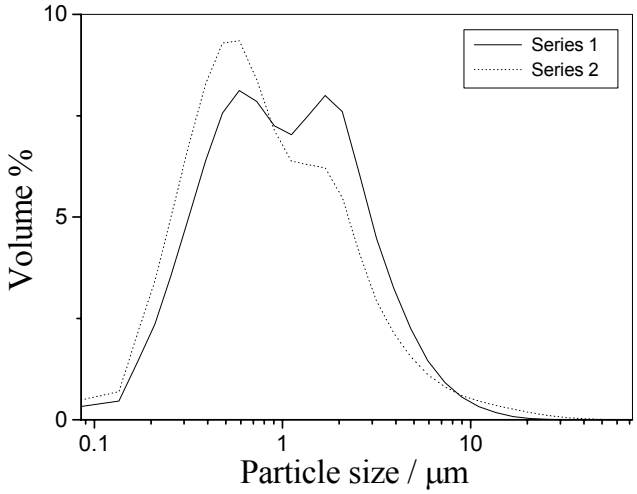

Fig. 3.2. Particle size distribution in C-layer slurry for series 1 and series 2 measured by light scattering. See table 3.1 for details on slurry compositions.

3.2.2. Electrochemical Characterisation

The samples were tested at three temperatures, 700°C, 850°C and 1000°C in air. Chronoamperometry measurements and impedance spectroscopy measurements were performed using a Solartron 1286 potentiostat and a Solartron 1250 frequency response analyser, respectively.

Impedance measurements were taken at open circuit voltage (OCV) and, while keeping the potential constant, after each chronoamperometry measurement. Impedance data

were typically obtained in the frequency range 65 kHz-1 mHz with an applied amplitude of 20 mV.

In the chronoamperometry measurements the current was measured at a constant potential over a 15 minute period. In some cases steady state conditions were not fully obtained after this time period. However, all data were taken after 15 minutes. Chronoamperometry measurements were performed at four different applied potentials, E_{appl}, for each sample. The cathodic overvoltage, η, was calculated using formula (3.1),

$$\eta = E_{appl} - IR_S \qquad (3.1)$$

where *I* was the measured current. In Fig. 3.3 examples of the obtained data are plotted after correction for ohmic losses. The lines are second degree polynomials fitted to the experimental data. From the second degree polynomial the dc current at -50 mV overvoltage was determined and the area specific polarisation resistance calculated. This number was used for comparison of the electrodes. At 1000°C it was necessary to extrapolate the i versus η characteristic. At this temperature the maximum applied potential was -300 mV, corresponding to cathodic overvoltages between 25 and 50 mV. Higher potentials were not applied to the sample due to the risk that the high current would cause localised heating (Primdahl et al., 1996).

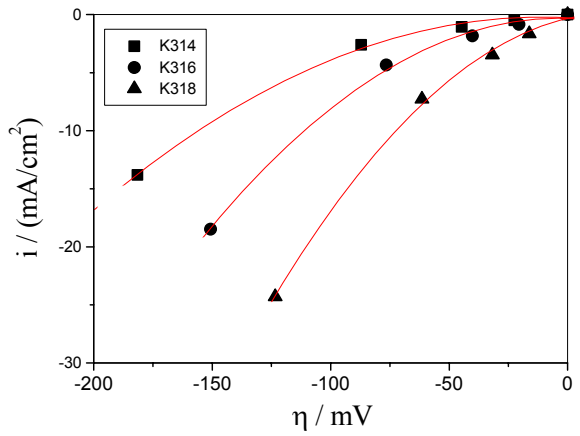

Fig. 3.3. i versus η characteristics obtained in air at 700°C. The curves are second degree polynomials fit to the experimental values.

3.2.3. Microstructural Characterisation

The electrochemical cells were embedded in epoxy before being cut and polished, to prepare the samples for scanning electron microscopy (SEM). The C-layer thickness was determined using a computer program called PCImage. The standard deviations on thickness measurements of 2 - 3 μm and 4 - 11 μm were 0.5 - 1 μm and 1 - 2 μm, respectively. Generalisations about the electrode structure were made by inspecting 10 - 12 micrographs taken at random locations on the sample.

3.3. Results and Discussion

3.3.1. Series 1, Effect of Thickness

Figs. 3.4 - 3.6 show R_p as a function of the C-layer thickness for different temperatures. The measurements obtained at -50 mV are dc measurements while those at OCV are impedance measurements. In the thickness range investigated, R_p decreases as the thickness increases. This implies some level of percolation in both LSM and YSZ for cathodes with thicknesses up to 11 μm. It is unlikely that all existing TPB lines are active, due to limited percolation in one or more phases.

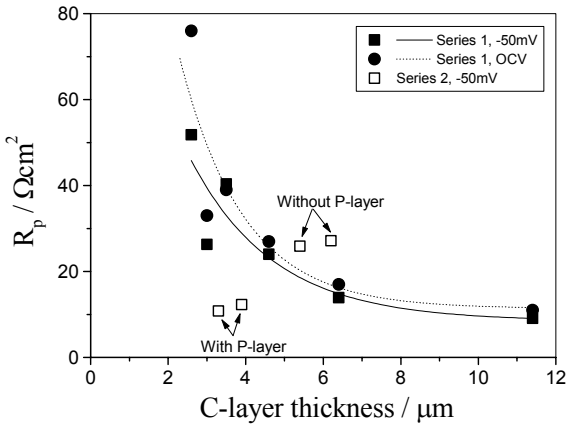

Fig. 3.4. Area specific polarisation resistance, R_p, determined in air at 700°C plotted as a function of the C-layer thickness.

Looking at the absolute values in Figs. 3.4 - 3.6 the sensitivity to changes in thickness is highest at 700°C and lowest at 1000°C. The data at 1000°C (Fig. 3.6) were determined from extrapolation of the iη-characteristics. This may influence the accuracy, but does not explain the observed trend.

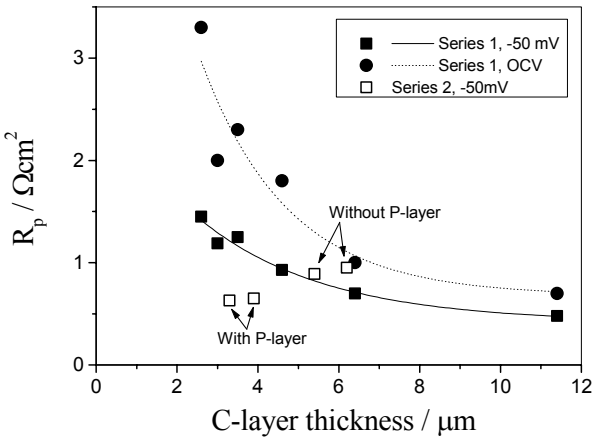

Fig. 3.5. Area specific polarisation resistance, R_p, determined in air at 850°C plotted as a function of the C-layer thickness.

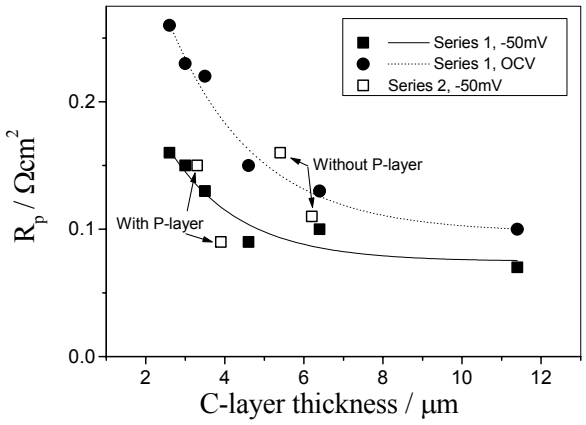

Fig. 3.6. Area specific polarisation resistance, R_p, determined in air at 1000°C plotted as a function of the C-layer thickness.

The relation between performance and temperature observed with dc measurements (Figs. 3.4 - 3.6) was confirmed by ac measurements (Fig. 3.7). At low temperature (700°C and 850°C) a majority of the impedance plots could be described by one dominant arc. However, what seems to be one dominant arc could actually be a number of overlapping arcs with similar time constants. At 1000°C four out of six impedance measurements contained two distinct arcs. It is uncertain what causes the presence of two distinct arcs in some impedance spectra. So far no correlation between the number of arcs and the electrode thickness has been found.

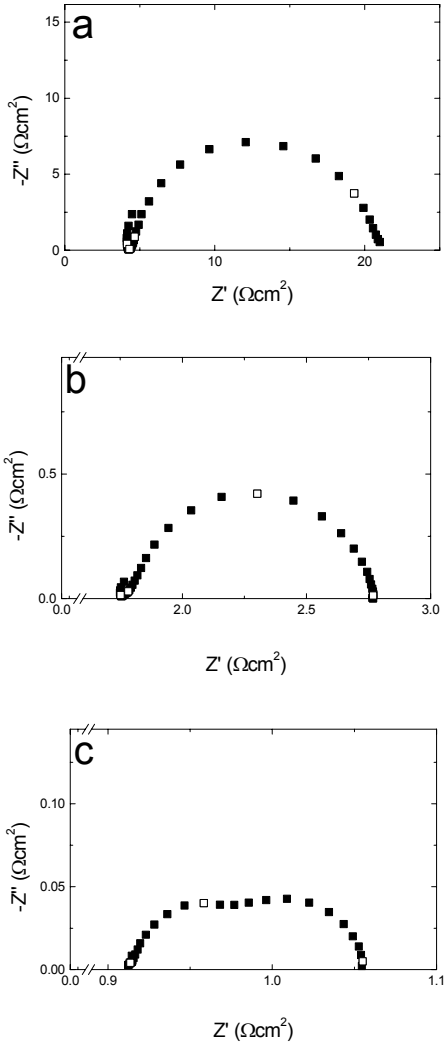

Fig. 3.7. Examples of impedance plots measured at OCV in air at varying temperature (sample K317), a) 700°C, b) 850°C and c) 1000°C. Data points at 10^{-2}, 1, 10^{2} and 10^{4}Hz are accentuated.

The apparent activation energy is not constant in the temperature range investigated (see Fig. 3.8). This may be due to the cathode reaction rate being limited by two or more reaction steps with different activation energies. Further, the bulk of the electrochemical reaction may not take place in the same volume fraction of the electrode at all temperatures (this will be dealt with in section 3.3.3). It is likely that the reaction zone along the active TPB is not identical at all measuring conditions (Kleitz et al., 1993). The reaction zone is believed to expand into a broader band as the temperature increases.

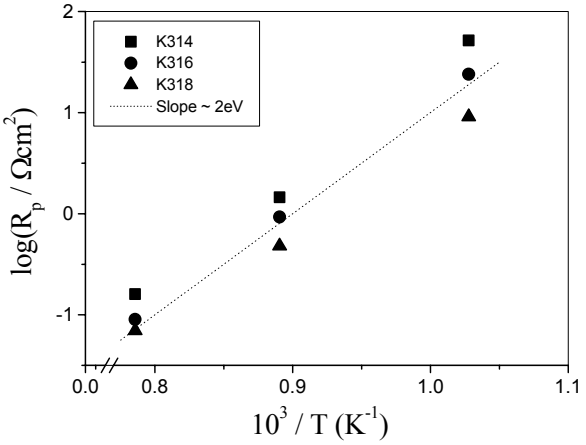

Fig. 3.8. Arrhenius plots obtained at –50 mV overvoltage in air, series 1. A reference line with a slope corresponding to an activation energy of –2 eV is shown for comparison.

The structural analysis in SEM revealed several trends. The micrographs in Fig. 3.9 and the following figures are obtained with backscattered electrons, i.e. in the images the LSM phase is brighter than the YSZ phase. The C-layers are generally dense and the porosity is not uniformly distributed, as illustrated in Fig. 3.9. A high fraction of the porosity is located between the C-layer and either the electrolyte or the CCC-layer. The amount of porosity tended to increase with the C-layer thickness. Adhesion of the C-layer to the electrolyte is extensive (Fig. 3.9).

Fig. 3.10 shows the C-layer most similar to the expected ideal structure. Besides good electrochemical properties this sample had i) good adhesion to both the electrolyte and the CCC-layer, ii) some percolation of LSM through the YSZ matrix, and iii) some porosity throughout the C-layer. An even higher porosity and a more uniform pore size distribution is expected to be preferable in ensuring percolation of gas through the C-layer, which could help to increase the active TPB length.

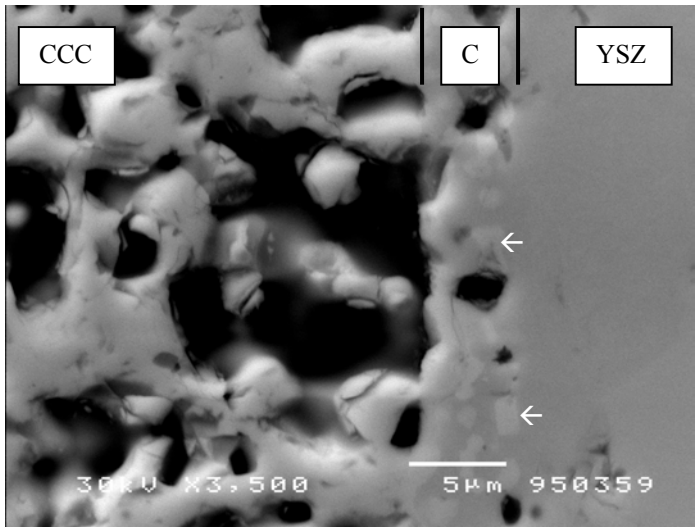

Fig. 3.9. SEM micrograph showing a cross section of sample K316 (series 1). The scale bar corresponds to 5 µm. The LSM phase is brighter than the YSZ phase, as the image is obtained with backscattered electrons. The arrows indicate some of the LSM grains.

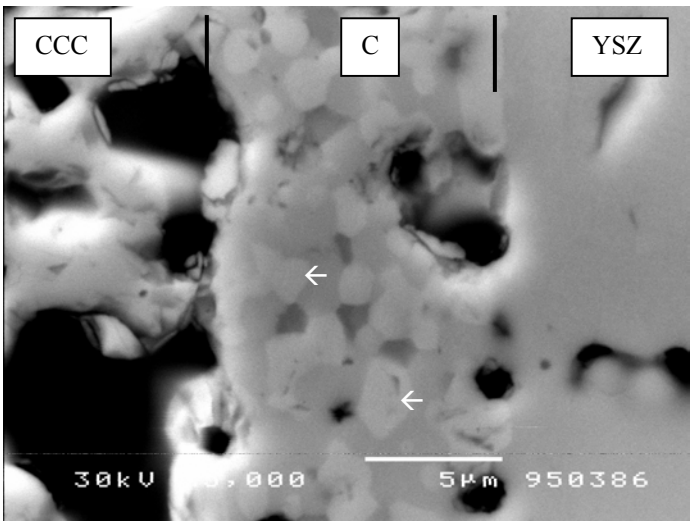

Fig. 3.10. SEM micrograph showing a cross section of sample K318 (series 1). The scale bar corresponds to 5 µm. The LSM phase is brighter than the YSZ phase, as the image is obtained with backscattered electrons. The arrows indicate some of the LSM grains.

The results are comparable to data obtained by Kenjo et al. (1992). They measured an area specific polarisation resistance of 0.16 Ωcm^2 for a LSM-YSZ composite electrode with equal amounts (by weight) of the two materials at 900°C in air. The results obtained for sample K318 correspond to a R_p of approximately 0.22 Ωcm^2 at 900°C in air (interpolated in Fig. 3.8). Also the effect of thickness seems similar. Kenjo et al. (1992) painted and isostatically pressed the green electrode. The electrodes in the present work are made by spray coating, an easy technique to scale up and commercialise. This indicates that it is possible to manufacture electrodes with good performance by industrial application methods.

3.3.2. Series 2, Effect of P-layer

The results of series 2 are shown in Table 3.2. Application of a P-layer improves the performance at the lowest temperatures tested (700°C and 850°C). The observed effect cannot be explained by variations in C-layer thickness, since the relationship between thickness and R_p is reversed in series 2 (Table 3.2). Thus, the P-layer had a significant effect. As observed in series 1 the performance of the electrodes in series 2 is less dependent on the C-layer structure at 1000°C than at lower temperatures. Comparing cathodes of similar thickness without a P-layer, cathodes prepared from partially precalcined LSM (series 1) have the lower R_p values (Figs. 3.4 - 3.6). Thus, the sintering activity of LSM affects the performance.

Arrhenius plots for the samples of series 2, given in Fig. 3.11, show the same trends as observed for series 1.

The ac measurements showed the same tendencies as the dc measurements. In the impedance plots one dominant arc was observed at both 700°C and 850°C. Fig. 3.12 shows impedance plots obtained at OCV and 1000°C for the samples in series 2. Two distinct arcs are observed for electrodes with a P-layer, while electrodes with no P-layer show only one

dominant arc. The appearance of the second arc for some electrodes suggests that the rate limiting steps at 1000°C are depending on the microstructure.

Table 3.2. Results obtained for the samples of series 2 with or without a P-layer. The measuring conditions are –50 mV overvoltage in air. Each number is an average of two values. Values at 1000°C are determined by extrapolation of the iη-characteristics.

Sample	Temperature / °C	C-layer thickness / µm	R_p(-50 mV) / Ω·cm^2
With P-layer	**704**	**4**	**12**
Without P-layer		**6**	**27**
With P-layer	**850**	**4**	**0.6**
Without P-layer		**6**	**0.9**
With P-layer	**1000**	**4**	**0.12**
Without P-layer		**6**	**0.14**

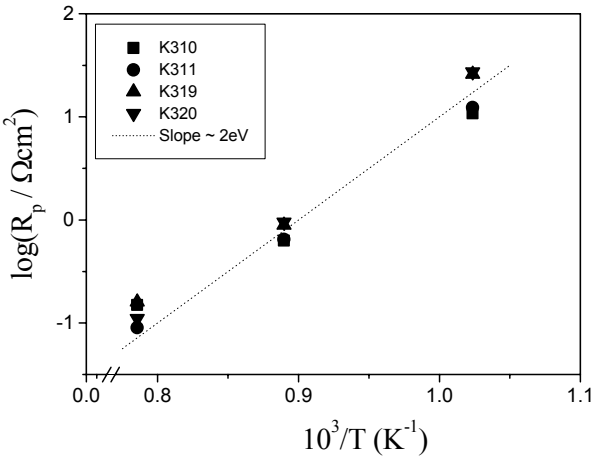

Fig. 3.11. Arrhenius plots obtained at –50 mV overvoltage in air, series 2. A reference line with a slope corresponding to an activation energy of –2 eV is shown for comparison.

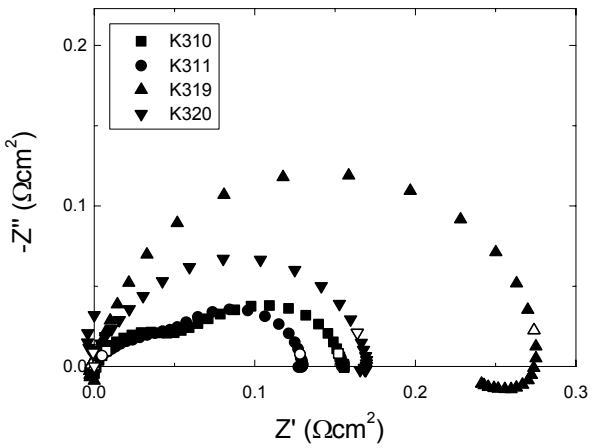

Fig. 3.12. Impedance plots measured at OCV and 1000°C on samples with and without a P-layer (K310 - 311 and K319 - 320, respectively). The data are R_s-corrected. Data points at 1 and 10^4Hz are accentuated.

For structural investigations using SEM two sintered TZ8Y-tapes were sprayed with a P-layer (Fig. 3.13). One of the samples was additionally sprayed with a C-layer (Fig. 3.14). As shown in Fig. 3.13 the P-layer was inhomogeneous in thickness and particle size distribution. However, the largest particles were distributed in a mono-layer. This is preferable to a multi-layer, since a thin layer has lower ohmic resistivity for ionic conduction through the P-layer. Cracks had formed on the sample surface after the C-layer was sprayed and sintered (Fig. 3.14). The cracks are believed to originate through a combination of contractions while drying the electrode and shrinkage while firing. The C-layer appeared dense in certain areas, i.e. the porosity was inhomogeneously distributed.

In addition to the above-described structural examinations of samples mounted on tapes, the electrochemically investigated electrodes were also examined by SEM. The C-layer was most porous for samples with a P-layer, as illustrated in Fig. 3.15 and 3.16. Additionally, the adhesion between the C-layer and the P-layer was good, but the number of contact points between the P-layer and the electrolyte was limited (Fig. 3.15). This caused an increase in the series resistance, but did not influence the polarisation resistance.

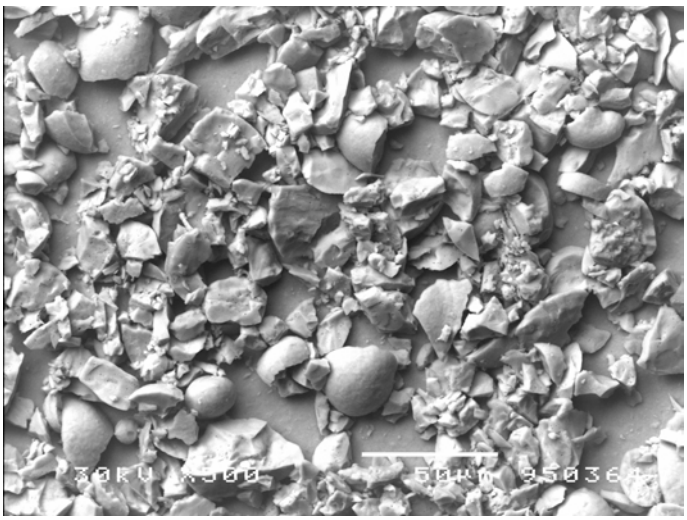

Fig. 3.13. SEM micrograph showing a TZ8Y-tape with a sprayed and sintered P-layer. The scale bar corresponds to 50 µm.

Fig. 3.14. SEM micrograph showing a TZ8Y-tape with a sprayed and sintered P-layer and C-layer. The scale bar corresponds to 50 µm.

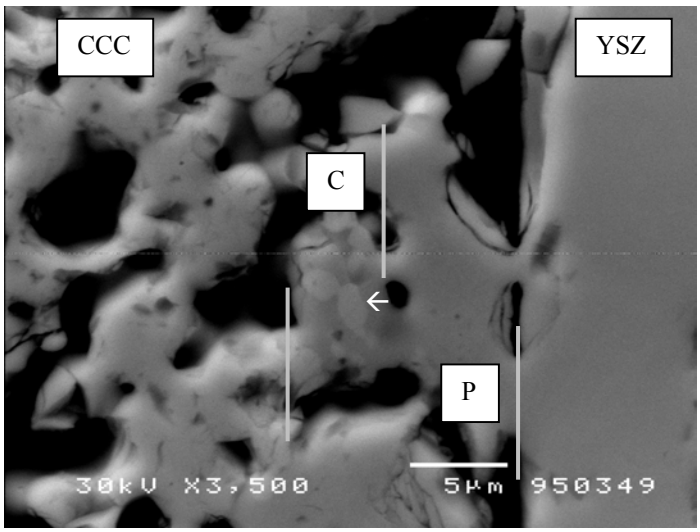

Fig. 3.15. SEM micrograph showing a cross section of an electrode with a P-layer (K311, series 2). The scale bar corresponds to 5 µm. The LSM phase is brighter than the YSZ phase, as the image is obtained with backscattered electrons. The arrow indicates an LSM grain.

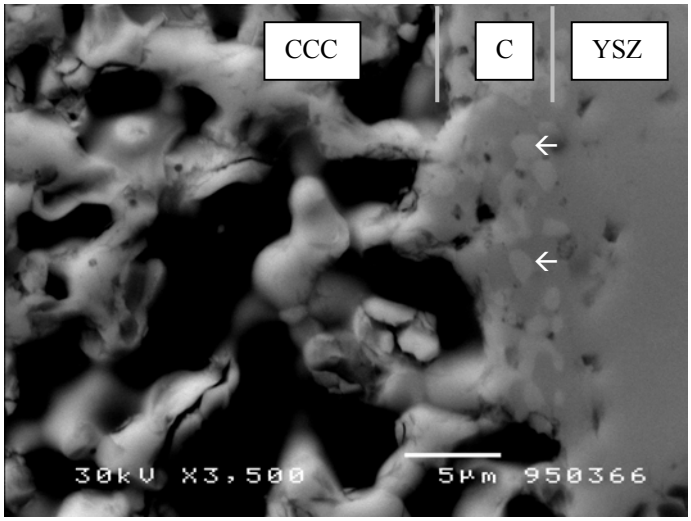

Fig. 3.16. SEM micrograph showing a cross section of an electrode without a P-layer (K320, series 2). The scale bar corresponds to 5 µm. The LSM phase is brighter than the YSZ phase, as the image is obtained with backscattered electrons. The arrows indicate some of the LSM grains.

In the C-layer YSZ tended to enclose the LSM particles (indicated by arrows in Fig. 3.16). Consequently, percolation through YSZ in the C-layer was more likely than percolation through LSM. Therefore, the density of active TPB was assumed to be relatively high near the interface between the C-layer and the CCC-layer. On samples with a P-layer the C-layer was broken into smaller islands rather than distributed in a continuous layer (Fig. 3.15). This formation of islands is expected to increase the contact area between the C-layer and the CCC-layer. The increased contact area in combination with the high density of TPB at this interface may explain the performance improvement observed at 700°C and 850°C by application of a P-layer.

Application of a P-layer does not improve the performance at 1000°C as observed at lower temperature. As discussed for series 1, this may be a consequence of an expansion of the reaction zone at high temperature.

3.3.3. Models

In order to estimate 1) the theoretical, active electrode thickness assuming percolation in all three phases through the C-layer and 2) the potential for electrode structure improvement, two simple models were used. The models were based on the assumption that performance of a composite cathode correlates directly to the active TPB and depends mainly upon the TPB density, percolation and series resistance in the composite.

Model 1

The model displayed in Fig. 3.17 was used to estimate the active thickness of a composite cathode limited by the ohmic resistance in the YSZ-fraction. A YSZ cylinder stretches from the electrolyte surface through the composite electrode to the current collecting layer. In the model the contact points between the cylinder and the LSM grains create active

TPB throughout the composite structure. The active thickness, t, of the composite structure was defined as the distance from the electrolyte where the polarisation resistance of one micrometer electrode, R_p^*, equals the ionic resistance, R_{ion}, in the YSZ cylinder, i.e.

$$R_p^* = R_{ion} \tag{3.2}$$

The resistances in equation (3.2) were defined as follows:

$$R_{ion} = \frac{R_{YSZ,spec}\, t}{A_{YSZ}} \tag{3.3}$$

$$R_p^* = \frac{R_{p,spec}}{L'_{TPB}} \tag{3.4}$$

where $R_{YSZ,spec.}$ is the specific resistance of YSZ, A_{YSZ} is the cross-sectional area of the cylinder, $R_{p,spec.}$ is the line-length specific reaction resistance of the TPB [Ωcm] and L'_{TPB} is the length of active TPB in one micrometer of the electrode. Equation (3.3) and (3.4) can be combined through (3.2), yielding the following expression for t:

$$t = \frac{R_{p,spec} A_{YSZ}}{R_{YSZ,spec} L'_{TPB}} \tag{3.5}$$

A cylinder diameter, $2r$, of 2 μm and a L'_{TPB} of πr μm were estimated from micrographs. The value $R_{p,spec}$ = 150 Ωcm is a rough estimate taken from Juhl et al. (1995). This value was measured with a point electrode, where the oxygen reduction reaction is assumed to occur along the perimeter of the contact area. Using a $R_{YSZ,spec.}$ of 10 Ωcm (Chiacchi et al., 1994) at 1000°C the model yields an active thickness t of 15 μm. This is in good agreement with the experimental findings.

Estimating t at other temperatures, apparent activation energies of -0.8 eV for $R_{YSZ,spec.}$ (Hohnke, et al. 1979) and –2 eV for $R_{p,spec.}$ (Kleitz et al., 1993) were considered appropriate. Using 15 μm at 1000°C as the reference value, the active thickness t was 60 μm at 850°C and 400 μm at 700°C.

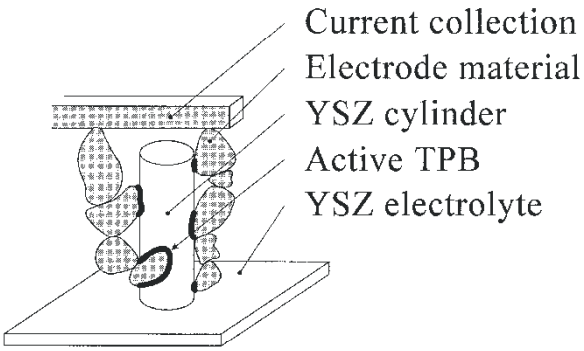

Fig. 3.17. Simple model illustrating the limitation of the active thickness of a composite electrode by the resistance in a YSZ cylinder.

The measured R_p values were apparently constant for C-layer thicknesses above 10 μm (Figs. 3.4 - 3.6). Compared with the calculations above this was not expected at 700°C and 850°C. One reason for this behaviour might be lack of electron and gas percolation paths through the entire C-layer thickness. Consequently, parameters other than ionic resistance in the YSZ phase could be limiting.

The observed insensitivity to structural changes at 1000°C compared to lower temperatures could, according to equation (3.5), be related to changes in the ratio between $R_{p,spec.}$ and $R_{YSZ,spec.}$ with temperature, due to different activation energies. Thus, the experimental findings may be explained qualitatively by a change of active thickness.

Model 2

To evaluate the performance which may be achieved for a composite cathode, a theoretical L_{TPB} in a mono-layer is calculated. An ideal-ordered mono-layer consisting of 1:1 LSM and YSZ is sketched in Fig. 3.18. A mono-layer with spheres of 2 μm is assumed to have 5/2 contacts per sphere, each with an ideal TPB length of 2 μm. This adds up to an area-specific triple phase boundary length, L^*_{TPB}, of $1.25 \cdot 10^4$ cm/cm^2 for the mono-layer. Using an analogy to equation (3.4) and maintaining $R_{p,spec.}$ yields an area specific polarisation

resistance, R_p, of 0.01 Ωcm^2 at 1000°C for the 2 μm mono-layer. Comparing this value to the best LSM/YSZ composite cathodes having R_p values of 0.1-0.14 Ωcm^2 for 3-6 μm thickness at 1000°C indicates a considerable potential for improving performance by controlling the structure.

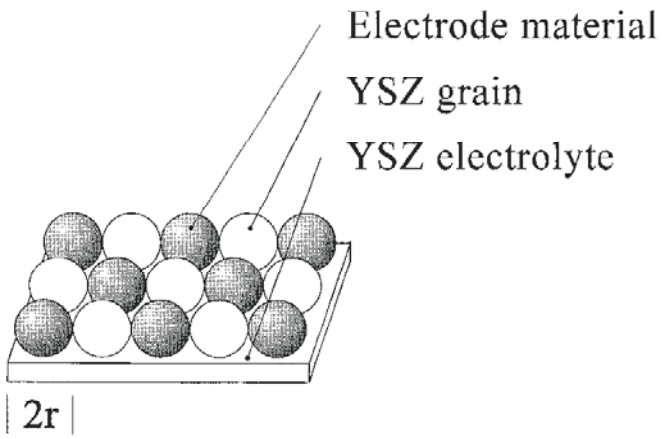

Fig. 3.18. Simple model illustrating the density of the triple phase boundary in an ordered composite consisting of a mono-layer of particles.

3.4. Conclusions

At low temperature (700°C and 850°C) increasing the composite cathode layer thickness had a positive effect on the electrode performance in the thickness range investigated. This implies that the bulk of the LSM/YSZ composite cathode is active for the oxygen reduction reaction. At 1000°C the polarisation resistance is less sensitive to thickness variations than at lower temperature.

Application of a porous layer of YSZ particles between the electrolyte and the composite cathode decreased the polarisation resistance at 700°C and 850°C, whereas no significant effect was observed at 1000°C. The particle layer is believed to extend the active triple phase boundary length locally at the interface between the composite cathode and the LSM current collecting layer.

The results suggest that with the materials and application method used, the largest potential for performance improvement by controlling the microstructure and thickness lies at temperatures well below 1000°C. Thus, these results can be utilised in relation to lowering the operation temperature of SOFCs.

Two simple models were used to estimate the theoretical active thickness and the minimum obtainable polarisation resistance. Although the two proposed models are simplified, they point out the potential in optimisation of electrode structure and thickness. The key to considerable improvement of the microstructure is to obtain a uniform blend of the three phases in the C-layer (LSM, YSZ and pores), leading to percolation of electrons, oxide ions and gas through the C-layer, since this will extend the active triple phase boundary line. Both the experimental and the theoretical part of the present work implies that large improvements in performance of composite electrodes are within reach.

3.5. Final Comments

The content of this chapter was published in 1996 (Juhl et al., 1996a). Since then several authors have reported results on similar subjects. Some of these are summarised in the following.

Murray et al. (1998) have investigated composite electrodes containing equal amounts by volume of $La_{0.8}Sr_{0.2}MnO_3$ and YSZ with 8 mol% Y_2O_3 with varying thickness up to 10 μm. A similar thickness dependence as reported in the present work was found, when measuring at 650-850°C. A minimum in polarisation resistance was not found for the thickness range investigated.

Fukunaga et al. (1996) have tested composite electrodes of $La_{0.81}Sr_{0.09}MnO_3$ and YSZ containing varying amounts of the two materials at 850°C. The effective thickness was

experimentally found to be less than 20 μm, and this result was confirmed by modelling. This is not contradicted by the results reported above, or by the results of Murray et al. (1998).

The effect of application of a layer of YSZ particles on the electrolyte surface and covering these particles with a thin layer (~80 nm) of LSM before application of an LSM current collector was studied by Herbstritt et al. (1999). The purpose of the YSZ layer is in essence the same as explained in the present work for the P-layer. An improved long term stability and a decrease in polarisation losses was found using this electrode structure. Thus, the improvements obtained when using a P-layer were confirmed.

In summary the results published after the results presented in this chapter confirm the findings and do not question any of the conclusions.

Chapter 4. Effect of Sintering Temperature on Microstructure and Performance[1]

4.1. Introduction

The performance of La(Sr,Ca)MnO_3/YSZ cathodes is sensitive to composition and processing (Chapter 3 and Mizusaki et al., 1988; Mizusaki et al., 1991; Kenjo et al., 1992; Østergård et al., 1995; Sasaki et al., 1996; van Heuveln et al., 1997a; van Heuveln, 1997b; Mitterdorfer et al., 1998). These parameters determine the length of the triple phase boundary (TPB) between electrode, electrolyte and gas. The TPBs are assumed to be the active sites with respect to the oxygen reduction proceeding in the electrode (Takahashi et al., 1969; Mizusaki et al., 1991; van Heuveln et al., 1997a).

The sintering conditions affect the microstructure, the adhesion of the electrode to the electrolyte and the reactivity between LSM and YSZ and are therefore important processing parameters. The sintering behaviour of LSM/YSZ cathodes and its effect on microstructure and performance is the subject of the present chapter.

In this work composite LSM/YSZ electrodes with a current collecting layer of LSM are investigated. Previously published work has indicated that the interface between the composite and the current collecting layer may affect the performance of LSM/YSZ composite electrodes (Chapter 3 and Murray et al., 1998, see also Chapter 5). Therefore, it is relevant to study the influence of the microstructure of both the composite and the current collecting layer on the electrode performance. For this purpose different combinations of sintering temperatures in the range of 1150°C-1300°C for the composite and the current collecting layer are used, and the effect on performance is investigated. The impedance of unsintered electrodes is measured as a function of increasing temperature in

[1]This chapter is based on: M.J. Jørgensen, S. Primdahl, C. Bagger and M. Mogensen, Accepted for publication in *Solid State Ionics* (2000b).

the range of 600-1050°C (in-situ sintering), in order to study the effect of lower sintering temperatures. The experimental techniques used for the investigations are electrochemical impedance spectroscopy and scanning electron microscopy.

4.2. Experimental

4.2.1. Sample Preparation and Test

Symmetrical two-electrode cells were used for this study. The geometry of the test cells is illustrated in Fig 2.2.

The C-layer consists of 50 weight% $(La_{0.75}Sr_{0.25})_{0.95}MnO_{3\pm\delta}$ and 50 weight% TZ8Y, and the two CCC-layers were made from of $(La_{0.75}Sr_{0.25})_{0.95}MnO_{3\pm\delta}$ and sintered separately.

The experiments were divided into two parts comprising electrodes sintered at varying temperatures and electrodes sintered in-situ, respectively.

Varying Sintering Temperature

The sintering temperature of the C-layer and the two CCC-layers was varied between 1150°C and 1300°C. Each layer was sintered for two hours before application of the next layer. The tested combinations of sintering temperatures are shown in Table 4.1. The table comprises results obtained for electrodes, where all layers were sintered at the same temperature (samples A - D), where the C-layer was sintered at 1300°C and the CCC-layers were sintered at 1250°C or 1200°C (samples E and F) and where the electrode layers were sintered using different combinations of 1200°C and 1300°C (samples G and H). The same powder processing procedure was used for all samples in Table 4.1, except that the CCC-layers of sample F contained a fraction of finer LSM particles than the other samples.

After the final sintering each sample was broken into test cells with an area of 0.2 - 0.5 cm^2. Pt-paste was painted on the electrode surfaces prior to test to ensure proper current collection. The current probe contacted the electrode in one point in the center of the electrode. Impedance measurements were performed at 1000°C in air at open circuit voltage (OCV). In addition the best sample with respect to polarisation resistance was tested at 850°C.

In-Situ Sintering

The C-layer and the two CCC-layers were applied with intermediate drying between the layers but without sintering. Test cells with areas of 0.18 cm^2 and 0.20 cm^2 were broken from the sample. The test cells were mounted between unsintered LSM foils made by tape casting. The foils were contacted by porous, sintered LSM pellets to ensure proper current collection. The electrodes were sintered in-situ during heating.

The test procedure was as follows. Impedance measurements were performed at 600°C, 700°C and 800°C. Thereafter, measurements were taken every 50°C up to 1050°C, which was the maximum temperature of the furnace. For test temperatures above 850°C an impedance measurement was first performed at the test temperature. Then the electrode was cooled to 850°C (reference temperature) and an impedance measurement was taken before the temperature was increased to the next level. The purpose of this was to investigate the development of the impedance at a given reference temperature as a function of the in-situ sintering temperature. The dwell time at each temperature was varying. The furnace temperature was changed twice a day and kept constant at the last temperature over night. The measurements were conducted in air at OCV.

4.2.2. Electrochemical Measurements

The measurements were carried out using an EG&G potentiostat/galvanostat model 273 combined with a frequency response analyser 1250 from Solartron. The measurements were performed at decreasing frequency from 65 kHz to 0.1 - 1 Hz. The amplitude applied over the cell was 14 mV RMS and 12 points per decade of frequency were measured.

4.2.3. Deconvolution of Impedance Spectra

For the electrodes sintered at varying temperature the summit frequency of the dominant arc in the impedance spectra was determined by the following method. The impedance data were deconvoluted by the software EQUIVCRT (Boukamp, 1986) using an equivalent circuit with two RQ-elements connected in series with an inductance, L, and a series resistance, R_s, which was mainly attributed to the electrolyte (see chapter 2 for further details). Here R is a resistance and Q is a constant phase element with the admittance $Y^* = Y_0(j\omega)^n$, where ω is the angular frequency and n is the frequency exponent. The summit frequency of the dominant arc was calculated using the formula $f_{max} = 1/(2\pi(RY_0)^{1/n})$ (Jacobsen et al., 1996).

4.2.4. Microstructural Investigations

The microstructure of a selection of the electrodes sintered at different temperatures was investigated using SEM. The instrument used was a low vacuum scanning electron microscope (Jeol LV5310). The electrolyte, C-layer and CCC-layer thicknesses stated in Table 4.1 are average values measured in 9, 10 - 20 and 6 random positions on the sample for the electrolyte and each of the two electrodes, respectively.

Table 4.1. Results obtained for electrodes sintered between 1150°C and 1300°C using different combinations of sintering temperatures for C-layer and CCC-layers. Measurement conditions: 1000°C, air and OCV.

ID	Sintering temperature, C-layer / °C	Sintering Temperature, CCC-layer 1 / °C	Sintering temperature, CCC-layer 2 / °C	Series resistance[1] R_s / Ωcm^2	Polarisation resistance R_p / Ωcm^2	Electrolyte thickness L_{elyt} / µm	C-layer thickness[2] L_C / µm	CCC-layer thickness[3] L_{CCC} / µm	L_{elyt}/R_s[4] σ_{app} / Scm^{-1}	Summit frequency[5] f_{max} / Hz
A	**1300**	**1300**	**1300**	**0.43**	**0.11**	**157**	**9**	**60**	**0.037**	**10**
B	**1250**	**1250**	**1250**	**0.36**	**0.07**	**145**	**13**	**15**	**0.040**	**48**
C	**1200**	**1200**	**1200**	**0.40**	**0.04**	**162**	**14**	**55**	**0.041**	**180**
D	**1150**	**1150**	**1150**	**0.17**	**0.03**	**149**	**13**	**80**	**0.088**	**337**
E	**1300**	**1250**	**1250**	**0.50**	**0.08**	**-**	**-**	**-**	**-**	**31**
F	**1300**	**1200**	**1200**	**0.18**	**0.05**	**160**	**4**	**70**	**0.089**	**103**
G	**1300**	**1200**	**1300**	**0.49**	**0.08**	**-**	**-**	**-**	**-**	**24**
H	**1200**	**1200**	**1300**	**0.48**	**0.07**	**147**	**10**	**85**	**0.031**	**22**

[1]Total series resistance, no division with two (see text). [2]Average thickness of the two electrodes in the symmetrical cell. [3]Average thickness of the CCC-layers on each side of the symmetrical cell. [4]Reference value: the specific conductivity of TZ8Y doped with Mn corresponding to 5 atomic percent of the cations is approximately σ_{YSZ} = 0.1 Scm^{-1} at 1000°C (Appel et al., 2000). [5]Summit frequency of the medium frequency arc (see text).

4.3. Results

4.3.1. Varying Sintering Temperature

The microstructure of the electrodes was strongly affected by the sintering temperature, as illustrated in Fig. 4.1 for electrodes sintered at temperatures between 1300°C and 1150°C (sample A - D, Table 4.1). The electrode having all layers sintered at 1300°C had an inhomogeneous pore size distribution (Fig. 4.1.a). Large areas in both the C-layer and the CCC-layers were sintered to high density. When decreasing the sintering temperature finer pores and smaller particles were observed in both the C-layer and the CCC-layers (Fig. 4.1.b - 4.1.d). The adhesion between the C-layer and the electrolyte in general seemed to be good for all the electrodes. The number of small pores at the C-layer/electrolyte interface was much larger for the electrode sintered at 1150°C (Fig. 4.1.d) compared to the electrode sintered at 1300°C (Fig. 4.1.a). Partial detachment of the composite layer was observed in the upper part of the micrograph in Fig. 4.1.d for the sample sintered at 1150°C. However, this was not observed on the opposite electrode on the sample.

Different combinations of sintering temperatures were used for the C-layer and the CCC-layers of the remaining samples in Table 4.1 (samples E - H). The C-layer seemed to have less fine pores, when sintered twice at 1200°C followed by 1300°C (Fig. 4.2.a), than when sintered at 1300°C followed by twice at 1200°C (Fig. 4.2.b). The CCC-layers of the electrode in Fig. 4.2.b contained finer powder than the CCC-layers in Fig. 4.2.a. This should not affect the sintering behaviour of the C-layer, but prevents direct comparison of the CCC-layer structure of the two electrodes.

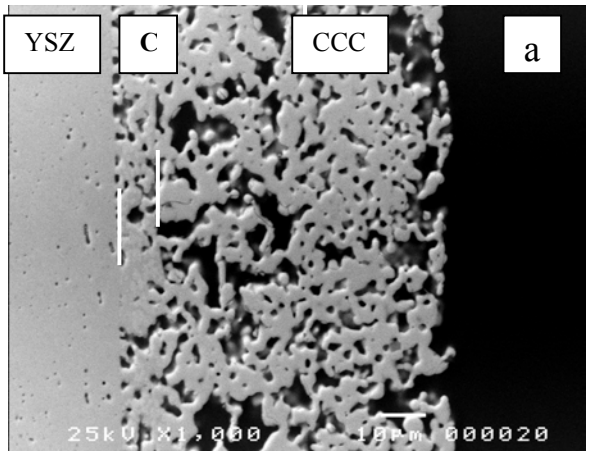

Sample A, Table 4.1, 3×1300°C

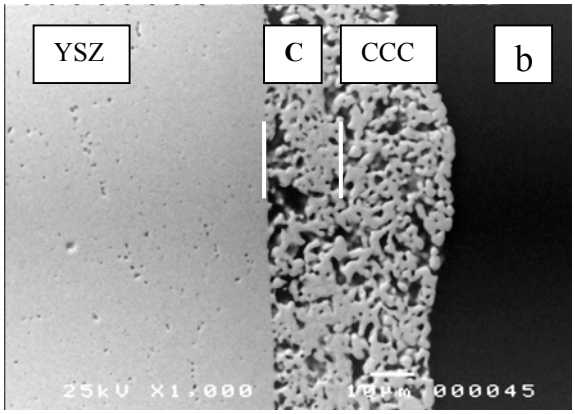

Sample B, Table 4.1, 3×1250°C

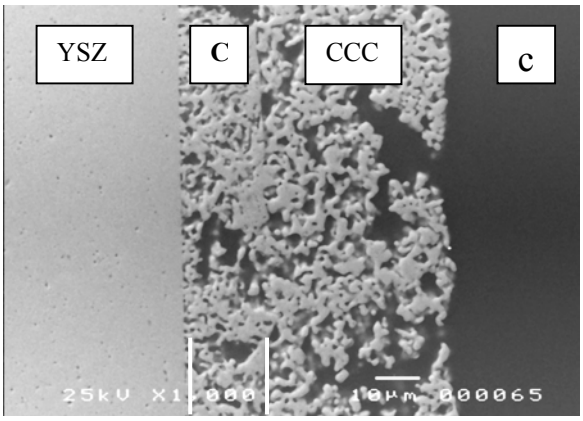

Sample C, Table 4.1, 3×1200°C

see following page

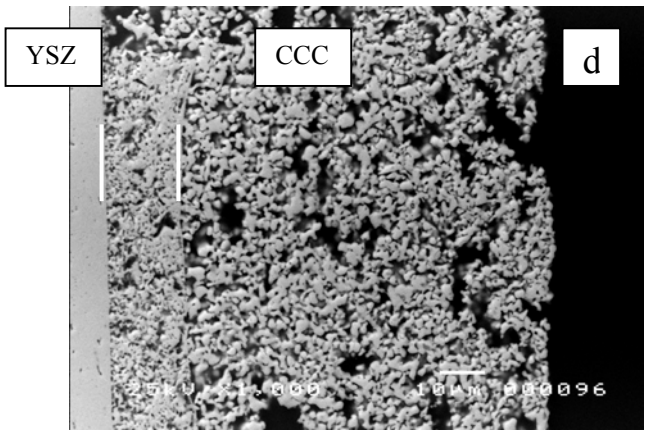

Sample D, Table 4.1, 3×1150°C

Fig. 4.1. Micrographs of electrodes having C-layer and CCC-layers sintered at the same temperature. The sample ID and the sintering conditions are stated below each micrograph. The scale bars correspond to 10 µm.

The variation in microstructure for the electrodes in Fig. 4.1 seemed reflected in the measured polarisation resistance, as illustrated for samples A - D in Table 4.1. Decreasing sintering temperature and thus less dense microstructure led to a decrease in the polarisation resistance, R_p. Also for the electrodes in Fig. 4.2, the sample with the less dense C-layer (sample F) had the lowest R_p.

R_p was not only affected by the sintering temperature (i.e. microstructure) of the C-layer. Samples E and F (Table 4.1) showed decreasing R_p with decreasing sintering temperature of the CCC-layers, when keeping the sintering temperature of the C-layer constant.

Fig. 4.3 shows impedance spectra for electrodes sintered at 1300°C and 1150°C, respectively. For the electrode sintered at 1150°C one dominant arc appears. For the electrode sintered at 1300°C a high frequency contribution was found in addition to the dominant low frequency arc. In the data obtained in the present work the high frequency arc appeared if at least one of the electrode layers was sintered above 1200°C.

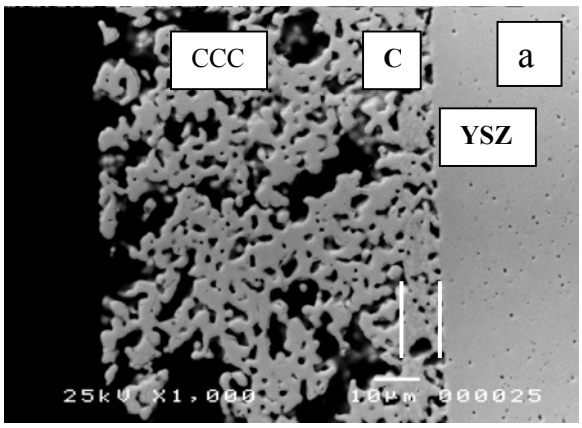

Sample H, Table 4.1, 2×1200°C + 1×1300°C

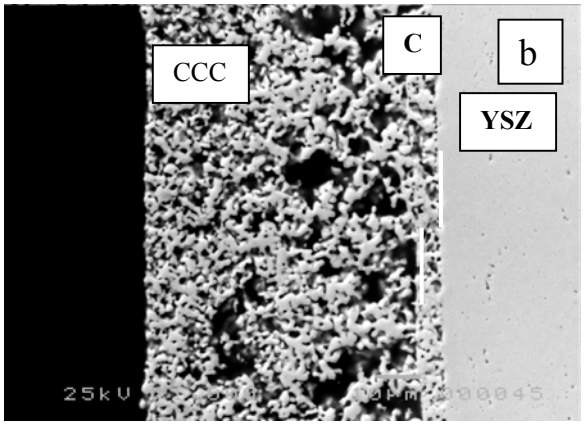

Sample F, Table 4.1, 1×1300°C + 2×1200°C

Fig. 4.2. Micrographs of electrodes sintered once at 1300°C and twice at 1200°C in different order. The sample ID and the sintering conditions are stated below each micrograph. The scale bars correspond to 10 µm.

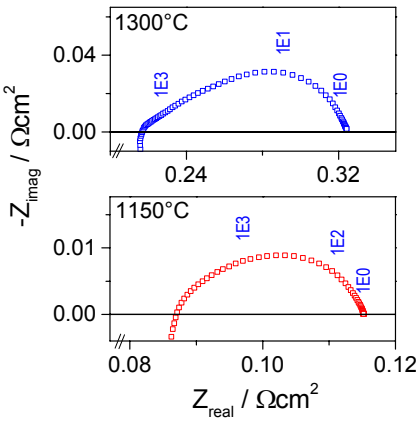

Fig. 4.3. Impedance spectra measured at OCV and 1000°C in air for electrodes fabricated with three sinterings at the temperature indicated in each spectrum. The numbers mark the frequency in Hz. Notice the different axis scaling.

The summit frequency of the dominant arc in the impedance spectra decreased with increasing sintering temperature, when all layers were sintered at the same temperature (Fig. 4.1 and samples A-D in Table 4.1). The summit frequency, and R_p, seems to depend more on the sintering temperature of the CCC-layers than on the sintering temperature of the C-layers (compare sample C, F and H).

The apparent electrolyte conductivity, σ_{app}, was determined from the measured series resistance, R_s, and the electrolyte thickness, L_{elyt}. σ_{app} was found to be closest to the reference value (conductivity of YSZ doped with Mn corresponding to 5 atomic percent of the cations (Appel et al., 2000)), when the electrodes were sintered at 1150°C (sample D, Table 4.1). The magnitude of σ_{app} was less than half of the reference value, when the electrodes were sintered at higher temperature (Table 4.1). σ_{app} was unexpectedly high for sample F in comparison with samples sintered at equally high temperatures.

The C-layer and CCC-layer thicknesses vary between 4 - 13 μm and 15 - 85 μm, respectively, for the samples in Table 4.1. The thickness variations of the C-layer do not seem to affect the trends observed for R_p with respect to sintering temperature. Neither is the CCC-layer thickness reflected in the magnitude of σ_{app}.

The electrode having the lowest R_p (sample D, Table 4.1) was also tested at 850°C, where R_p was found to be 0.12 Ωcm^2.

4.3.2. In-Situ Sintering

Two nominally identical electrochemical cells were sintered in-situ in this experiment. The cells behaved in a similar manner as a function of temperature. Bode plots of the impedance measured at intervals of 100°C between 600°C and 1000°C are shown in Fig. 4.4 for one sample. One dominant arc was observed at 600°C and 700°C. At higher sintering temperatures an additional arc appeared at low frequency. This arc was

independent of temperature. It is found that at 950°C the contributions from the two arcs were approximately equal, and at higher temperatures the low frequency arc dominated.

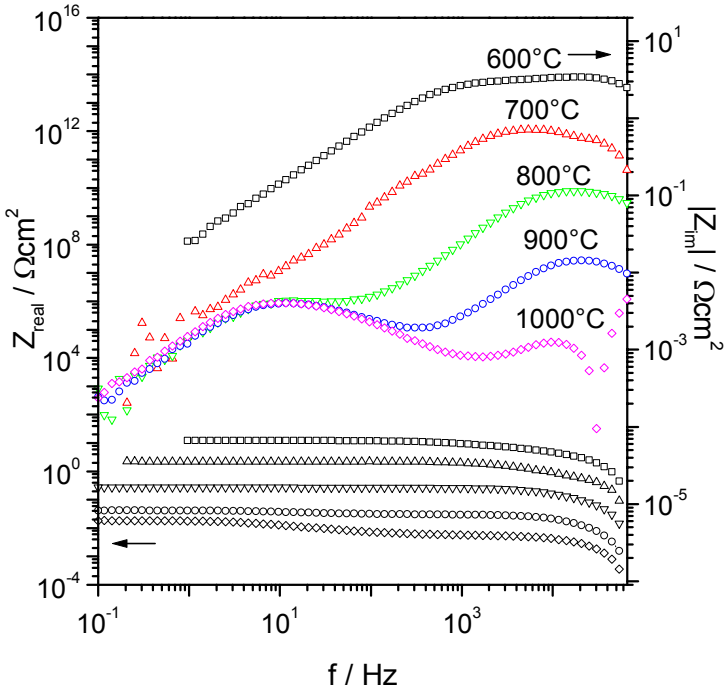

Fig. 4.4. Bode plot of impedance measurements taken at OCV in air for an electrode sintered in-situ. The real part is corrected with respect to the series resistance. The sintering/measurement temperature is indicated for each curve.

Arrhenius plots for R_p and R_s are shown in Fig. 4.5. For R_s the slope of the Arrhenius curve is fairly constant with an activation energy of approximately 0.9 eV. For R_p a distinct bending point is found around 950°C. The change in R_p with temperature is much lower above 950°C than below this temperature.

The measurements taken at the reference temperature, 850°C, are plotted in Fig. 4.6. The optimum sintering temperature with respect to R_p is 950-1000°C. When increasing the sintering temperature further to 1050°C a small increase in R_p is observed. However, R_s decreases continuously with increasing sintering temperature. The total resistance (R_p + R_s) is equal for 1000°C and 1050°C.

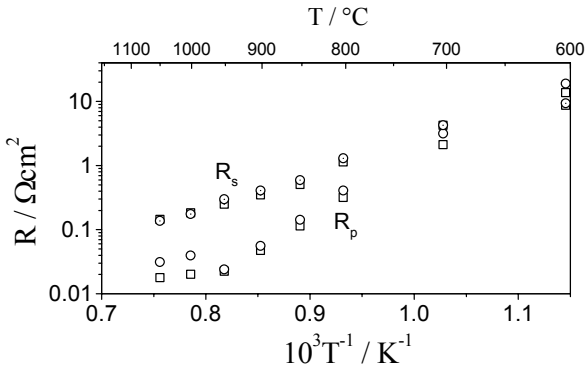

Fig. 4.5. Arrhenius plots of R_p (open symbols) and R_s (symbols with dot in center) against the inverse measurement temperature determined for electrodes during in-situ sintering. Measurement conditions: air, OCV.

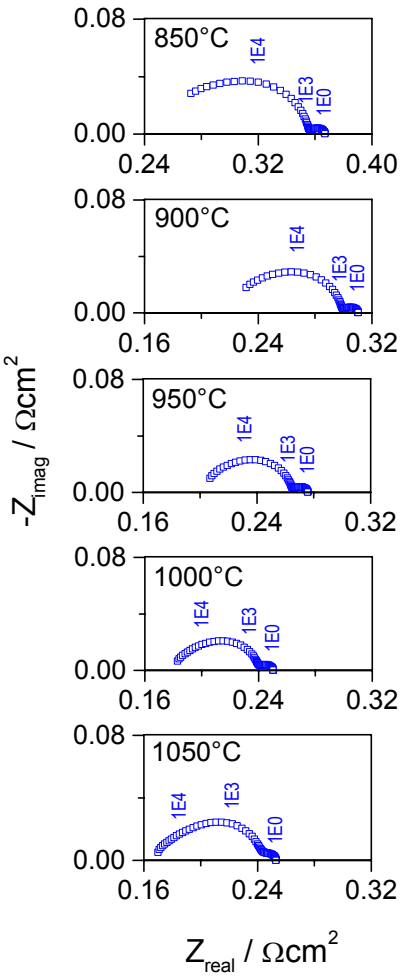

Fig. 4.6. Impedance measurements obtained at OCV and 850°C in air for the electrode in Fig. 4.4 after in-situ sintering at the temperature indicated in each spectrum. The numbers mark the frequency in Hz. Notice that the axis scaling of the upper spectrum differs from the others.

The impedance spectra in Fig. 4.6 comprise the same two arcs as reflected in Fig. 4.4, the high frequency arc, which is dominant, and the low frequency arc which is more or less independent of the sintering temperature. At the highest sintering temperatures (1000°C and 1050°C) high frequency distortion of the dominant arc appears. The summit frequency of the dominant arc decreases with increasing sintering temperature (Fig. 4.6), as also described for the electrodes sintered at various sintering temperatures.

4.4. Discussion

4.4.1. Interpretation of Impedance Measurements

In the data presented above three different arcs may appear in the impedance spectra. The high frequency arc is ascribed to transport of species within the composite structure (Appendix A). The arc found at medium frequency often dominates the impedance. The summit frequency of this arc decreases with increasing sintering temperature of the CCC-layers. The low frequency arc, which is found to be insensitive to temperature changes, is ascribed to gas diffusion limitation. In the following these processes are denoted transport arc, medium frequency arc and diffusion arc, respectively. The impedance of LSM/YSZ composites and the nature of the processes related to the observed arcs are discussed in Chapter 7.

4.4.2. Varying Sintering Temperature

Only one sample of each type in Table 4.1 is tested. The correlation between R_p and the sintering temperature (i.e. microstructure) found in Table 4.1 is assumed to be a true effect, as it follows a clear trend. A further argument is that the summit frequency of the dominant arc also changes systematically with the sintering temperature.

The thickness of the C-layer should be taken into account when interpreting the results in Table 4.1, as R_p has previously been found to decrease with increasing thickness (Chapter 3). However, considering the C-layer thickness, when evaluating the correlation between R_p and sintering temperature, does not change any of the trends described in the result section (section 4.3.1).

For all the electrodes the medium frequency arc dominates the impedance spectra. The observed change in summit frequency of this arc with sintering temperature has been reported elsewhere (van Heuveln et al., 1997b; Mitterdorfer et al., 1998; Holtappels et al., 1998). When the electrodes are sintered at least once at temperatures above 1200°C the transport arc appears at high frequency (Fig. 4.3).

The electrode microstructure and R_p are found to correlate. High porosity and small particles in the C-layer, i.e. long TPB length, results in low R_p-values. This trend is supported by literature findings (Mizusaki et al., 1991; Sasaki et al., 1996; van Heuveln et al., 1997a; van Heuveln et al., 1997b; Mitterdorfer et al., 1998). Also, the microstructure of the CCC-layers is important with respect to the oxygen reduction reaction (sample E and F, Table 4.1). The sintering conditions of the CCC-layers affect the microstructure and thus R_p. If the CCC-layers are sintered at the same sintering temperature as the C-layer or higher, the C-layer microstructure may densify during sintering of the CCC-layers. This is not the case if the CCC-layers are sintered at lower temperature than the C-layer. Therefore, the order of the sinterings is reflected in the microstructure (Fig. 4.2).

The effect of microstructure is also reflected in the apparent electrolyte conductivity, which is closest to the conductivity of YSZ doped with Mn corresponding to 5 atomic percent of the cations, when the sample is sintered at 1150°C. The observed variations in σ_{app} are not considered to be an effect of differences in the quality of the current collection, as no correlation between the thickness of the CCC-layers and σ_{app} are found (Table 4.1). Pt paste is applied on the upper CCC-layer to improve the current

collection. It is attempted to keep the thickness of the Pt layer constant, thus the differences in σ_{app} are assumed not to be related to the thickness of this layer. The origin of the variations in σ_{app} is assumed to be differences in the C-layer microstructure, as discussed in the following.

As discussed in Chapter 3, micrographs of this type of composite electrode sintered at 1300°C suggest that the LSM particles in the C-layer are more or less enclosed in a dense YSZ matrix (see Fig. 3.8). Thus, the occurrence of active TPB in the composite phase is diminished when the electrode is sintered at high temperature. Thereby, the C-layer interfaces become relatively more important with respect to oxygen reduction as the sintering temperature is increased. If the C-layer becomes so dense that gas access to the C-layer/electrolyte interface is limited, the C-layer/CCC-layer interface becomes the primary source of active sites. In this case the oxide ions generated have to be transported from the active sites through the bulk of the C-layer to the electrolyte. This will add noticeably to the ohmic resistance, and may contribute to the experimental findings with respect to σ_{app}. The transport arc is only observed at sintering temperatures above 1200°C, suggesting that transport of species through the bulk of the C-layer is not a relevant process for electrodes sintered at low temperature.

A relatively high σ_{app} is observed for sample F (Table 4.1) considering that the C-layer is sintered at 1300°C. However, this may be due to the low C-layer thickness of this sample, as this should result in a relatively smaller increase in the ohmic resistance and thus σ_{app} should be high.

The fact that the electrode performance depends on the sintering conditions of the CCC-layers (Table 4.1) confirms that a significant part of the active sites are situated at the interface between the C-layer and the CCC-layers. The importance of this interface with respect to oxygen reduction is also reported elsewhere (Chapter 3, Chapter 5 and Murray et

al, 1998), where application of CCC-layers is found to affect the performance and the durability.

In summary the results indicate that TPB inside the composite layer and at the C-layer interfaces may be active with respect to oxygen reduction. For samples with a dense C-layer the interface between the C-layer and the CCC-layers becomes relatively more important.

Optimum performance is assumed to be obtained, where a long TPB length in the bulk of the composite in addition to many active sites at the C-layer interfaces are present. To obtain a microstructure with these properties, it appears to be advantageous to sinter at lower temperature, as suggested by the results of the in-situ sintering experiments.

4.4.3. In-Situ Sintering

In the in-situ sintering experiment the measurements performed at 850°C show a decrease in R_p with increasing sintering temperature until 950-1000°C (Fig. 4.6). This is interpreted as enhanced contact between grains (LSM-LSM, YSZ-YSZ and LSM-YSZ) in the electrode, which is assumed to lower the resistance for transfer of species across particle interfaces. When the temperature is increased to 1050°C an increase in R_p is found. This may be ascribed to enhanced sintering of the electrodes, which will lead to coarsening, loss of porosity and a decrease in the active TPB. This mechanism continues when the sintering temperature is increased, as R_p measured at 850°C for the sample sintered three times at 1150°C (sample D, Table 4.1) is higher (0.12 Ωcm^2) than observed for the sample in Fig. 4.6 sintered at 1050°C (0.09 Ωcm^2). Sasaki et al. (1996) also found a lower limit for R_p as a function of sintering temperature.

Mitterdorfer and Gauckler (1998) investigated the impedance of $La_{0.85}Sr_{0.15}Mn_{0.98}O_3$ electrodes during in-situ sintering and after sintering. A severe increase in the impedance was found after sintering. This was interpreted as an effect of

formation of low-conductive La-zirconate at the TPB during sintering. In the present work LSM containing excess Mn is used, as this composition suppresses the formation of La-zirconate (Clausen et al., 1994; Mitterdorfer et al., 1998).

When measuring at the reference temperature (850°C) R_s decreases with increasing sintering temperature (Fig. 4.6). This behaviour is ascribed to improved physical and electrical contact between the composite and the electrolyte and between LSM particles in the current collecting layer. This observation is in agreement with Sasaki et al. (1996), who found a decrease in R_s going from 1050°C to 1100°C. Thereafter, R_s was found to increase with increasing temperature as also found for the results in Table 4.1.

The total resistance ($R_s + R_p$) at 850°C is the same for sintering temperatures of 1000°C and 1050°C, as the increase in R_p, when going from 1000°C to 1050°C, is counterbalanced by a decrease in R_s (Fig. 4.6). If R_s could be lowered at 950°C and 1000°C, for instance by addition of sintering aids, which could improve the adhesion of the electrode to the electrolyte, the total resistance may be lowered.

The two observed arcs in the impedance spectra are the medium frequency arc and the gas diffusion arc, respectively. For measurements taken at the reference temperature (850°C) the transport arc becomes noticeable at high sintering temperatures (1000°C and 1050°C), as high frequency distortion of the medium frequency arc is observed (Fig. 4.6). For the data measured at increasing sintering temperature the gas diffusion arc is approximately equal to the medium frequency arc at 950°C (Fig. 4.4). Above this temperature gas diffusion, which is independent of temperature (Fig. 4.4 and 4.6), dominates the impedance. This explains the bend at 950°C in the Arrhenius plots for R_p (Fig. 4.5) and that R_p is almost independent of temperature above 950°C.

The diffusion arc does not seem to be affected by changes in porosity during in-situ sintering above 800°C (Fig. 4.4). This may suggest that the gas diffusion limitation is restricted to a volume outside the electrode structure (see Chapter 7). The current pick-up

system used consists of an LSM tape and an LSM pellet, which may cause the gas layer above the electrode to be stagnant. Therefore, the gas diffusion limitation may be changed by altering the current pick-up system and ensuring a high gas flow.

4.4.4. Final Remarks

The results emphasise that the microstructure and the performance of LSM/YSZ composite cathodes are strongly related. The results also illustrate the importance of the microstructure of the LSM current collecting layer. It is found that it may be advantageous to sinter the composite and the current collecting layer at different temperatures, to achieve desired microstructures.

A microstructure can be established in multiple different ways by varying for instance the powder fabrication technique, the powder processing and the sintering temperature. When optimising the sintering temperature for a given electrode composition both R_p and R_s must be taken into consideration. For R_s a certain sintering temperature is required to achieve good physical and electrical contact. However, if the sintering temperature is too high the electrode microstructure becomes coarse, which may lead to current constriction (Sasaki et al., 1996). With respect to R_p the optimum sintering temperature is where the TPB is at its maximum.

Densification of the electrode structure during extended operation has been reported in the literature (Tsukuda and Yamashita, 1994; Weber et al., 1996a; Weber et al., 1996b; see also Chapter 5). It is reasonable to assume that the electrodes sintered at low temperature are most likely to densify during operation, since the operation temperature is closest to the sintering temperature for these electrodes. Thus, it is necessary to include durability studies in the determination of the optimum sintering temperature for a given cathode.

4.5. Conclusions

The correlation between performance and microstructure of SOFC cathodes consisting of a composite LSM/YSZ layer and two current collecting layers of LSM sintered at different temperatures was studied in air at open circuit voltage. With decreasing sintering temperature in the range from 1300°C to 1150°C the electrode microstructure was found to be less dense and to contain smaller grains. This led to a longer triple phase boundary line in the composite structure, resulting in a decrease in polarisation resistance with decreasing sintering temperature.

Decreasing the sintering temperature of only the current collecting layers improved the performance, too. Thus, it may be advantageous to sinter the composite and the current collector at different temperatures, depending on the desired microstructures.

The triple phase boundary lines, which are active for reduction of oxygen, are situated in the bulk of the composite and at the composite interfaces with electrolyte and current collector. With increasing sintering temperature the composite/current collector interface is assumed to become more important, as gas access to the composite/electrolyte interface and to LSM/YSZ contacts in the composite structure may be obstructed if the composite structure becomes too dense.

With respect to the polarisation resistance measured at 850°C in air an in-situ sintering experiment showed an optimum value at sintering temperatures around 950 - 1000°C. However, when increasing the sintering temperature to 1050°C the increase in the polarisation resistance was counterbalanced by a decrease in the series resistance. The optimum sintering temperature, where both the polarisation resistance and the series resistance are low, is a trade off between good physical and electrical contact between LSM and YSZ and a long triple phase boundary line.

Chapter 5. Durability of LSM/YSZ Cathodes[1]

5.1. Introduction

As discussed in Chapter 3 and 4 the performance of LSM/YSZ composite cathodes depends on the microstructure. Therefore, microstructural changes during operation may change the performance considerably. Furthermore, the performance and degradation may depend on the formation of low-conductive reaction products such as lanthanum zirconate at the cathode-electrolyte interface during cell fabrication.

To increase the understanding of the degradation mechanism of SOFC composite cathodes it is relevant to investigate whether temperature, current load or kinetic processes are responsible for the degradation. In this chapter the degradation of SOFC cathodes operated at realistic conditions for up to 2000 hours was studied. Nominally identical cathodes, which were annealed at high temperature, but not exposed to current during the annealing period, were studied for comparison. The aim was to separate the effects of temperature and current on the degradation of the cathodes.

The study combines electrochemical methods with scanning electron microscopy (SEM) and energy dispersive x-ray spectrometry (EDS). Changes in electrochemical performance are compared with the changes in microstructure and composition of the cathode and the electrolyte.

[1]This chapter is based on: M.J. Jørgensen, P. Holtappels and C.C. Appel, Durability Test of SOFC Cathodes, *J. Appl. Electrochem.*, **30** (2000a) 413-420.

5.2. Experimental

5.2.1 Sample Preparation

The electrochemical test geometry is the three-electrode cell shown in Fig. 2.1.b. Two types of electrodes were tested; type A comprising a C-layer and type B comprising a C-layer and a CCC-layer.

The C-layer was made from a mixture of 60 weight percent LSM and 40 weight percent YSZ. The LSM material was $(La_{0.85}Sr_{0.15})_{0.9}MnO_{3\pm\delta}$ (nominal composition) and the YSZ fraction of the C-layer is TZ-3YB. The C-layer was sintered at 1300°C for 2 hours. After sintering the thickness of the C-layer was 5 - 20 μm.

On electrodes of type B a CCC-layer consisting of two layers of $(La_{0.85}Sr_{0.15})_{0.9}MnO_{3\pm\delta}$ (nominal composition) were applied on the sintered C-layer. The layers were sintered individually at 1300°C for 2 hours. The total thickness of the two layers was 15 - 30 μm after sintering.

On electrodes of both type A and B an unsintered tape cast LSM foil for current collection was applied on the working electrode immediately before the electrochemical test. A dense, channelled LSM pellet was pressed into contact with the LSM foil to ensure optimum current pick-up from the working electrode during the test (see Fig. 2.1.b).

The construction and the electrochemical treatment of the electrodes are shown in Table 1 together with an ID code for each type of treatment. In the following the ID codes A or B have the subscript “galv” (for instance A_{galv}), when a galvanostatic durability test is performed, whereas no subscript is used for the electrodes in the non-loaded durability test. The subscript “ref.” is used for reference samples, which were produced in parallel with the other samples and used only for structural analysis.

Table 5.1. Description of the electrodes tested

ID	Construction	Durability test	Aim
A	**C + tape**	**0 $mAcm^{-2}$**	**Determine effect of temperature. Compare with $A_{ref.}$, A_{galv} and B.**
A_{galv}	**C + tape**	**-300 $mAcm^{-2}$**	**Determine effect of temperature and current. Compare with $A_{ref.}$, A and B_{galv}.**
$A_{ref.}$	**C + tape**	**No test**	**Reference used for structural analysis. Not tested electrochemically.**
B	**C + CCC + tape**	**0 $mAcm^{-2}$**	**Determine effect of temperature. Compare with A and $B_{ref.}$, B_{galv}.**
B_{galv}	**C + CCC + tape**	**-300 $mAcm^{-2}$**	**Determine effect of temperature and current. Compare with A_{galv} and $B_{ref.}$, B.**
$B_{ref.}$	**C + CCC + tape**	**No test**	**Reference used for structural analysis. Not tested electrochemically.**

5.2.2. Electrochemical Test

The test procedure used for the different types of electrodes is shown in the flow chart in Fig. 5.1. The durability tests were performed as follows. Impedance measurements at open circuit voltage (OCV) and under four fixed cathodic polarisations were performed at 850°C, 950°C and 1000°C in air before and after the durability test. The impedance measurements were performed after an equilibration period of 15 minutes at each potential. The durability test at 1000°C in air was performed with or without a galvanostatic load of -300 $mAcm^{-2}$ up to 2000 hours.

The measurements were carried out using different combinations of instruments from Solartron (1260 + 1287, 1250 + 1286 or 1280). The maximum frequency used in the impedance measurements varied with the used frequency response analyser (20 - 65 kHz). The lowest measuring frequency was 5 mHz for the first OCV measurement and 50 mHz

for all other impedance measurements. The amplitude applied between the working and the reference electrode was 14 mV RMS and 6 points per decade were measured.

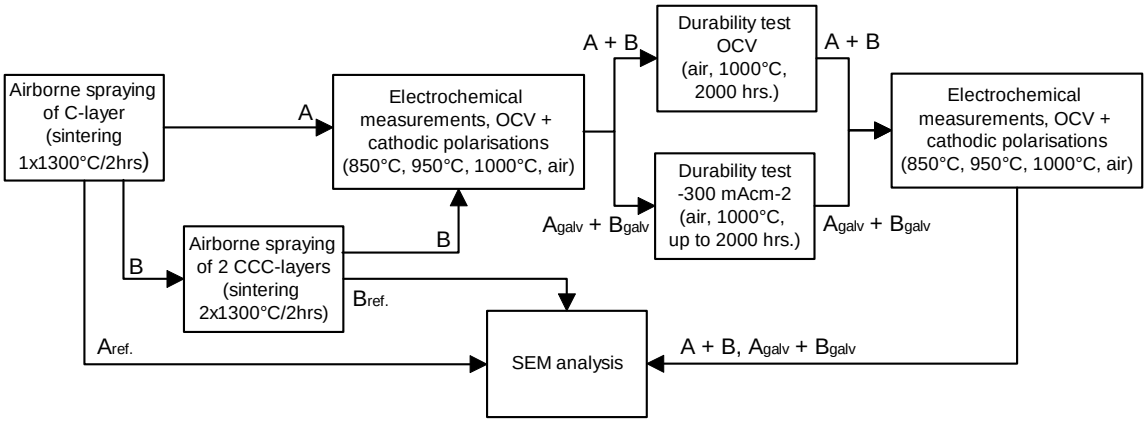

Fig. 5.1. Flow chart showing the sample preparation and test. The electrode type (A or B) is marked in the flow chart.

During the galvanostatic durability test a constant current of -300 $mAcm^{-2}$ was applied between the working and the counter electrode. The voltage drop at each cathode was measured between the reference electrode and a potential probe connected to the working electrode (four-wire, three-electrode set-up). Impedance measurements were performed approximately every 200 hours at the actual measured potential. The current was supplied by a Danica TPS 20 constant current supply. The voltage difference between the working and the reference electrode was measured by a Fluke multimeter.

In the unloaded durability tests the samples were placed in a separate furnace for two periods of 1000 hours at 1000°C. The electrode performance was measured before and after each heat treatment (see Fig. 5.1).

5.2.3. SEM Investigations

The samples were examined by scanning electron microscopy (SEM) (JEOL LV5310). X-ray element mapping was performed on a Philips XL40 SEM with a Noran Vantage EDS system.

5.3. Results

5.3.1. Durability Test

Current-overvoltage curves measured at 1000°C for electrodes of type A and B before and after the durability test are shown in Figs. 5.2.a and 5.2.b, respectively. The ohmic resistance, R_S, which was used for correction for the ohmic drop of the electrolyte substrate, was obtained from impedance data using the EQUIVCRT program (Boukamp, 1986). The current-overvoltage curves are assumed to be linear at low overvoltages, i.e. the slope of the curve corresponds to the inverse DC resistance.

According to Fig. 5.2.a almost no degradation is found after the unloaded durability test (type A), while the electrodes degrade considerably during the galvanostatic durability test (type A_{galv}). Similar results were obtained for electrodes of type B and B_{galv}, respectively (Fig. 5.2.b). The same difference between the degradation of the electrodes in the galvanostatic and the unloaded test, respectively, is found at 850°C.

Fig. 5.3 shows the change in overvoltage with time for electrodes of type A_{galv} and B_{galv} during the galvanostatic durability test. For three of the electrodes the degradation rate was smaller during the first 800 hours compared to the last 1000 hours (concave overvoltage-time curve). For the fourth electrode the degradation rate was constant within the tested period (linear overvoltage-time curve). After 2000 hours galvanostatic durability test the increase in overvoltage at 1000°C exceeded 100 % of the initial value for all the

electrodes. The increase in overvoltage with time is most severe for electrodes without a sintered CCC-layer (type A_{galv}) compared to electrodes with this layer (type B_{galv}).

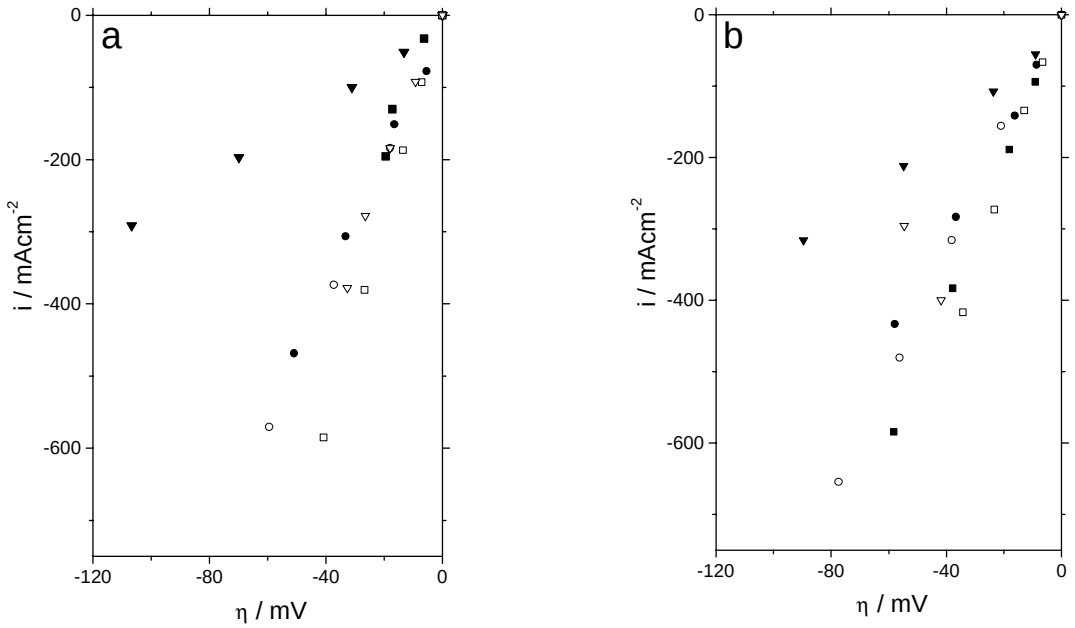

Fig. 5.2. Steady state current versus overvoltage curves. Measurement conditions: 1000°C, air. a) Type A: (○) *before test,* (□) *after 1000 hrs,* (∇) *after 2000 hrs. Type* A_{galv}*:* (●) *sample 1, before test,* (■) *sample 2, after 1000 hrs,* (▼) *sample 3, after 2000 hrs. b) Type B:* (○) *before test,* (□) *after 1000 hrs,* (∇) *after 2000 hrs. Type* B_{galv} (●) *sample 1, before test,* (■) *sample 1, after 1000 hrs,* (▼) *sample 2, after 2000 hrs.*

Examples of the time dependence of the ohmic resistance R_s, which is mainly ascribed to the electrolyte, are also plotted in Fig. 5.3. The increase in R_s with time is ascribed to a decrease in conductivity of the electrolyte pellet (Appel et al., 2000). The observed change in R_s is comparable with the degradation rate measured for YSZ (with 8 mol% Y_2O_3) slightly doped with Mn (Appel et al., 2000).

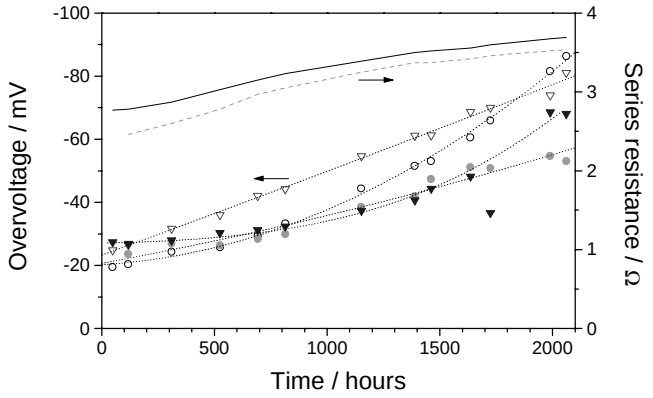

Fig. 5.3. Overpotential and series resistance versus time obtained in durability tests at 1000°C in air. Overvoltage: (○,∇) A_{galv}, (●,▼) B_{galv}. *Series resistance: solid line:* A_{galv}, *dashed line:* B_{galv}..

Impedance spectra measured at OCV before and after the galvanostatic durability test on an electrode of type A_{galv} are shown in Fig. 5.4. The initial impedance (Fig. 5.4.a) applied well to the model presented by Holtappels et al. (1998). After the durability test the impedance was changed considerably at both high and low frequencies (Fig. 5.4.6). This is discussed further in Chapter 7.

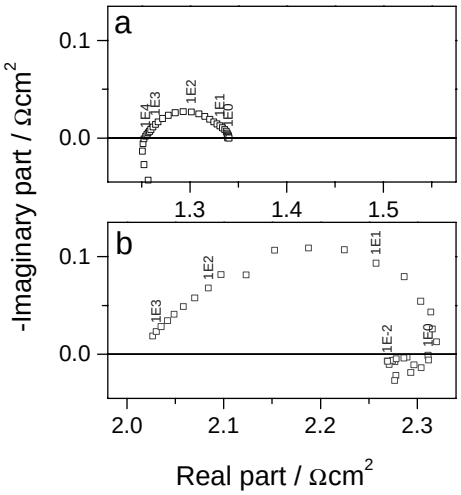

Fig. 5.4. Impedance spectra taken at open circuit voltage a) before and b) after current loaded durability test (-300 mAcm^{-2} for 2000 hours) for an electrode without CCC-layer (type A_{galv}*). Measurement conditions: 1000°C, air.*

5.3.2. SEM Investigations

Six types of electrodes were investigated using SEM, reference samples ($A_{ref.}$ and $B_{ref.}$), electrodes subjected to non-loaded durability test (A and B), and electrodes tested galvanostatically (A_{galv} and B_{galv}). A number of micrographs taken systematically along the electrode-electrolyte interface were studied for each type of electrode. Along this interface for one particular electrode considerable variations in the microstructure and pore size distribution were found. Also variations in the thickness of the C-layer and CCC-layer across the interface were found. Due to these variations for each sample the microstructural results presented in the following only include trends where significant microstructural changes were observed after the durability test.

Micrographs with the same magnification for electrodes of type $A_{ref.}$, A, A_{galv} and $B_{ref.}$, B, B_{galv} are shown in Fig. 5.5 and Fig. 5.6, respectively. The micrographs of the reference electrodes in Figs. 5.5.a and 5.6.a show that the C-layers in general have very dense areas with a random distribution of 3 - 10 μm pores. The adhesion between the C-layer and the electrolyte is good. No obvious change in the C-layer microstructure seemed to occur during the non-loaded durability test (compare Fig. 5.5.a with 5.5.b and 5.6.a with 5.6.b) The microstructure of type A may have seemed more open after the non-loaded durability test (compare Figs. 5.5.a and 5.5.b). This is considered to be within the expected structural variation of the C-layer.

For the electrodes tested galvanostatically (type A_{galv} and B_{galv}) changes in the microstructure at the C-layer interfaces were found. This is illustrated in Figs. 5.5.c, 5.6.c and 5.6.d, where small pores (~1 μm) along the interfaces of the C-layer are visible. These pores were not found in the reference electrodes (Figs. 5.5.a and 5.6.a), nor in the electrodes tested without current load (Figs. 5.5.b and 5.6.b).

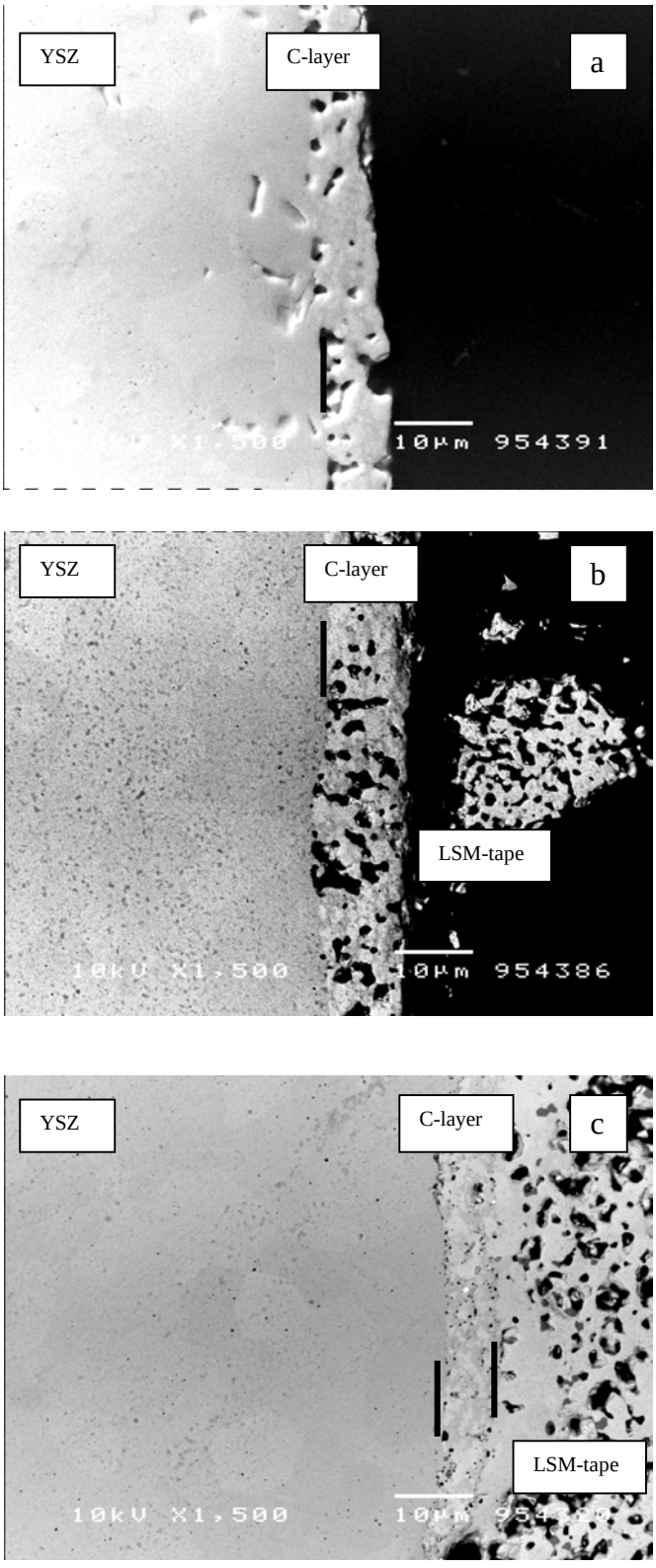

Fig. 5.5. Back-scattered electron images of electrodes without CCC-layers (type A) tested in air at 1000°C. a) reference sample (type $A_{ref.}$), b) after 2000 hours without current load (type A), c) after 2000 hours with current load (type A_{galv}).

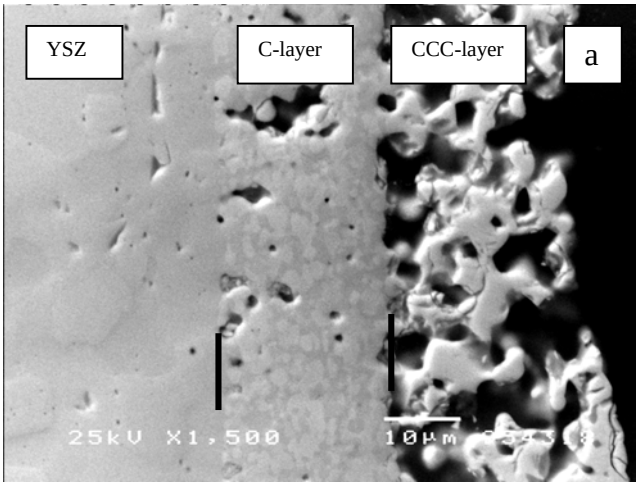

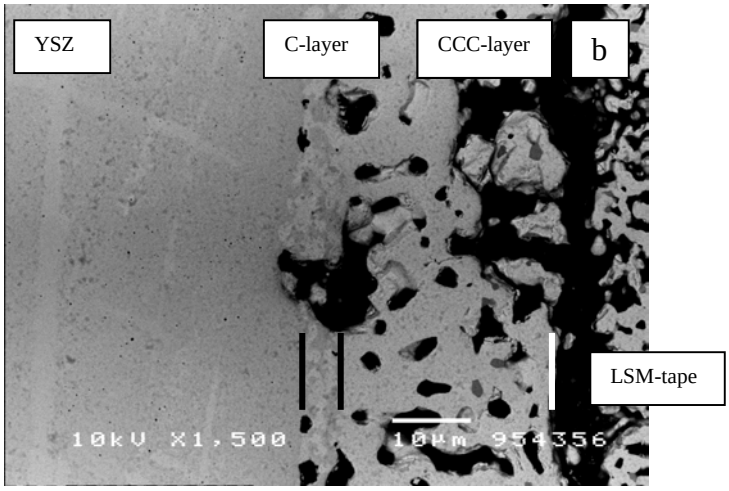

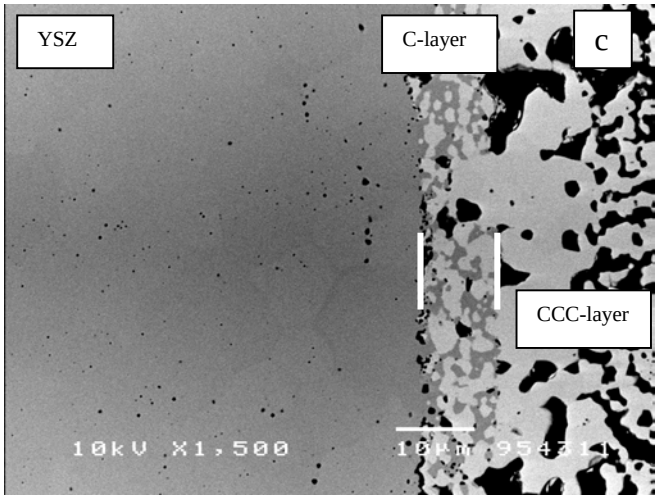

see following page

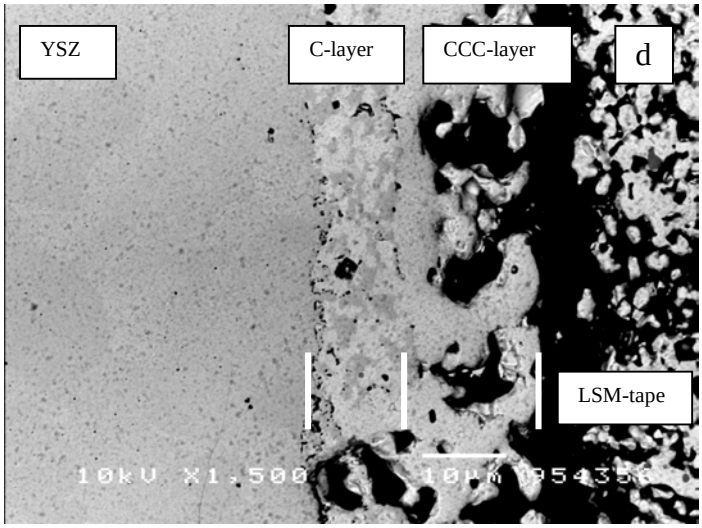

Fig. 5.6. Back-scattered electron images of electrodes with CCC-layers (type B) tested in air at 1000°C. a) reference sample (type $B_{ref.}$), b) after 2000 hours without current load (type B), c) after 1000 hours with current load (type B_{galv}), d) after 2000 hours with current load (type B_{galv}).

For electrodes with only a C-layer (type A_{galv}) the C-layer and the current collecting LSM-tape closest to the C-layer interface was found to be densified during the galvanostatic test (compare Figs. 5.6.a and 5.6.c). For electrodes including CCC-layer (type B_{galv}) the possible densification of the C-layer after 2000 hours galvanostatic durability test (Fig. 5.6.d) was not as pronounced as for type A_{galv}.

X-ray element mappings at the interface between the C-layer and the electrolyte were made for electrodes of type B and B_{galv}. In both cases the Mn concentration was found to be higher along the grain boundaries of the electrolyte material close to the interface than inside the electrolyte grains (Fig. 5.7). No difference in the Mn concentration at the grain boundaries was found for electrodes tested with and without current load (type B and B_{galv}).

Variations in the relative concentration of the elements in the C-layer-electrolyte interface were examined by EDS point analyses. This did not show formation of reaction

products such as La-zirconate. The white particles seen in the C-layer in Fig. 5.5.c were found to consist of Pt. Deposition of Pt in the electrode structure during operation is not likely, as there is no Pt in the vicinity of the electrode during the experiments. Therefore, Pt is assumed to be a contamination from the cutting and polishing process.

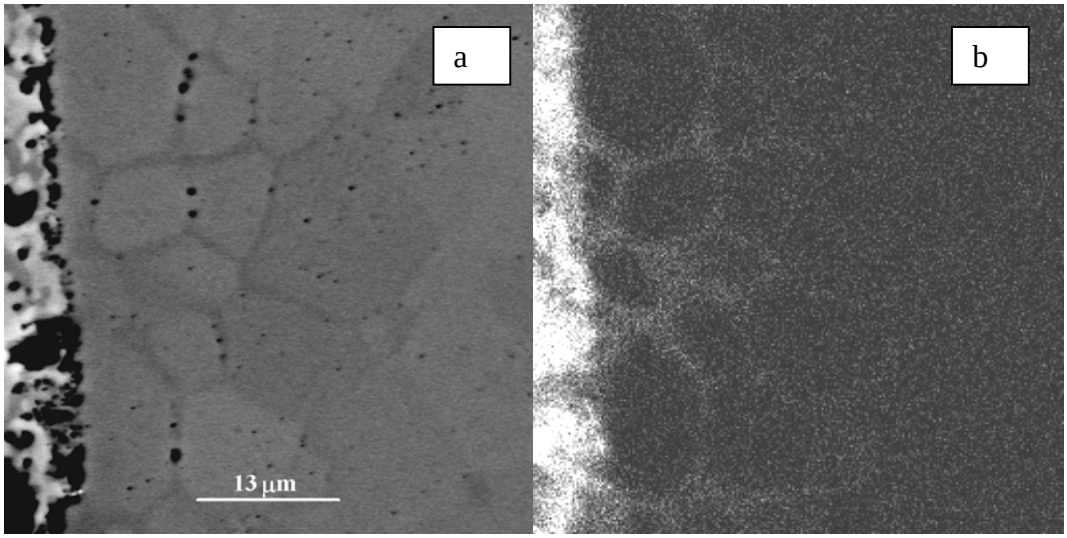

Fig. 5.7. a) Backscattered electron image of a cathode-electrolyte interface type B_{galv}. The grain boundaries in YSZ close to the interface are dark. b) X-ray map of Mn Kα. A higher concentration of Mn in the grain boundaries than in grains of YSZ is observed.

5.4. Discussion

The results of the unloaded durability tests (type A and B) showed that keeping the electrodes at OCV and 1000°C for 2000 hours does not cause considerable degradation. However, when current is passed through the electrodes at otherwise identical conditions the degradation is severe. Therefore, the current load of -300 $mAcm^{-2}$ rather than the operation temperature of 1000°C is responsible for the degradation.

In the following, emphasis will be put on the microstructural changes observed by SEM after the galvanostatic durability test. The results do not indicate formation of

reaction products such as La-zirconate or enhanced migration of cations from the C-layer to the electrolyte for galvanostatically tested electrodes. Therefore, the degradation is not considered to be related to these phenomena, and they will not be discussed further.

5.4.1. Microstructural Changes

Two types of microstructural changes were observed for galvanostatically tested electrodes; pore formation at the C-layer interfaces and densification of the C-layer and the current collecting tape on electrodes of type A_{galv}. These two phenomena will be treated separately in the following.

The observed pore formation at the C-layer interfaces may have caused a decrease in the length of active triple phase boundary (TPB) between electrode, electrolyte and gas phase, as the contact area between C-layer and electrolyte was decreased considerably (see for instance Fig. 5.6.c). As the polarisation resistance scales with the inverse of TPB length, the microstructural changes may be responsible for the observed increase in polarisation resistance during galvanostatic tests.

In electrodes of type A_{galv}, densification of the C-layer during galvanostatic durability testing (compare Figs. 5.5.a and 5.5.c) may have decreased the length of the TPB further, causing these electrodes to degrade more than electrodes of type B_{galv} (see Fig. 5.3). The densification is presumably related to sintering of the structure due to ohmic heating. Electrodes of type A_{galv} were more likely to sinter during the test, as they were only sintered once at 1300°C, while electrodes of type B_{galv} were sintered three times at these conditions (see Fig. 5.1).

The densification of the current collecting LSM-tape on electrodes of type A_{galv} during galvanostatic test (compare Figs. 5.5.a and 5.5.c) is ascribed to sintering of the tape-structure during current load, as this layer is unsintered at the beginning of the test. This densification may also decrease the electrode performance, as the interface between the C-

layer and the current collecting layer has previously been found to affect the electrode performance (see Chapter 3 and 4).

The pore formation observed after the galvanostatic durability test was a common feature for all the cathodes investigated. Since closed pores may contribute as extra capacitive contributions in the electrode impedance (Lauvstad, 1995), the appearance of an extra capacitive arc at high frequencies in Fig. 5.4.b supports the assumption that the pore formation was a major cause of the degradation of the electrochemical performance. In the following this feature is discussed in more detail.

Pore formation between LSM and YSZ induced by current load has also been found by Tsukuda and Yamashita (1994). They observed voids at the interface between LSM and YSZ grains in some samples after 18.5 hours testing at 0.5 Acm^{-2} at 1000°C. An increase in polarisation resistance due to the voids was not measured; on the contrary the performance improved. The reason for this might be that the pore formation was much less extensive than in the present work, probably due to the short test period.

Other authors have found microstructural changes at the interface between an electrode and a YSZ electrolyte after current load. Bay and Jacobsen (1997a and 1997b) found that the morphology of the interface between a Pt point electrode and a YSZ electrolyte changed during potentiostatic experiments at 1000°C. The changes were related to passage of current, as the material at the YSZ surface did not redistribute after annealing at 1000°C without current load (Bay and Jacobsen, 1997b). No explanations about possible driving forces for this severe mass transport were given.

Mass transport by so-called ‘kinetic demixing’ of multi-compound ceramic oxide materials due to electrotransport has been described in the literature (Yurek and Schmalzried, 1975; Monceau et al., 1994; Hong and Yoo, 1998; Yoo and Lee, 1998). When such materials are exposed to an electric field local thermodynamic equilibrium does not exist, causing the materials composition to change locally (Yurek and

Schmalzried, 1975). Hong and Yoo (1998) found that differences in both the diffusivity and the effective charge of the cations in a multi-compound ceramic oxide are responsible for the redistribution of the elements. Yoo and Lee (1998) warned that kinetic demixing could be relevant for SOFC materials such as YSZ and LSM.

When exposing a cation deficient oxide material to an oxygen potential gradient, cations can migrate towards the higher oxygen potential interface, while vacancies move in the opposite direction. This may lead to pore formation and pore movement (Yurek and Schmalzried, 1975). The pores will preferably form at the interface with the lowest oxygen potential in places where there is an indentation or a notch, as this part of the interface is unstable. The pores are transported towards the interface with the highest oxygen potential. This prediction seems also to be fulfilled in our studies, where the pores presumably are formed at the C-layer-electrolyte interface (low-potential interface) and transported towards the CCC-layer (see for instance Fig. 5.5.c). The applied current creates an oxygen potential difference across the C-layer and this difference may be the driving force of the pore formation.

From the above discussed results it is concluded that among other factors e.g. sintering properties of the cathode layers, the thermodynamic stability of the multi-component ceramic mixture under operating conditions turns out to be an important factor determining the long time performance of SOFC cathodes. However, the SEM resolution is too low to prove that redistribution of the cathode components occurs during galvanostatic testing, and measurement techniques with higher resolution should be used to confirm this. The composite nature of the cathode complicates matters, as the YSZ phase in the electrode might affect the expected demixing.

5.4.2. Impact on Fuel Cell Operation

The above mentioned theory about electrotransport phenomena suggests that the magnitude of the current load will affect the pore formation rate. This is confirmed by

comparison of the results obtained in the present work with results reported in the literature (Bagger et al., 1996). Cells comprising cathodes produced with the same materials compositions and manufacturing procedures as the cathodes in the present work have been tested for 2000 hours in a stack (Bagger et al., 2000). During the first 1100 hours the stack was operated at approximately 0.13 Acm^{-2}, after that the current load was varying. The degradation of the electrodes was considerably lower than what could be expected from the results reported above. For some cells essentially no degradation was found after 2000 hours of operation. No voids at the C-layer interfaces were found after the test (Appel, 2000). The reason for this is presumably that the stack was operated at a smaller current load/overvoltage than the electrodes tested in the present work.

The thermodynamic stability of LSM-YSZ composite cathodes may vary with parameters such as materials compositions and microstructure. Furthermore, the operating conditions (current load/overvoltage) may affect the long time performance, as illustrated by the example presented above. In order to secure a long lifetime for SOFC cathodes, it is crucial to explore the cause of the deterioration further and to find precautions against it. It is relevant to search for electrode compositions and microstructures, which are stable when exposed to current flow across the material.

In section 8.3.1 an experiment to verify the hypothesis about the degradation rate being dependent on the current density is suggested.

5.5. Conclusions

Composite LSM/YSZ electrodes tested without current load showed little or no degradation after 2000 hours at 1000°C in air. For electrodes tested galvanostatically at -300 $mAcm^{-2}$ and 1000°C in air an increase in overvoltage exceeding 100 % of the initial value was found after 2000 hours testing.

Characterisation of the electrodes by SEM showed that a large amount of sub-micron pores were formed close to the interfaces of the composite cathode layer for electrodes tested galvanostatically. No such structural changes were observed after the unloaded durability tests.

For electrodes without a sintered current collecting layer, densification of the composite layer and the LSM-tape occurred during galvanostatic testing.

The morphology change due to pore formation and densification of the composite layer for electrodes without a sintered current collecting layer were proposed as the main reasons for the increase in the polarisation resistance during galvanostatic durability tests, due to a decrease in the active triple phase boundary length.

The current load created an oxygen potential difference across the composite cathodes. This may lead to the observed pore formation and pore movement. Electrotransport of components in the LSM may lead to redistribution of the cathode material. The mechanisms of the structural changes needs further examination, in order to find precautions against the deterioration of the LSM containing cathodes.

Chapter 6. Evaluation of the Measurement Approach[1]

6.1. Introduction

As discussed in Chapters 3 - 5 the overall reaction rate of the oxygen reduction process proceeding in LSM/YSZ composite cathodes depends on the microstructure. In order to optimise the performance and durability of such cathodes a detailed understanding of the oxygen reduction mechanism is of interest. Electrochemical impedance spectroscopy (EIS) is considered to be a very suitable method for mechanistic studies (Mogensen et al., 1997). One approach to gain knowledge about the oxygen reduction mechanism is to study the effect of deliberate changes in for instance electrode thickness and microstructure on the impedance (Chapter 3 and 4, Appendix A; Østergård et al., 1995).

The composite electrodes examined here have a fairly low area-specific polarisation resistance. A three-electrode measurement cell must be carefully designed to give reliable measurement results with low errors (discussed in section 2.1). A critical parameter is the frequency stability of the equipotential lines in the electrolyte body at the point where the reference electrode is in contact. This requirement is relatively easy to handle for thick electrolyte cells (≥1 mm), but for thin electrolyte cells (~200 μm) the requirements for alignment of working and counter electrode are extreme (Winkler et al, 1998). On the other hand, the combination of high-performance electrodes and thick electrolytes renders measurements sensitive to phase errors in the characterisation equipment at high frequencies. Therefore, a symmetric two electrode cell on a thin (~180 μm) substrate is used for verification of measurements in the linear current-voltage regime around open circuit voltage (OCV).

[1]This chapter is based on: M.J. Jørgensen, S. Primdahl and M. Mogensen, Characterisation of Composite SOFC Cathodes using Impedance Spectroscopy, *Electrochimica Acta*, **44** (1999) 4195-4201.

For practical reasons the tested electrode areas are 0.2 – 0.5 cm^2. This results in a measured polarisation resistance in the order of only 250 mΩ at 1000°C, for three-electrode cells (Fig. 2.1). The electrode resistance is low compared with the series resistance of about 2 Ω. This implies a relative high uncertainty on the polarisation resistance.

This chapter describes some of the problems and limitations encountered during investigation of these electrodes. Parameters which are not directly related to the oxygen reduction process, but which can affect the measured impedance, are discussed.

6.2. Experimental

Three-electrode cells (Fig. 2.1.) and two-electrode cells (Fig. 2.2.) were tested. LSM powders with the nominal composition $(La_{1-x}Sr_x)_{0.9}MnO_{3\pm\delta}$, where x = 0.15 or 0.25 were used for fabrication of C-layer and CCC-layers. The YSZ component in the composite electrodes was TZ3YB. In electrodes with x = 0.15 a LSM to YSZ weight ratio of 3:2 was used, while this ratio was 1:1 for electrodes with x = 0.25. The cells were sintered at 1300°C for two hours after application of the C-layer and each CCC-layer.

The tests were performed in air at 850°C or 1000°C. Impedance measurements were carried out using a Solartron 1250 frequency response analyser with either an EG&G potentiostat/galvanostat model 273 or a Solartron 1286 electrochemical interface. Alternatively, a Solartron 1280 electrochemical measurement unit was used. The frequency range was typically from 65.5 kHz to 5 mHz and 20 kHz to 50 mHz, respectively, for Solartron 1250 and Solartron 1280. The voltage amplitude applied over the cell was 14 mV RMS and 6 points per decade were measured at decreasing frequency.

6.3. Results and Discussion

The results show how several parameters with no relation to the oxygen reduction process under investigation can influence the measurement results. These parameters must be identified and taken into consideration when interpreting the impedance of LSM/YSZ composite electrodes. Three topics are addressed. The first deals with contributions to the measured impedance introduced by the measurement equipment, whereas the second comprises electrode activation i.e. the effect of the previous electrochemical history. The third topic is sample reproducibility in combination with the impact of the test cell geometry on the measured impedance.

6.3.1. Equipment Induced Errors

A consequence of doing polarised measurements on high-performance electrodes is the inherent high dc current and thus a low sensitivity for the ac signal of interest. Ideally, the standard resistor on the electrochemical interface should always be selected to give maximum sensitivity at a given current range in the EIS measurement. If the measurements are performed with too small a standard resistor the dominant effect should in principle be a higher noise to signal ratio. Using too large a resistor will unfortunately not yield evidently invalid measurements, in practice systematic distortions in the high frequency part of the impedance spectra can appear. The distortion at high frequencies described below using too large standard resistors has been observed to be reproducible using a Solartron 1250 frequency response analyser both in combination with a PAR EG&G 273 and a Solartron 1286.

Fig. 6.1 shows an example of the influence of the standard resistor on the measured impedance of an LSM/YSZ composite cathode at 850°C in air. The spectra a and b were obtained in this order changing only the standard resistor from 100 Ω to 1 Ω. Measurements with a 10 Ω standard resistor recommended for the obtained 2 to 4 mA have

also been performed and are similar to data obtained with a 1 Ω standard resistor (Fig. 6.1.b). In the measurements shown in Fig. 6.1 data with little scatter (noise) were obtained. However, the shape of the spectra differed at high frequency. An imaginary error-range on data points at high frequency has been introduced in Figs. 6.1.a and 6.1.b (dotted lines) according to the specifications of the analyser phase angle error (Solartron, 1985). Within this error-range the high frequency tail of Fig. 6.1.a might well be described by a poorly defined arc with a real part of anywhere between 0.1 Ωcm^2 and 0.4 Ωcm^2, thereby arriving at a significantly higher polarisation resistance and somewhat lower series resistance than what is indicated by Fig. 6.1.b.

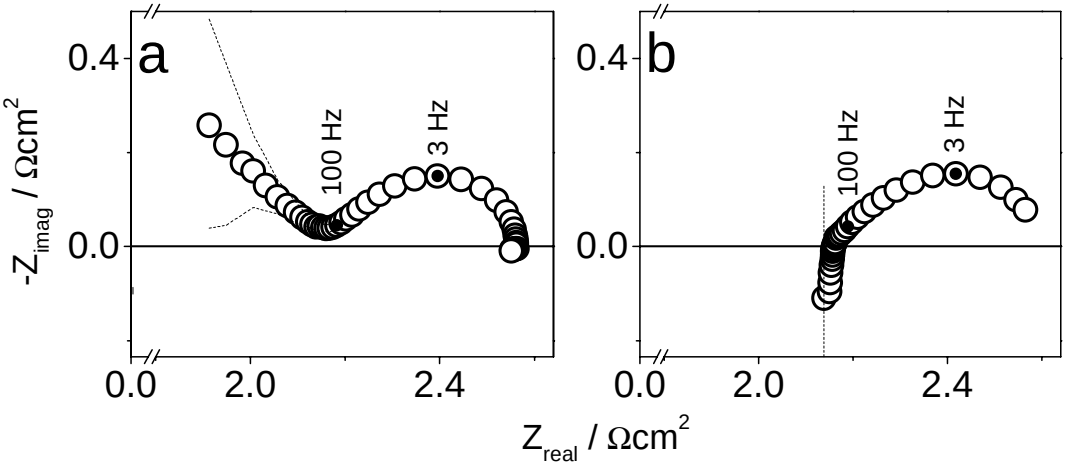

Fig. 6.1. Nyquist plot showing the influence of the standard resistor used on the electrochemical interface on the impedance of a composite $(La_{0.75}Sr_{0.25})_{0.9}MnO_{3\pm\delta}$/YSZ cathode. a: 100 Ω, b: 1 Ω. The dotted lines mark the maximum errors given by equipment specifications considering only the phase error. Sample geometry: pellet. Measurement conditions: 850°C, air, OCV.

Based on the impedance spectrum in Fig. 6.1.b, the high frequency tail of Fig. 6.1.a can be recognised as an artefact. It is therefore reasonable to correct the data in Fig. 6.1.a for the high frequency tail before fitting the data to an equivalent circuit. When fitting the data to the equivalent circuit shown in Fig. 6.2 (Appendix A) using EQUIVCRT

(Boukamp, 1986) high quality fits with relative errors below 1 % were obtained. Comparing the data extracted from Fig. 6.1.a and Fig. 6.1.b the deviation between the R_s-values was around 1.5 %, and the variation in the polarisation resistance ($R_p = R_{high} + R_{low}$) was 1 - 2 %. The largest variation in the resistances (up to 13 %) was found for R_{high}.

The conclusion of this example is that although the standard resistor affects the measured impedance, the total polarisation resistance may be determined with low error once the artefact has been recognised. However, in the detailed analysis larger errors are found in the high frequency part. Therefore, when examining electrodes having impedance characteristics with low phase angles it is recommended to pay particular attention to the current sensitivity of the chosen standard resistor.

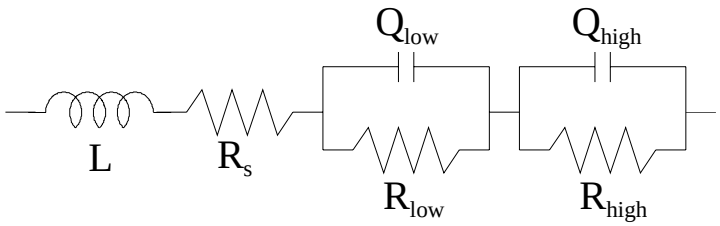

Fig. 6.2. The equivalent circuit used for fitting the data in Fig. 6.1. L is an inductance, R is a resistance and Q is a constant phase element. High and low refers to the frequency range.

6.3.2. Electrode Activation

For composite LSM/YSZ electrodes the previous electrochemical history can affect the measurement results. A composite cathode deposited on the pellet geometry was measured at 850°C in air. A series of impedance measurements were performed, first at OCV, then the electrode was polarised cathodically (-54 mA/cm^2) for 30 min, then anodically (54 mA/cm^2) for 30 min. After about 45 min of equilibration at OCV another measurement was taken at OCV. The two measurements at OCV are given in Fig. 6.3. After passing current the polarisation resistance at OCV was significantly lower than the initial value, i.e. the electrode was activated. The activation was reversible as the

polarisation resistance increased with time after interruption of the current. In another experiment made on the same electrode at a constant current density of -100 mA/cm^2 the stabilisation time under current load was established to be 10 hours.

It has been observed that nominally identical composite electrodes do not always have comparable performance at open circuit voltage in an initial measurement. Indeed, some electrodes have been found to exhibit no activation at all. This indicates that nominally identical electrodes treated the same way might not be at the same activated state at the start of a test sequence. McEvoy (1995) has recommended to handle this aspect of activation by defining an electrochemical treatment by which the minimum polarisation resistance of an electrode, i.e. a fully activated state, can be obtained. At Risø it has so far not been possible to determine a current treatment, which activates all electrodes fully, so that the same level of performance is reached after activation of electrodes prepared identically.

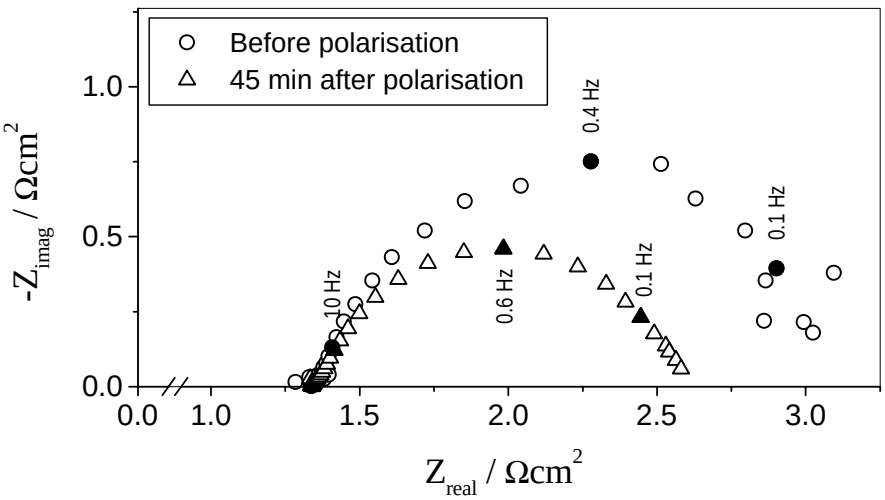

Fig. 6.3. Example showing how a composite $(La_{0.85}Sr_{0.15})_{0.9}MnO_{3\pm\delta}$/YSZ electrode can be activated due to current load. Sample geometry: pellet. Test conditions: 850°C, OCV, air.

The activation effect seems to be a common feature for LSM electrodes (McEvoy, 1994; Lee, 1995; Odgaard and Skou, 1996; van Heuveln and Bouwmeester, 1997b; Jiang et al., 1999). For instance, McEvoy has reported similar phenomena for porous electrodes of LSM (McEvoy, 1995). With point electrodes of LSM tested in contact with YSZ high time constants for equilibration have been observed (Juhl et al., 1995). Jacobsen et al. have observed similar phenomena using a $LaMnO_{3+\delta}$/YSZ system (Jacobsen et al., 1994). In potential sweeps inductive hysteresis was observed at cathodic conditions, i.e. the current at a given overpotential was higher when decreasing the overpotential compared to increasing it. At present the origin of the activation process is not clear. Understanding of the activation mechanism might be a fundamental step in understanding the oxygen reduction process for this type of electrode. This is discussed further in chapter 7.

The activation process of LSM based cathodes has two consequences. First of all the electrodes have to experience a polarisation and equilibration cycle in order to obtain comparable results. Secondly, once the electrode has been polarised it is activated for a considerable period of time due to the large time constants.

6.3.3. Reproducibility of Electrode Characterisation

The performance of a composite LSM/YSZ electrode reflects the sum of active TPBs in the particular electrode. As the characteristic particle size in the electrode is a few microns, the total number of active sites in the composite is expected to assure a statistically representative measurement for the electrode areas tested here (0.4 cm^2 and 0.25×2 cm^2, respectively), and reproducibility is expectable. Nevertheless, variations in both the polarisation resistance and the shape of the impedance plots were found for nominally identical electrodes.

Figs. 6.4 and 6.5 each shows the impedance of 8 nominally identical composite electrodes, produced on three-electrode pellets and on symmetrical cells, respectively. The

electrodes on pellets in Fig. 6.4 were sprayed together at the same time, aiming at producing as identical electrodes as possible. To optimise current collection a tape cast LSM foil was added to the sintered current collecting layers, and a dense LSM pellet with channels was pressed into contact with the foil during the measurements (Fig. 2.1.b). The symmetrical cells in Fig. 6.5 were all cut from the very same 45×45 mm^2 cell after sintering. The electrodes in Fig. 6.4 were investigated using a combination of a Solartron 1286 and Solartron 1250, while the data in Fig. 6.5 were obtained using a Solartron 1280.

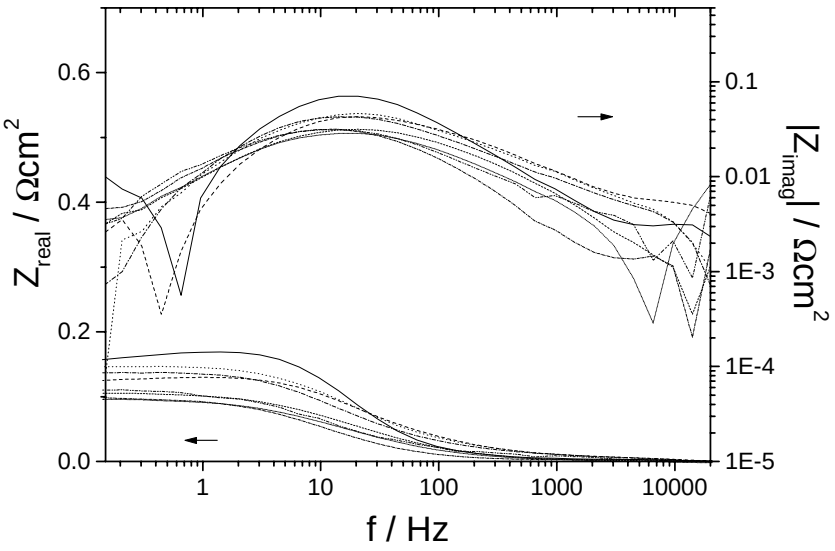

Fig. 6.4. Bode plot of 8 nominally identical composite $(La_{0.85}Sr_{0.15})_{0.9}MnO_{3\pm\delta}$/YSZ electrodes on pellets. An un-sintered LSM-tape and a dense, channeled LSM pellet were used as extra current collector (applied on two sprayed and sintered LSM-layers). The real part was normalised with respect to the series resistance. Measurement conditions: 1000°C, OCV, air.

For the electrodes on electrolyte pellets rather large scatter was observed, especially at frequencies below approximately 1 Hz and above 100 Hz (Fig. 6.4). The polarisation resistance varied between 0.10 and 0.17 Ωcm^2 and the summit frequency of the dominating arc was between 10 and 20 Hz. The variation in both real and imaginary

part of the impedance for the electrodes produced on electrolyte tape was somewhat smaller (Fig. 6.5). The polarisation resistance varied between 0.14 and 0.16 Ωcm^2 for seven of the cells and was 0.20 Ωcm^2 for the eighth. The summit frequency of the dominant arc was about 3 to 5 Hz. Overall, the reproducibility in polarisation resistance and frequency dependence for the electrodes characterised on pellets was not quite as good as what is obtained on symmetrical cells. At high frequencies close to the maximum range of the equipment (20 kHz) some scatter was observed for the symmetrical cells (Fig. 6.5). There might, however, be several reasons for the scatter.

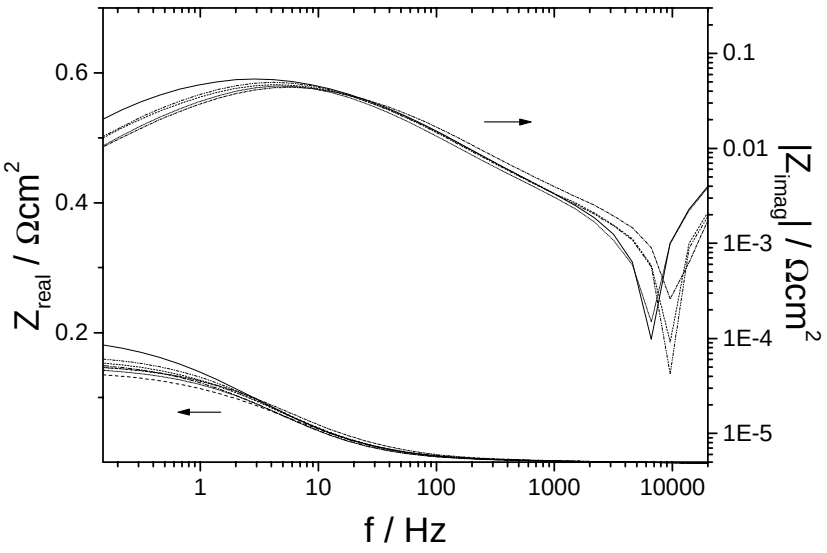

Fig. 6.5. Bode plot of 8 nominally identical symmetrical cells with composite $(La_{0.85}Sr_{0.15})_{0.9}MnO_{3\pm\delta}$/YSZ electrodes. The real part was normalised with respect to the series resistance. Measurement conditions: 1000°C, OCV, air.

At high frequency some of the scatter measured on pellets can be due to variations in the electrode thickness from sample to sample, as this parameter previously has been demonstrated to influence this part of the impedance (Appendix A). Due to the aerodynamic effects of the spraying mask used at the edge and due to the surface tension of the low viscous slurry, a certain difference in thickness and homogeneity at the rim of cathodes on pellets has been observed. Compared to this, cathodes on thin electrolyte

substrates are rather uniform in thickness and homogeneity, as they are cut from the centre of a substrate. Furthermore, it is assumed that it is easier to spray a uniform cathode on a substrate of 45×45 mm^2 than on a number of pellets placed next to each other.

The ratio between R_p and R_s is rather low in the case of the pellets (~0.1). The resulting low phase angle is sensitive to phase errors in the characterisation equipment, leading to poor resolution at high frequencies as the imaginary part approaches zero. This might explain the observed scatter. One way to increase the phase angle is to lower the electrolyte thickness considerably. This approach must be optimised against the trade off on frequency stability of the equipotential lines in the electrolyte where the reference potential is measured (Winkler et al., 1998). For the electrodes on symmetrical cells the ratio between R_p and R_s was significantly higher (~2), and higher phase angle was obtained.

In addition to the above discussed, other effects which might affect the impedance, can be considered. The current collector structure applied on top of electrodes is not necessarily perfectly reproducible. Even with the rather extreme precautions taken here to ensure optimum current collection, it has been observed that the electrode performance is sensitive to the quality of the current collection (Jørgensen et al., 1996-2000). Also the influence of gas access with respect to diffusion limitation has been demonstrated (see chapter 7).

6.3.4. Measurement Strategies and Possibilities

With both geometries one could argue that the electrode area should be decreased in order to enhance the signal from the working electrode. For the symmetrical cells it is difficult to handle smaller cells in practice due to the need for mounting current collectors. If the electrode area is decreased on the pellets before application of the electrode, the afore mentioned problems with inhomogeneities in the structure at the rim are expected to

escalate. An alternative could be cutting away the rim of the electrodes on pellets after sintering using a diamond tool. This would both decrease the sample area and minimise the rim effect.

At the moment the best compromise to obtain reliable measurements seems to be use of the two geometries in combination. In this way the symmetrical cells serve as a reliable development tool, whereas a higher number of pellets must be used for polarised studies with the option of verification of the impedance at OCV against the symmetrical cells.

The examples described previously show that the influence of parameters not related to the oxygen reduction process may be important to take into account when interpreting the impedance data obtained on composite cathodes. It appears essential to build up experience with the particular type of electrodes and measurement equipment, before a reliable analysis of obtained data can be successful. Furthermore, the investigated electrode characteristics (e.g. polarisation resistance) must exhibit variations, which are significantly larger than the effects of the undesirable phenomena discussed above, to be considered as true variations.

Despite the experimental difficulties and the overlapping processes in the impedance spectra, useful information about the oxygen reduction process has been gained using composite LSM/YSZ electrodes. For instance, the impedance measurements taken at 1000°C presented in this paper all have a dominating arc with a summit frequency in the range of 3 - 20 Hz. It has been proposed that this arc is related to a Gerischer type impedance, implying that a chemical reaction coupled with surface diffusion and charge transfer is one of the rate limitations (Holtappels et al., 1998). The high frequency arc, which appears clearly in some measurements, has previously been related to structure, as the resistance of this arc increased with increasing thickness of the composite (Appendix

A). At present a detailed correlation between this arc and the microstructure has not been found. The impedance of LSM/YSZ composite cathodes is discussed further in Chapter 7.

Apparently, a statistical evaluation is necessary, i.e. it takes a quite high number (~10 or more) of electrodes in order to characterise a given type of composite LSM/YSZ cathode.

6.4 Conclusions

Electrochemical impedance spectroscopy has been used to investigate composite LSM/YSZ cathodes for solid oxide fuel cells. Obtained impedance spectra on high-performance electrodes are found to be influenced by i) the equipment settings during test; ii) the previous electrochemical history of the specific cell; and iii) the geometry of the measurement cell.

The choice of standard resistor on the potentiostat was found to have an impact on the high frequency part of the impedance spectra, where an artefact tail can be introduced. This artefact can, when recognised, be corrected for and has hereafter little impact on the determination of the total polarisation resistance. However, in detailed analysis the high frequency part of the electrode response may be significantly affected.

Some composite YSZ/LSM electrodes were activated by passing current. The activation process was reversible. Time constants in the order of 10 hours have been observed. This implies a long equilibration time at the given conditions before reliable steady state measurements can be obtained.

Two measurement cell geometries were compared, symmetrical two-electrode cells with thin electrolyte (~180 μm) and three-electrode cells on electrolyte pellets with a distance of ~2 mm from the reference electrode to the working electrode. Symmetrical cells, which are only suitable for OCV measurements, indicated better reproducibility than

electrodes on pellets, especially at high frequency. The poorer reproducibility of data obtained on the pellets was partly ascribed to low phase angles due to the electrolyte resistance being high compared with the electrode resistance, and partly to variations in electrode structure due to rim effects introduced under production. The best compromise to obtain reliable results is to use the two cell geometries in combination.

Electrochemical impedance spectroscopy was found to be useful for investigating composite cathodes, although the data were not straight forward to interpret due to several overlapping processes and the influence of parameters not related to the oxygen reduction process. A substantial statistical evaluation is needed in order to gain confidence in the data and understand the parameters influencing the impedance of composite cathodes.

Chapter 7. The Impedance of LSM/YSZ Composite Cathodes[1]

7.1. Introduction

In the previous chapters LSM/YSZ composite cathodes were investigated using impedance spectroscopy. These chapters described determination of the series resistance and the polarisation resistance from the impedance data. However, important information about the oxygen reduction mechanism may be gained by interpreting these data further, as impedance spectroscopy allows separation of the various processes affecting the reaction rate. This chapter looks at the detailed interpretation of these data.

The impedance of a composite cathode is complex. In a Nyquist plot (minus imaginary part plotted against the real part) the impedance is composed of a number of more or less overlapping arcs each reflecting a physical or chemical process. These processes usually cannot be separated from a single impedance measurement. Therefore a number of impedance experiments must be carried out to distinguish all the involved processes. Further, the impedance is affected by many features, which are not all known. These features are not all directly related to the oxygen reduction process (Chapter 6). Therefore, it is necessary to perform many experiments varying parameters like temperature, oxygen partial pressure, overpotential and electrode geometry in order to interpret the impedance data using a simple physical or chemical model.

To make an unambiguous model describing the oxygen reduction kinetics in LSM/YSZ electrodes, the dependence of the electrode performance on composition, processing and electrochemical prehistory has to be included. The strategy followed in this

[1]This chapter is based on: M.J. Jørgensen and M. Mogensen, The Impedance of SOFC LSM/YSZ composite cathodes, submitted for *J. Electrochemical Soc.* (2000c).

chapter is to look for general features in a large number of data obtained for electrodes with different composition and processing.

In the following some literature regarding the impedance of the LSM/YSZ system is first summarised. Then, after an experimental section, examples of impedance spectra obtained for LSM/YSZ composite cathodes in this work are presented and the apparent number of processes affecting the impedance is determined. Finally, the characteristics of the processes found in this work are compared to literature, and the nature of each of the processes is suggested.

7.2. Literature Findings

In this section some literature concerning the LSM/YSZ electrode system is discussed. This will be used as background for interpreting the results obtained in this work.

Various authors have found different numbers of rate limiting processes for the LSM/YSZ system, and the nature of the individual processes is uncertain. Composite LSM/YSZ electrodes are of main interest for this study; however, results obtained for LSM point electrodes in contact with YSZ and for porous LSM electrodes applied on YSZ may help to reveal the oxygen reduction mechanism for the composite cathodes.

For the simplest possible LSM/YSZ system, namely a model system consisting of a pointed LSM electrode in contact with YSZ, one or two limiting processes can be found. Siebert et al. (1995) found that at OCV the oxygen reduction process was mainly limited by one process. The dependence on oxygen partial pressure was found to be $p_{O_2}^{-0.5}$, and an activation energy of 1.8 eV was found in air. At low anodic and cathodic polarisation, oxygen adsorption at the TPB was assumed to be rate limiting.

Odgaard and Skou (1996 and 1997) found two limiting processes for an LSM cone electrode in contact with YSZ. A charge transfer process was assumed at high frequency and a mass transfer process at lower frequency. It was found that the electrode could be activated by current passage, but not by changing the electrode potential by changing the oxygen partial pressure (Odgaard and Skou, 1997). The activation process was found to be reversible, and was ascribed to a broadening of the active reaction zone on the free YSZ surface along the triple phase boundary (TPB) between electrode, electrolyte and gas phase (Odgaard and Skou, 1996; Odgaard and Skou, 1997). According to Kleitz et al. (1993) this type of extension is expected to be smaller than 1 µm. By modelling on the basis of the constriction resistance in the electrolyte van Heuveln et al. (1997a) found the extension to be in the order of 0.03 - 0.07 µm. However, finite element modelling suggested the extension of the reaction zone to be as low as 0.1 - 1 nm (van Heuveln et al., 1997c). Oxygen exchange experiments indicate that the reaction zone is close to the TPB or spreads at the interface between LSM and YSZ (Horita et al., 2000). Adler et al. (1996) suggest that the extension of the reaction zone on the free electrode surface is small for LSM. Altogether this indicates that the extension of the reaction zone on LSM or YSZ is relatively small and therefore cannot solely account for the observed activation.

For an LSM point electrode in contact with YSZ Hammouche et al. (1991) found that at high cathodic overvoltages a different regime, where LSM has some ionic conductivity in addition to electronic conductivity, is entered. The infliction point above which significant ionic conductivity is obtained is approximately -0.5 V and -0.65 V for LSM doped with 25% and 15% Sr, respectively (Hammouche et al., 1991). As also discussed by Mogensen (1993) the ionic conductivity of LSM is assumed to be negligible in the present work as the test conditions are OCV or cathodic overvoltages far below the overvoltages stated above. Further, the self-diffusion constant for oxygen in LSM has been

found to be in the order of 10^{-13} cm^2/s at 900°C (Berenov et al., 1999), suggesting that self-diffusion of oxygen in LSM will not play an important role at the conditions studied here.

Youngblood et al. (1993) have investigated the oxygen reduction process at 900-1000°C using a roughened $La_{1-x}Sr_xMnO_{3\pm\delta}$ (x = 0.1 or 0.3) electrode in contact with a roughened YSZ surface. Two processes were found to be rate limiting. At high frequency charge transfer was suggested to be limiting, while oxygen dissociation was indicated to dominate the low frequency regime.

For porous $La(Sr,Ca)MnO_{3\pm\delta}$ electrodes on YSZ impedance spectra have revealed between one and three arcs (Østergård et al., 1993; Murray et al., 1998; Mizusaki et al., 1991; Mitterdorfer and Gauckler, 1998; Jiang et al., 1999; van Heuveln et al., 1997b). Murray et al. (1998) have investigated $La_{0.8}Sr_{0.2}MnO_3$ electrodes sintered on YSZ at 1100°C in the temperature range 550 - 850°C. One dominant arc was found. It had an activation energy of 1.6 eV, an oxygen partial pressure dependency of $p_{O_2}^{-0.14}$ and a summit frequency of 3 - 4 kHz at 850°C in air. This arc was ascribed to oxygen dissociation and adsorption. A low frequency arc, attributed to diffusion, was observed at high temperature and low p_{O_2}.

Mizusaki et al. (1991) have investigated $La_{0.6}Ca_{0.4}MnO_3$ electrodes in contact with YSZ and found that the impedance mainly consisted of one slightly depressed arc. The reaction rate was found to be proportional to the length of TPB, and the kinetics of the rate limiting process was assumed to be independent of the electrode microstructure. Oxygen atoms on the electrode surface were considered to contribute to the rate limiting process.

Østergård and Mogensen (1993) found three limiting processes at 1000°C when investigating $La_{0.85}Sr_{0.15}MnO_3$ cathodes sintered on YSZ at 1300°C. The medium frequency process was ascribed to dissociation of adsorbed oxygen molecules. Thus, a surface related process in correspondence with the references sited above. The high and low frequency arcs were tentatively suggested to be charge transfer of oxide ions from the

electrode/electrolyte interface to vacancies in the electrolyte and diffusion of oxide ions to the electrode/electrolyte interface, respectively.

Alteration of the interface between a porous LSM electrode and YSZ due to formation of reaction products and its influence on the electrode kinetics has been studied by Mitterdorfer and Gauckler (1998). It was thought that charge transfer, dissociation of adsorbed oxygen ions and surface diffusion of atomic oxygen may contribute to the impedance depending on electrode composition (LSM stoichiometry), preparation and measurement conditions.

Also Jiang et al. (1999) found that the impedance of a $La_{0.8}Sr_{0.2}MnO_3$ electrode in contact with YSZ could comprise up to three processes. The two contributions at the lowest frequencies were insignificant after a substantial cathodic current treatment, showing that some of the electrode processes change with current load. This behaviour was interpreted as the presence of a passive reaction layer formed during sample preparation preventing adsorption and dissociation of oxygen species on the electrode surface. The passive layer was assumed to dissolve as a consequence of current load.

The effect of current load was also investigated by van Heuveln et al. (1997b) on porous $La_{0.85}Sr_{0.15}MnO_{3\pm\delta}$ electrodes in contact with YSZ. Two processes, charge transfer (high frequencies) and diffusion of adsorbed O^- species along the LSM surface to the TPB (low frequencies), were suggested to limit the performance at moderate overpotentials. When passing a cathodic current through the electrode the performance was found to improve considerably, and the process was reversible. The performance improvement was mainly due to lowering of the low frequency contribution, and was therefore attributed to enhanced diffusion of oxygen intermediates.

The references cited above clearly show that discrepancies exists about the nature of the rate limiting steps of the oxygen reaction mechanism on porous LSM electrodes. When a composite structure is made by adding YSZ to the LSM electrode the impedance

becomes even more complex, as geometric effects related to the YSZ phase of the composite may contribute to the impedance (Appendix A; Murray et al., 1998). Juhl et al. (1996b, Appendix A) have studied the effect of thickness and microstructure of an $(La_{0.75}Sr_{0.25})_{0.9}MnO_3$/YSZ composite electrode on the impedance in the temperature range 700-1000°C. Two limiting processes were found. For the low frequency process an apparent activation energy of 2 eV was found (Appendix A), suggesting that this process is related to the rate limiting process found for LSM point electrodes (Siebert et al., 1995). For this process the resistance decreased with increasing composite thickness, presumably due to an increase in the number of active reaction sites per nominal electrode area. The process was attributed to a chemical elementary process in the overall oxygen reduction mechanism. The high frequency resistance increased with increasing composite thickness and was strongly dependent on microstructure. This process was ascribed to transport phenomena in the composite layer rather than an elementary process in the overall oxygen reduction mechanism.

For composite LSM/YSZ electrodes Murray et al. (1998) found a high frequency arc in addition to the one or two limiting processes found for porous LSM electrodes. The high frequency contribution, which had an activation energy of approximately 1 eV and no oxygen partial pressure dependence, was ascribed to YSZ grain boundary resistance in the electrode. The thickness dependence of the composite electrode performance was in agreement with the findings of Juhl et al. (1996a).

One or two rate limiting processes depending on the measurement conditions have been reported by Holtappels et al. (1998 and 2000a) for $(La_{0.85}Sr_{0.15})_{0.9}MnO_{3\pm\delta}$/YSZ composite electrodes sintered at temperatures between 1100°C to 1300°C. At 850°C the impedance mainly consisted of one arc, which was fitted well to a Gerischer type impedance, and therefore ascribed to fundamental reaction steps involving chemical bond breaking coupled with diffusion on the electrode surface. The summit frequency of this arc

was found to decrease with increasing sintering temperature. At 1000°C an additional contribution was sometimes found at low frequency. This additional arc was sensitive to the gas composition (the type of inert gas) and was tentatively ascribed to gas diffusion.

A low frequency inductive loop may sometimes appear in the impedance spectra of LSM/YSZ composite electrodes (see section 7.4). This feature can be explained by the activation of a passive layer at the electrode surface (Bonanos et al., 1987) or by adsorption phenomena (see e.g. Lasia (1999)). Low frequency inductive loops have been found for Sr and Ca doped $LaMnO_3$, Pt and Au electrodes in contact with YSZ under high anodic or cathodic polarisations (Gharbage et al., 1994; Narita et al., 1993; Schouler and Kleitz, 1987; van Hassel et al., 1992). In correspondence with these observations inductive hysteresis has been found for an LSM point electrode in contact with YSZ using potential sweeps (Juhl et al., 1995). For the $La_{0.5}Sr_{0.5}MnO_3$/YSZ system the low frequency inductive loop was attributed to adsorption of several species at the same site (Hammouche, 1989). Closely related to this, van Hassel et al. (1992) assumed that the inductive loop for an Au/YSZ system was connected to adsorption of intermediate oxygen species, and that the occupation of the adsorption sites depends on the polarisation. A different interpretation was given for the Pt/YSZ system as the inductive loop was ascribed to formation of electronic defects in the electrolyte leading to a drastic increase in the reaction rate (Schouler and Kleitz, 1987). Narita et al. (1993) ascribed the low frequency inductive loop to partial reduction of the electrolyte or the electrode at the counter electrode interface. Thus, the nature of the inductive phenomenon is far from clear and it may depend on the electrode material.

Summarising the literature for various kinds of LSM and LSM/YSZ electrodes in contact with YSZ it is clear that the impedance strongly depends on the nature of the electrode. Various processes may be limiting depending on electrode composition, processing parameters and the measurement conditions. Some trends can be revealed for

the high, medium and low frequency regime. At high frequency a contribution presumably related to the electrode structure may appear for both porous and composite electrodes. The arc often observed at medium frequency having an activation energy of 1.5 - 2 eV is assumed to be of the same nature for LSM point electrodes, porous LSM electrodes and LSM/YSZ composites. Disagreement about the nature of this process exists. Finally, at low frequency a diffusion limitation is observed at some conditions.

7.3. Experimental

7.3.1. Sample preparation

LSM/YSZ composite cathodes applied on YSZ pellets or tapes were tested (Fig. 2.1 and 2.2, respectively).

The LSM used in the examples below was $(La_{1-x}Sr_x)_yMnO_{3\pm\delta}$ with x = 0.15 or 0.25 and y = 0.9 or 0.95. The YSZ fraction of the C-layer was TZ8Y or TZ3YB. Three composite cathode compositions were tested: type I containing 50 weight% $(La_{0.75}Sr_{0.25})_{0.9}MnO_{3\pm\delta}$ and 50 weight% TZ3YB, type II containing 60 weight% $(La_{0.85}Sr_{0.15})_{0.9}MnO_{3\pm\delta}$ and 40 weight% TZ3YB, and type III containing 50 weight% $(La_{0.75}Sr_{0.25})_{0.95}MnO_{3\pm\delta}$ and 50 weight% TZ8Y. In the following the sintering temperature of the C-layer is stated for each example.

A CCC-layer consisting of LSM with the same composition as used for the C-layer was in most cases applied for current collection. If made by application of two nominally identical LSM sprayings with intermediate drying and sintering the CCC-layer was sintered at the same temperature as the C-layer. In cases where a CCC-layer was not applied by spraying, an unsintered LSM tape was used for current collection.

7.3.2. Electrochemical measurements

The composite electrodes were tested electrochemically using the three-electrode, four-wire set-up shown in Fig. 2.1 or by a simple two-electrode, four-wire measurement using the symmetrical cell shown in Fig. 2.2. In the three-electrode test an unsintered LSM tape cast foil and a channelled LSM pellet were in some experiments attached to the working electrode to improve current collection (2.1.b).

Impedance measurements were performed in air at open circuit voltage (OCV) or at applied cathodic potentials (three electrode measurements only) at temperatures between 800°C and 1000°C. The measurements were carried out using different instruments from Solartron (1250 + 1286 or 1280). The maximum frequency used in the impedance measurements varied with the used frequency response analyser (20 - 65 kHz). The lowest measuring frequency was 1 - 100 mHz. The amplitude applied between the working and the reference electrode was 14 mV RMS and 6 - 12 points per decade of frequency were measured going from high to low frequency.

The type of electrochemical cell and the measurement conditions are stated for each example in the following.

In order to illustrate the number of processes hidden in the impedance spectra some of the data presented in the following are deconvoluted by EQUIVCRT (Boukamp, 1986) using the equivalent circuit in Fig. 2.4.

7.4. Results

At Risø National laboratory composite LSM/YSZ cathodes have been studied for a number of years (Appendix A; Clausen et al., 1994; Østergård et al., 1995; Juhl et al., 1996a; Holtappels et al., 1998; Jørgensen et al., 1999; Jørgensen et al., 2000a; Jørgensen et al., 2000b). Various LSM compositions, LSM/YSZ ratios, processing procedures and

sintering temperatures have been tested using impedance spectroscopy. In general the impedance data includes a high frequency induction tail ascribed to the measurement leads, an ohmic resistance (the high frequency intercept adjusted for induction) mainly originating from the electrolyte and usually two to four processes which contribute to the electrode impedance spectrum. A process is here defined as a chemical or physical phenomenon, which gives rise to an arc in the impedance spectra. Some of the processes may contribute to limiting the rate of the electrode reaction. The number of processes and the magnitude of each contribution may vary with the electrode composition, the fabrication procedure and the test conditions. The different features found for the impedance of composites cathodes are illustrated by examples obtained for the three types of electrodes defined in section 7.3.1.

Before investigating the impedance of LSM/YSZ composite electrodes, it is useful to look at the impedance of a pointed LSM electrode pressed into contact with a YSZ electrolyte (Juhl, 1994). The purpose of such an experiment is to have a small, uniform and well-defined contact area between the working electrode and the electrolyte, whereby a measurable TPB is obtained (Fabry and Kleitz, 1972; Fabry and Kleitz, 1974). This in principle allows quantification of the characteristics of oxygen reduction on LSM, as the effect of geometry is minimised. The impedance of a pointed LSM electrode in contact with YSZ can appear as quite simple, as illustrated in Fig. 7.1. One dominant arc with some low frequency distortion is observed.

The impedance of composite LSM/YSZ electrodes can be much more complex (Fig. 7.2), as additional high and low frequency processes may be observed. In Fig. 7.2.a at least four processes, one of which gives a low frequency induction tail, are included in the impedance, while only two distinct processes are visible in Fig. 7.2.b.

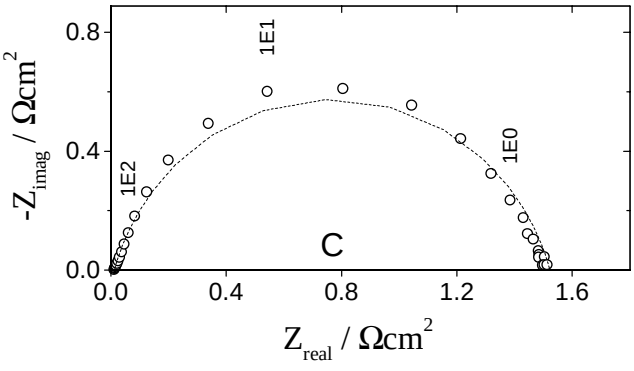

Fig. 7.1. Impedance of a $(La_{0.85}Sr_{0.15})_{0.9}MnO_{3\pm\delta}$ pointed electrode pressed into contact with a TZ8Y electrolyte (Juhl, 1994). The numbers mark the frequency in Hz. The dotted line shows the deconvolution of the data. The contact area between electrode and electrolyte is in the order of 10^{-5} cm^2. Measurement conditions: 1000°C, air, OCV, three-electrode measurement.

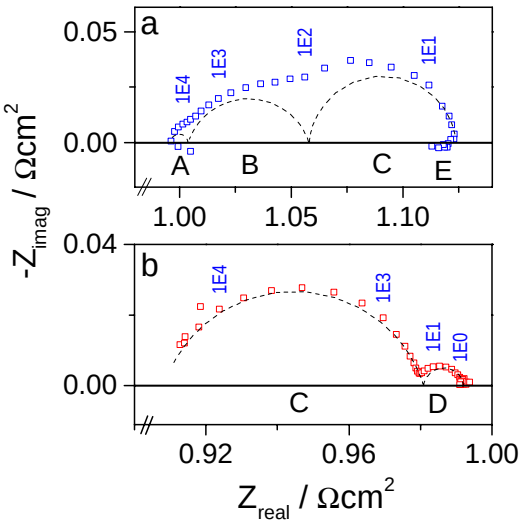

Fig. 7.2. Impedances obtained for two different LSM/YSZ composite cathodes at OCV and 1000°C in air. Notice the different axis scaling. The numbers mark the frequency in Hz. The dotted line shows the deconvolution of the data, three-electrode measurement. a) Cathode type I sintered at 1300°C/2 hours. b) Cathode type II sintered at 1100°C/2 hours, three-electrode measurement.

Fig. 7.3 shows an example of how different the impedance of two composite electrodes produced in parallel with nominally identical composition can be. In Fig. 7.3.a an inductive loop is visible at low frequency. Considering the polarisation resistance, R_p, as the difference between the high and the low frequency intercept with the real axis, values of 0.10 and 0.07 $\Omega \cdot cm^2$ are obtained for Fig. 7.3.a and 7.3.b, respectively (for Fig. 7.3.a the dc point is used for determination of R_p). Hence, considering the very different impedance spectra obtained for these nominally identical electrodes, the performance at OCV is found to be in reasonable agreement.

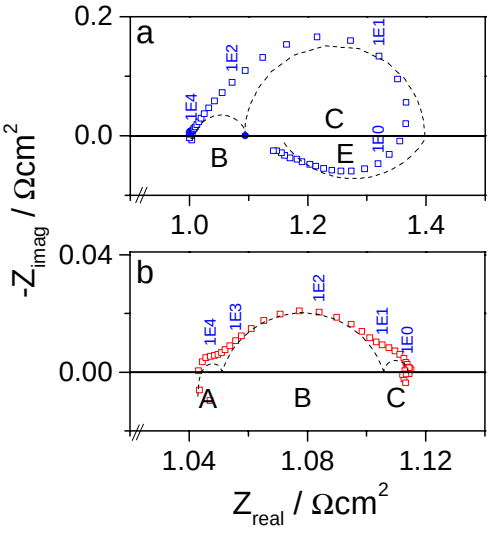

Fig. 7.3. Example showing the impedance of two nominally identical electrodes produced in parallel. Notice the different axis scaling. The numbers mark the frequency in Hz. The dotted line shows the deconvolution of the data. The solid circle in curve a) marks the dc point as determined by chronoamperometry. Cathode type II sintered at 1300°C/2 hours. Measurement conditions: 1000°C, air, OCV, three-electrode measurement.

Fig. 7.4 shows the impedance of three electrodes which are nominally identical except for the C-layer thickness (increasing thickness from Fig. 7.4.a to 7.4.c). In Fig. 7.4.a one distinct arc is visible. Fig. 7.4.b shows at least three arcs, as a high frequency

contribution and a low frequency induction loop appear. In Fig. 7.4.c one dominant arc with some high frequency distortion is found. The magnitude of the high frequency process and the low frequency process does not scale with thickness in a simple manner. It may be sensitive to variations in the microstructure and composition, which are yet outside our control. These variations seems to overshadow the effect of thickness.

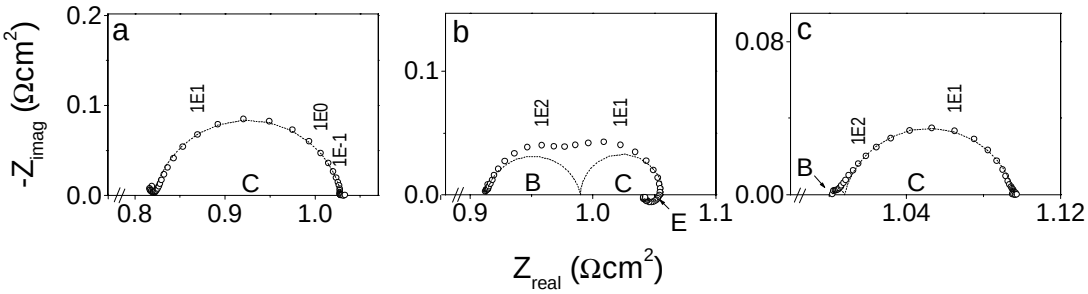

Fig. 7.4. Illustration of non-systematic influence of the C-layer thickness on the impedance of electrodes with nominally identical composition: a) 4 µm, b) 6 µm, c) 11 µm. Notice the different axis scaling. The numbers mark the frequency in Hz. The dotted line shows the deconvolution of the data. Cathode type I sintered at 1300°C/2 hours. Measurement conditions: 1000°C, air, OCV, three-electrode measurement.

The influence of the sintering temperature on the impedance is illustrated in Fig. 7.5. It shows Bode plots from the in-situ sintering experiment described in Chapter 4 measured at temperatures from 800°C to 1050°C with intervals of 50°C. This electrode shows at least two limiting processes. A high frequency process, which decreases in magnitude as the measurement temperature is increased, and a low frequency process which is independent of temperature.

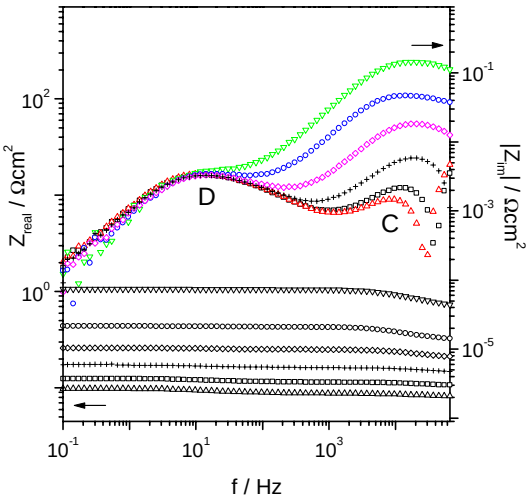

Fig. 7.5. Bode plot obtained at different temperatures for an unsintered composite cathode, ∇ 800°C, ○ 850°C, ◊ 900°C, + 950°C, □ 1000°C, Δ 1050°C. Cathode type III. Measurement conditions: air, OCV, two-electrode measurement.

The measurements taken at the reference temperature (850°C) during the in-situ sintering experiment (Chapter 4) show that the low frequency arc is almost independent of sintering temperature (Fig. 7.6). The summit frequency of the high frequency arc decreases with increasing sintering temperature. In these measurements the summit frequency is taken as the frequency at the measurement point having the maximum imaginary value. This value changes from approximately 15 kHz at 850°C to 1.5 kHz at 1050°C. Taking that the summit frequency is equal to the inverse of the resistance times the capacity, this is equivalent to capacitances of 75 µF/cm^2 to 1 mF/cm^2.

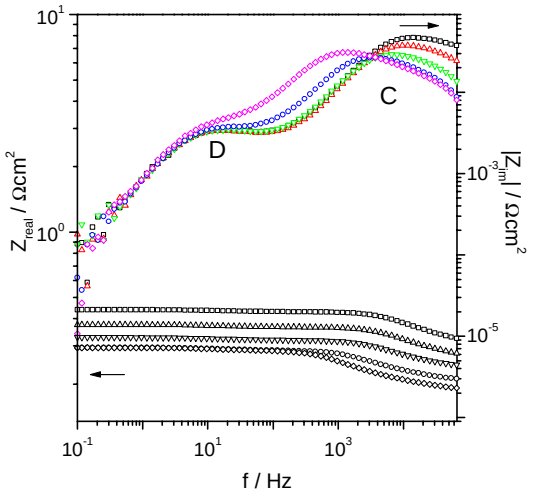

Fig. 7.6. Bode plot obtained at 850°C for the electrode shown in Fig. 7.5 after sintering at different temperatures, □ 850°C, Δ 900°C, ∇ 950°C, ○ 1000°C, ◊ 1050°C. Cathode type III. Measurement conditions: air, OCV, two-electrode measurement.

Passing current through the composite electrode may affect the impedance on both a short and a long time scale, as discussed in Chapter 6 and Chapter 5, respectively. Some cathodes can be activated by current load, i.e. the polarisation resistance measured at OCV is lower after a certain current load than before. An example is given in Fig. 7.7.a where the performances of an electrode measured before and 45 min. after anodic and cathodic current flow (±54 mA/cm^2 for 30 min each) are compared. As the current is interrupted R_p increases with time and eventually reaches the original level. Whether or not the electrodes can be activated by current load seems to depend on the processing (e.g. sintering temperature) and the measurement conditions. For example the activation can be negligible when measuring at 1000°C but distinct at 850°C, as illustrated in Fig. 7.7. It could be argued that the behaviour in Fig. 7.7 is due the overvoltage being higher at 850°C than at 1000°C, as the electrode experienced the same current density at the two temperatures. However, the lower sensitivity observed at 1000°C is in correspondence with previous findings (Chapter 3). Whether nominally identical electrodes which initially have different

impedances (like in Fig. 7.3) can have the same performance and similar impedances after a certain current treatment needs further investigation.

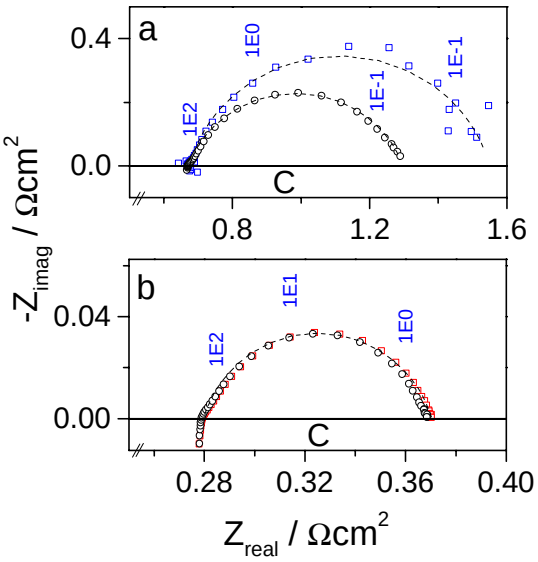

Fig. 7.7. Impedance obtained before □ and 45 min. after ○ current load (+54 mA/cm^2 for 30 min. and -54 mA/cm^2 for 30 min). a) 850°C, b) 1000°C. Notice the different axis scaling. The numbers mark the frequency in Hz. The dotted line shows the deconvolution of the data. Cathode type II sintered at 1300°C/2 hours. Measurement conditions: air, OCV, two-electrode measurement.

Short term cathodic polarisation (10 - 15 min) can affect the impedance in different ways. When the impedance reveals one distorted arc it seems to be little affected. The magnitude of this arc may decrease somewhat, but otherwise the response can be rather unaffected. When the impedance comprises two distinct arcs, the low frequency arc may be strongly affected by polarisation, as illustrated in Fig. 7.8. The low frequency impedance grows as the polarisation increases, while the high frequency impedance decreases slightly. When the current is released, the magnitude of low frequency impedance decreases to a level close to the starting point (compare the two OCV curves in Fig. 7.8). At the highest cathodic polarisations an inductive loop seems to evolve at low frequencies (marked E in Fig. 7.8).

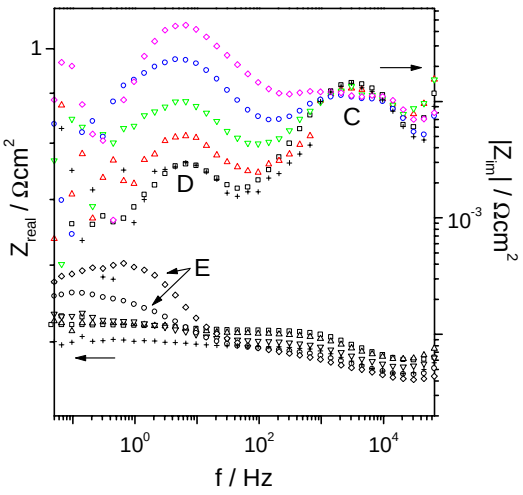

Fig. 7.8. Bode plot as measured after equilibration of the electrode for 15 min. at the overvoltage, η, □ η = 0 mV, Δ η = -22 mV, ∇ η = -48 mV, ○ η = -50 mV, ◊ η = -45.5 mV, + η = 0 mV. The points marked E are of inductive nature. Cathode type II sintered at 1100°C/2 hours. Measurement conditions: 1008°C, air, three-electrode measurement.

Exposing a composite electrode to a constant current load on a larger time scale affects the impedance differently than a short term polarisation. For composite cathodes subjected to a current load of –300 mA/cm^2 for 2000 hours at 1000°C (Chapter 5) OCV measurements performed before and after the current loaded test reveal that the magnitude of the dominant arc has increased considerably, while its summit frequency decreases slightly (Fig. 7.9). Furthermore, a small arc seems to have evolved at high frequencies (relaxation frequency ~ 10^3 Hz) during the test. The change in the high frequency intercept during test is related to degradation of the YSZ electrolyte (Appel et al., 2000). Changes in the microstructure are also found after the test, as a large number of 1 µm pores are formed along the interfaces of the composite electrode and the composite layer is densified (Chapter 5).

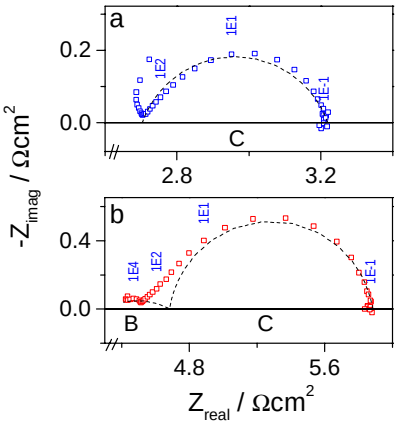

Fig. 7.9. Impedance measured before (a) and after (b) 2000 hours durability test at -300 mA/cm^2 at 1000°C on a sample of type A_{galv} (see Chapter 5). Notice the different axis scaling. The numbers mark the frequency in Hz. The dotted line shows the deconvolution of the data. Cathode type II sintered at 1300°C/2 hours. Measurement conditions 850°C, air, OCV, three-electrode measurement.

The aim of the examples presented above, which are chosen from a large number of measurements obtained on electrodes with different characteristics (in the order of 500 electrodes have been investigated of which only a few have been published previously, see for instance Appendix A; Clausen et al., 1994; Østergård et al., 1995; Juhl et al., 1996a; Holtappels et al., 1998; Jørgensen et al., 1999; Jørgensen et al., 2000a; Jørgensen et al., 2000b), is to illustrate that quite different features can be found in the impedance of electrodes with different chemical and electrochemical prehistory. It appears that at least five processes can affect the electrode performance. The arcs corresponding to these processes are named A - E going from high to low frequency and are marked in Figs. 7.1 - 7.9. The positioning of the arcs in the figures is only tentative, as more arcs than indicated may be present in the impedance spectra due to overlapping with other arcs.

In Table 7.1 some of the characteristics of each of these arcs are presented. These will be discussed in section 7.5. It will be argued why it is believed that each of the arcs reflects a specific process or inter-linked processes.

Table 7.1. *Overview of the processes found to affect the impedance of LSM/YSZ composite cathodes.*

Arc	f_{max} / Hz	E_a/ eV	z in $p_{O_2}^{-z}$	Characteristics	Process
A B	~10^4 (this work) 10^2-5·10^3 (this work) ~5·10^3 (1)	1 (1)	0 (1)	These arcs depend strongly on microstructure. The two arcs may have similar f_{max} and are therefore not always separable. Increases with increasing composite thickness (2).	Transport/transfer of oxygen intermediates/oxide ions at LSM/YSZ. interfaces and through the YSZ of the composite.
C	f_{max} = f(T_s ,T_m), 0.1 < f_{max} < 10^4 Example (this work): Ts = 1300°C T_m = 1000°C 5 < f_{max} < 30 T_m = 850°C 0.5 < f_{max} < 20	2 (2), 1.8-1.9 (3), 1.5-1.6 (1)	0.5 (3,4 [LCM]), 0.3 (5), 0.14-0.3 (1)	Summit frequency decreases with increasing sintering temperature (Fig. 7.6). The magnitude of this arc is strongly related to the length of TPB and decreases with increasing composite thickness (2). Magnitude changes with current passage (activation) (Fig. 7.7), assumed to be related to segregates at the TPB.	Reflects competitive elementary processes in the overall oxygen reaction mechanism. The processes are assumed to be dissociative adsorption, transfer of species at TPB and surface diffusion.
D	5-10 (this work), 2 (1), 1.4 (4 [LCM]), 5 (6)	0 (this work)	0.6-0.8 (1), 1 (4 [LCM], 6)	Magnitude increases with increasing cathodic overvoltage (Fig. 7.8). Independent of measurement temperature (Fig. 7.5) Most pronounced for electrodes with high $f_{max,C}$ (e.g. electrodes sintered at 1100°C or below).	Gas diffusion in a stagnant gas layer above the electrode structure.
E	~0.03-0.4 (this work)	-	-	Inductive arc, possibly related to electrode activation. More than one process may be present.	Assumed to be related to segregates at the TPB.

References are stated in parenthesis: (1) Murray et al., 1998; (2) Appendix A; (3) Siebert et al., 1995; (4) Tsuneyoshi et al., 1989; (5) Østergård et al., 1993; (6) Eguchi et al., 1991; f_{max} = summit frequency, T_s = sintering temperature, T_m = measurement temperature, E_a = activation energy, LCM = (La,Ca)MnO_3.

7.5. Discussion

The impedance of composite LSM/YSZ cathodes contains several depressed arcs, which are usually not well-separated. The individual processes may be affected by electrode composition, processing and measurement conditions. Impedance spectroscopy is a very sensitive method, which may be influenced by small variations in any of these parameters; variations, which may be difficult to detect. This is reflected in the quite different spectra obtained for nominally identical electrodes (Fig. 7.3). Taking this into account the discrepancies found in literature regarding the number of rate limiting processes for the oxygen reduction mechanism and the nature of these are not any longer surprising.

The differences observed in the impedance of nominally identical electrodes (Fig. 7.3) and before and after polarisation (Figs. 7.7-7.9) may reflect that the LSM/YSZ system is dynamic during operation (Chapter 5). With a Pt/YSZ system redistribution of the materials during current flow has been observed (Bay and Jacobsen 1997a and 1997b). Others have pointed out that kinetic demixing may occur during operation for a LSM/YSZ system (Yoo and Lee, 1998). Therefore, the impedance depends on the electrochemical prehistory of the electrochemical cell (Chapter 6).

In this work it has been revealed that a model with at least five processes is necessary to describe the impedance of all the composite electrodes investigated. The number of processes is larger than reported in literature, presumably because more different types of composite electrodes than normally reported have been investigated and thereby more different characteristics have been observed. All of the five processes found do not appear simultaneously in the impedance due to the different dependence of the processes on composition, fabrication and electrochemical prehistory. If two processes

have similar time constants their corresponding arcs may be overlapping in the impedance spectrum.

In the following the nature of the individual processes found will be discussed. The processes are discussed in order of appearance from high to low frequency, although this order does not reflect the relative importance and magnitude of the processes.

7.5.1. Process A & B

In several studies on composite electrodes the high frequency contribution to the impedance was assumed to be a geometric effect related to the composite microstructure, and it was fitted to one depressed arc using equivalent circuits (Appendix A; Murray et al., 1998). However, Juhl et al. (1996b, Appendix A) found that this arc reflected more than one simple process. The activation energy changed within the tested temperature range and the summit frequency and the frequency power (n-value) varied considerably (Appendix A). On the background of this and the results presented above (Figs. 7.2.a and 7.3.b) it is suggested that the high frequency impedance of composite electrodes may comprise contributions from two rate limiting processes, here called A at the highest frequencies and B (arc B reflects process B).

In some cases the magnitude of one or both of the processes may be insignificant, or the time constants of the processes may be so close, that the two arcs are not well-separated in the impedance. Further arc B may be overlapping with arc C, when the sintering temperature is low. At such conditions the time constant of arc C are close to that of arc B, and the magnitude of arc B is usually found to be small compared to arc C. If there is only one arc present in the impedance spectrum, it is assumed to be arc C rather than arc B. This is argued in the discussion of arc C. The two high frequency processes, A and B, are in most cases not separable with reasonable accuracy, and they are therefore treated together in the following.

These processes seem strongly related to the electrode microstructure (Figs. 7.3 and 7.4). The durability results in Fig. 7.9 show that after 2000 hours with -300 mA/cm^2 at 1000°C a high frequency process appears in the impedance. This is presumably related to a change in microstructure during the test, as densification of the composite structure and pore formation at the composite interfaces was observed (Chapter 5).

Whether process A and B are of the same nature is not possible to decide at present, as they are so difficult to separate. Tentatively, both processes are ascribed to transport phenomena in the composite structure as suggested previously (Appendix A), and the arc is denoted arc B in the following in case only one of the two high frequency arcs is visible.

Murray et al. (1998) found an activation energy of around 1 eV for process B, and it was ascribed to YSZ grain boundaries. However, using literature data for the grain boundary capacity (assuming that the grain size is 2 μm and that the grain boundary capacity is independent of temperature) and the grain boundary resisitivity of YSZ at 850°C (Badwal and Drennan, 1987; Badwal, 1992), a summit frequency in the range of 40 MHz is found. As the summit frequencies found in this work are orders of magnitude lower than this value (Table 7.1), this interpretation is not likely to be valid. Transport across YSZ grain boundaries may affect the high frequency impedance, but cannot account for the observed arcs A and B.

Sunde (1996) has simulated the polarisation resistance of composite electrodes using random resistor networks. It was found that contacts between electrode and electrolyte particles for which at least one of the phases is not connected to its corresponding bulk phase (lack of percolation) may affect the impedance (Sunde, 1996), and this effect will most likely appear at high frequencies (Sunde, 1997). It is reasonable to assume that such contacts are present in the composite electrodes investigated here. The observed thickness dependence (increase of the high frequency impedance with increasing thickness (Appendix A; Murray et al., 1998)) may be due to the increasing number of

LSM-YSZ interfaces oxygen intermediates/oxide ions have to pass on their way to and from the active sites with increasing composite thickness.

Data in literature show that for some porous LSM electrodes a contribution to the impedance can be observed at frequencies higher than what is expectable for arc C (Østergård et al., 1993; van Heuveln et al., 1997b). Thus, type A or B arcs may also be present for non-composite structures. This may indicate that a rough interface in a non-composite structure may on the very local scale (e.g. grain size or below) contain similar reaction paths as a composite structure.

Mitterdorfer and Gauckler (1998) found that reaction products such as La-zirconate may affect the impedance. It is therefore suggested that the high frequency arcs may also reflect the presence of such phases, as these phases due to their low conductivity may affect adversely the transport of oxygen intermediates through the electrode-electrolyte interface structure. A-site substoichiometric LSM was used in this work to suppress the formation of La-zirconate (Clausen et al., 1994), however, traces of such phases may be present.

Based on the above analysis the processes involved are suggested to be transport of oxide ions/oxygen intermediates across LSM/YSZ interfaces in addition to transport through YSZ grains and across YSZ grain boundaries in the composite. It was argued previously that transport across YSZ grain boundaries cannot solely account for the observed high frequency arc. However, it cannot be excluded that the high frequency impedance reflects a combination of different phenomena, whereof one could be transport across YSZ grain boundaries. Based on the present data it is not possible to give a more precise interpretation, nor is it possible to define which species are involved in the transport processes.

It is expected that the high frequency impedance can be minimised by ensuring good percolation of LSM and YSZ through the electrode structure and by suppressing the formation of secondary phases.

7.5.2. Process C

For porous $La_{0.6}Ca_{0.4}MnO_3$ electrodes Mizusaki et al. (1991) suggested that the same process limits the performance independently of the electrode microstructure. The process limiting the performance of an LSM point electrode (Fig.7.1) is assumed to be the same as for $La_{0.6}Ca_{0.4}MnO_3$. Siebert et al. (1995) found an activation energy of 1.8 - 1.9 eV for this process using an LSM point electrode. In reasonable agreement with this Murray et al. (1998) and Juhl et al. (1996b, Appendix A) found the activation energy of this process to be close to 1.5 - 1.6 eV and 2 eV, respectively, for LSM/YSZ composite electrodes. This process, which seems to limit the performance of $La(Sr,Ca)MnO_3$ electrodes and which nature is independent of microstructure, is here called C. The associated arc seems to be the only one of the five arcs presented above, which appears in all impedance measurements and it is often found to be the dominant contribution to the overall impedance. Thus, this arc seems to be essential for the oxygen reduction mechanism.

The magnitude of arc C seems to depend strongly on the length of TPB (Appendix A; Mizusaki et al., 1991; Jørgensen et al., 2000a; Juhl et al., 1996a). This is reflected in the results presented in Fig. 7.9. The increase in arc C during the durability test is ascribed to a decrease in TPB length due to the described pore formation and densification of the composite layer (Chapter 5). Thus, a minimisation of the contribution of arc C to the overall impedance may be obtained by optimising the TPB-length.

The summit frequencies of arc C found in the present work are in reasonable agreement with the findings in literature (Mizusaki et al., 1991; van Heuveln et al., 1997b; Holtappels et al., 1998; Murray et al., 1998; Mitterdorfer et al., 1998). Sintering

temperature is the only fabrication parameter, which so far has been found to affect the time constant of arc C significantly. Probably this is related to the changes in electrode particle size and particle interconnection, which occur as a function of sintering temperature. According to Fig. 7.6 the summit frequency of arc C, $f_{max,C}$, decreases with increasing sintering temperature. Similar dependence of $f_{max,C}$ on the sintering temperature has been found in literature (van Heuveln et al., 1997b; Holtappels et al., 1998; Mitterdorfer et al., 1998). In Fig. 7.9 $f_{max,C}$ decreases slightly during the durability test, i.e. the same trend as observed for increasing sintering temperature. This corresponds well with the observed densification of the composite structure after durability test, which is ascribed to sintering due to local heating during current passage (Chapter 5).

When the sintering temperature is high, the summit frequency of arc C is low. At such conditions other low frequency processes may be difficult to distinguish from arc C. At low sintering temperatures arc C is shifted to higher frequencies and may overlap with arcs A and B. Thus, the process reflecting arc C seems to contribute significantly to the rate limitations of all LSM electrodes even though the appearance of the total impedance spectrum may vary substantially.

Disagreement about the nature of this process exists in literature (section 7.2). Apart from the presence of secondary phases, which may affect the impedance, the reason for this may be the above-mentioned overlap between arc C and other processes, which makes it difficult to reveal the nature of the individual processes. According to section 7.2 the dominant arc in the impedance (arc C) may be related to adsorption of oxygen species or dissociation of adsorbed oxygen. In some cases arc C can be described by a Gerischer type impedance, suggesting that bond-breaking and surface diffusion may be rate limiting for the oxygen reduction process (Holtappels et al., 1998; Holtappels et al., 2000a).

As shown in table 1 several authors found an oxygen partial pressure dependence of $p_{O_2}^{-z}$, z = 0.14 - 0.5. The varying p_{O_2} dependence and activation energy indicate that

more than one process may contribute to arc C. Each of the processes may dominate at certain conditions depending on parameters as electrode composition, processing and electrochemical prehistory. One of these processes is, based on literature (section 7.2) and the oxygen partial pressure dependence, suggested to be dissociative adsorption. Another is assumed to be transfer of oxygen intermediates/oxide ions at the TPB, since the TPB length is found to affect the magnitude of arc C. At conditions where the typical Gerischer impedance features are found to be distinct (Holtappels et al., 1998; Holtappels et al., 2000a), bond-breaking (dissociative adsorption) may be coupled with surface diffusion. The competition of several processes is in agreement with the fact that the possibility of activating the electrode with current flow may vary from electrode to electrode and at different measurement conditions (Fig.7.7).

The activation process illustrated in Fig. 7.7.a has also been reported in literature (Jørgensen et al., 1999; Odgaard et al., 1996; Jiang et al., 1999; van Heuveln, 1997b; McEvoy, 1994; Lee et al., 1995). This process may be related to the accessible TPB length, as a decrease in the magnitude of arc C is found, when current is passed through the electrode. The activation process has previously been interpreted as a broadening of the active reaction area along the TPB-line. However, as discussed in the literature survey there are various indications that the extension of the reaction area may be rather small, and this explanation may therefore not solely account for the rather extensive activation, which can be observed for composite electrodes upon current load.

It is suggested that the activation process is related to segregations along the TPB-line. These may comprise constituents from the electrode and electrolyte material (Mn and Y, respectively), impurities (from the electrode and electrolyte material and contaminations related to the fabrication procedure) and reaction products formed during fabrication. The presence of a passive layer, which is affected by current passage was also suggested by Jiang et al. (1999). Such segregations may limit the reaction rate due to their

low conductivity and may be affected by current passage. For instance, Tricker and Stobbs (1993) observed that $La_2Zr_2O_7$ may redistribute during operation. This observation was explained thermodynamically by Yokokawa et al. (1994) who suggested that the zirconate formation is a reversible process, which is sensitive to the oxygen potential. A change of the oxygen potential is not enough to initiate the activation, this requires passage of current (Odgaard and Skou, 1996). Redistribution of segregates due to current load may improve the accessibility of the TPB leading to the observed decrease in the reaction resistance (arc C), and it may explain the reversibility of the activation process. Also it may explain both that the electrode resistance and the electrochemical prehistory is connected and that the activation process is not observed at all measurement temperatures (Fig. 7.7).

This hypothesis may explain some of the differences observed by different laboratories as the amount of segregates will depend considerably on the raw materials and the processing. Although the formation of reaction products was suppressed in this work by the choice of an A-site substochiometric LSM composition the presence of small amounts of segregations other than La- and Sr-zirconates cannot be excluded. Also, the presence of impurities in the electrode and electrolyte material is inevitable. Further, the composition of LSM is not likely to be completely homogeneous from grain to grain. For instance the LSM stoichiometry and thereby the reactivity may vary within the electrode (Mitterdorfer and Gauckler, 1998). This may explain the significantly different impedance spectra observed for nominally identical electrodes (Fig. 7.3).

The capacity related to arc C may vary considerably. For instance values of 80 $\mu F/cm^2$ and 0.4 F/cm^2 can be found in AC measurements with an amplitude of 20 mV (Fig. 7.6 and 7.7.a, respectively). The reason for the different capacities in this example is assumed to be that the electrodes are sintered at different temperatures, which has proven to affect the summit frequency of arc C considerably. The decrease in polarisation resistance with decreasing sintering temperature is relatively much smaller than the

corresponding increase in summit frequency, reflecting the decrease in capacity. This correlation between sintering temperature and capacity implies that the capacity is not related to the accessible electrode surface area, which could be the case if it was related to for instance adsorbed oxygen species, as the accessible surface area or at least TPB length is assumed to be largest for electrodes sintered at low temperature.

The capacity of Fig. 7.7.a is much larger than expected for interfacial polarisation, suggesting that it reflects a bulk process. Three bulk processes related to LSM, YSZ and the gas phase, respectively, may therefore be considered.

Adler et al. (1996) have suggested that bulk oxidation/reduction of a mixed conducting electrode material may explain the large capacitances. In the case of LSM this process would involve Mn^{3+}/Mn^{4+} in the LSM crystal lattice. However, in the example presented above the charge necessary to explain the observed capacity (0.4 F/cm^2 for an electrode area of 0.25 cm^2) at an applied voltage amplitude of 20 mV is $2 \cdot 10^{-3}$ C. This charge corresponds to $1.3 \cdot 10^{16}$ electrons. This amount exceeds the amount of Mn-ions present in the composite electrode. Also, this amount by far exceeds the amount of Mn, which may be dissolved in the YSZ crystal lattice. Thus, oxidation and reduction of Mn in the electrode and electrolyte crystal lattice cannot account for the observed capacity. Further, the oxygen volume necessary to ascribe the charge to reduction/oxidation of oxygen is larger than the electrode volume. Therefore, reduction and oxidation of oxygen in pores in the electrode structure can be excluded as the origin of the capacity.

This leads to the suggestion that the observed capacity is really a pseudo capacity reflecting in the time domain a decreasing current related to a slow passivation phenomenon. The passivation process may be related to adsorbed oxygen intermediates, e.g. O^-, and/or segregates onto the TPB-zone at the LSM side of the LSM/YSZ interface. However, more work is necessary in order to determine the detailed nature of this phenomenon.

7.5.3. Process D

Several authors have reported the presence of a low frequency arc attributed to diffusion (Tsuneyoshi et al., 1989; Eguchi et al., 1991; Østergård et al., 1993; Holtappels et al., 1998; Murray et al., 1998; Mitterdorfer et al., 1998). The presence of this process, denoted D, is also found in several of the data presented in this work (Figs. 7.2.b, 7.5, 7.6 and 7.8). In Fig. 7.8 the magnitude of arc D is found to increase considerably with polarisation. This is interpreted as oxygen depletion. Fig. 7.5 shows that the magnitude and summit frequency of arc D is independent of measurement temperature. These observations suggest that the origin of this arc is gas diffusion. This is in correspondence with Adler et al. (1996) who predicted that gas diffusion limitations should be found at lower frequency than other limiting processes with comparable resistance.

The gas diffusion limitation can either be related to the porous electrode structure or a stagnant gas layer above the electrode structure. The approximate thickness of the gas layer involved can be estimated using the procedures of Adler et al. (1996) and Primdahl et al. (1999c). Both models involve the binary diffusion coefficient of oxygen and nitrogen (Welty et al., 1984). For both models the thickness of the gas layer is found to be in the order of several millimeters at 850°C and 1000°C. This strongly indicates that the gas diffusion limitation is related to a stagnant gas layer above the electrode surface. This assumption is supported by the findings in Chapter 4, which show that the gas diffusion limitation is independent of the electrode microstructure.

For the results presented in this work arc D is only visible for electrodes sintered at 1100°C or below. For such electrodes the summit frequency of arc C is significantly higher than for arc D, i.e. the processes do not overlap in the impedance. When the summit frequencies of arc C and D are close, arc C tends to dominate the impedance. In such cases arc D may just cause a low frequency distortion of arc C.

7.5.4. Process E

The impedance spectrum in Fig. 7.3.a suggests that the low frequency inductive loop in the electrode impedance may reflect more than one process. However, in this work it was chosen to treat the low frequency induction contribution as one process (arc E), as the amount of information about the possible processes is much too limited to separate them. The appearance of arc E is rather irregular which complicates a detailed investigation of this feature. In literature the presence of a low frequency inductive loop has been observed at high cathodic polarisations (see section 7.2). As the inductive loop in the present work has been observed at quite different circumstances (OCV, Figs. 7.2.a and 7.3.a) it may be another phenomenon than what is reported in literature. The fact that the inductive loop only appears for one of the two nominally identical electrodes in Fig. 7.3 suggests that this feature is not an inherent property of LSM.

Due to the high time constant of this process inductive loops may not always be observed as this requires measurements at very low frequency. The time constant depends on the measurement temperature and possibly also on the oxygen potential and the electrode history. If for instance the measurement before current load in Fig. 7.7.a had been extended to lower frequencies an inductive loop may have appeared. This leads to the suggestion that the low frequency inductive process may be related to the activation phenomenon described for arc C. Thus, process E is tentatively related to segregates at the TPB. As discussed for arc C the segregates may redistribute depending on the operating conditions. At OCV the time constant of this process is expected to be high, as observed for arc E.

7.5.5. Strategy of Further Studies

The discussion above is summarised in Table 7.1 by listing the limiting processes found. The interpretation of each process is stated together with the literature findings.

The next steps in revealing the oxygen reduction mechanism is to investigate in more details the nature of each of the identified processes further by experiments and by modeling of the data. An equivalent circuit model dealing with the five limiting processes will contain a large number of parameters, and the work involved with data treatment may seem enormous. However, many of the parameters will turn out to be zero, as all five processes normally do not appear simultaneously. Further, if for instance a Gerischer type impedance can be used successfully in the equivalent circuit (Holtappels et al., 1998; Holtappels et al., 2000a), the number of parameters can be reduced. Although it is time consuming, it is important to fit the data to an equivalent circuit in order to reduce the impedance data to the smallest possible number of characteristic parameters, which are adequate for all electrode compositions, structures etc. Important information about the nature of the individual processes may be gained from the dependence of these parameters on composition, processing and test conditions.

7.6. Conclusions

LSM/YSZ composite cathodes with different composition and processing parameters have been studied using impedance spectroscopy. By studying electrodes with fundamentally different characteristics, it was found that more processes than reported in the literature may determine the performance of such electrodes. At least five processes were found to affect the impedance. Going from high to low frequency these processes are:

- At least two processes, A and B, related to the transport of oxide ions/oxygen intermediates within the electrode structure and at the electrode/electrolyte interface. It is often difficult to separate the two processes in the impedance spectrum.
- An overall process, C, reflecting competitive elementary steps in the overall oxygen reduction reaction. This process depends on the triple phase boundary length and is often found to be the dominant contributor to the impedance. It is assumed that this process may be dominated by dissociative adsorption, transfer of species at the triple phase boundary or surface diffusion depending on the circumstances.
- Gas diffusion in a stagnant gas layer above the electrode structure (arc D).
- An activation process, which decreases the TPB-line resistance, resulting in an inductive arc E at very low frequencies. It is suggested that this process is related to segregation of materials including impurities at the TPB.

The processes are usually not all present in the impedance spectra simultaneously.

Further studies should include modelling using equivalent circuits, as this may reduce the impedance data to a definite number of characteristic parameters.

Chapter 8. Conclusions and Recommendations

8.1. General Conclusions

The subject of this thesis is an investigation of composite cathodes of lanthanum strontium manganate (LSM) and yttria stabilised zirconia (YSZ) for solid oxide fuel cells. The composite electrode was applied on a YSZ substrate by spraying. Two layers of LSM were applied on the composite to ensure proper current collection. The experimental techniques used were primarily electrochemical impedance spectroscopy and scanning electron microscopy (SEM). The electrochemical investigations were carried out in air at temperatures between 700°C and 1000°C using either symmetrical two-electrode cells for measurements at open circuit voltage (OCV) or three-electrode cells for OCV and polarised measurements.

The polarisation resistance was found to decrease with increasing thickness between 2.5 and 11.5 µm at 700 - 1000°C (Chapter 3). Application of a layer of YSZ particles on the electrolyte surface prior to application of the composite layer improved the performance compared to electrodes without such a layer. Thus, the electrode performance was sensitive to the thickness and the microstructure of the electrode. The polarisation resistance was most sensitive to microstructural changes at 700°C and 850°C compared to at 1000°C. This implies a potential for low temperature operation.

Changing the sintering temperature from 1300°C to 1150°C altered the microstructure, which was most porous and contained the smallest particles when sintered at low temperature (Chapter 4). Thus, the triple phase boundary line was longest in the electrodes sintered at low temperature. This was reflected in the polarisation resistance, which was lowest for these electrodes. The electrode performance was sensitive to the sintering conditions of the current collecting layers, as a lower polarisation resistance was obtained by lowering the sintering temperature of these layers only. This implies that a

large fraction of the active triple phase boundary lines were present at the interface between the composite and the current collecting layers.

The degradation of LSM/YSZ composite cathodes operated at realistic conditions (-300 mA/cm^2, 1000°C, air) involved pore formation at the composite interfaces in addition to densification of the composite structure, which led to a severe increase in the polarisation resistance (Chapter 5). It was found that current passage rather than temperature caused the degradation. The effect of current flow was ascribed to kinetic demixing. Thus, when constructing an alternative electrode microstructure it is important to investigate whether it deteriorates during current flow by performing durability measurements.

The impedance of composite LSM/YSZ cathodes was affected by parameters which are not directly related to the oxygen reduction process. Small variations in the microstructure or the composition, outside our control, may affect the impedance. It seems necessary to investigate a large number of nominally identical electrodes to obtain a proper characterisation of a given type of cathode (Chapter 6), due to the observed variations in the impedance of such electrodes. It is advantageous to combine simple two-electrode tests performed at OCV with polarised measurements using three-electrode cells, in order to get a good description of the electrode performance. The two-electrode test is suitable for an initial screening of the electrodes, while the more time consuming three-electrode test can give information about the polarisation behaviour of the electrodes.

At least five processes (physical and chemical) affected the impedance response of the investigated LSM/YSZ composite electrodes (Chapter 7). Two high frequency processes were ascribed to transport phenomena across LSM-YSZ interfaces and in the YSZ phase of the composite. A medium frequency arc was ascribed to competitive elementary steps in the overall oxygen reduction mechanism such as dissociative adsorption (bond-breaking), surface diffusion and transfer of species at the triple phase

boundary. A low frequency arc related to gas diffusion limitation in a stagnant gas layer above the electrode structure was sometimes found. An inductive process related to electrode activation, probably involving segregates at the triple phase boundary between electrode, electrolyte and gas may also appear. These findings provide a new basis for future modelling the impedance of LSM/YSZ composite cathodes.

8.2. Major Achievements

A major finding of this work is that the SOFC composite cathode comprising LSM and YSZ is indeed a dynamic system. The electrochemical properties of the system do not only depend on physical parameters such as microstructure and thickness, they are also affected by the measurement conditions and the electrochemical prehistory. In addition it appears that the electrolyte (purity and Y-content) and the cathode current collector structure also affect the electrode performance. Passing current through the LSM/YSZ composite electrode has been found to affect both the short term performance (activation) and the long term performance (degradation). This is believed to be the reason why the LSM/YSZ system cannot be described in a simple manner, and explains why no unambiguous model has been presented in the literature despite the extensive amount of work performed in this field.

A maybe surprising, but important observation is the influence of the CCC-layer microstructure on the performance of the electrode. The hypothesis that the interface between the C-layer and the CCC-layer contains a large fraction of the active sites is important with respect to choosing processing parameters, as the microstructure of both layers must be carefully tailored.

Another achievement of this work is to show that more processes than reported in the literature may contribute to limiting the performance of SOFC cathodes. The reason

why more processes are found is probably that many electrodes with different compositions and processing parameters are compared in this work. At least five processes were found. However, more processes may contribute to the electrode impedance. It is essential to take all these processes into account when proposing a model for the oxygen reduction mechanism. Otherwise an unambiguous model may not be found. This work provides a new basis for making such a model.

Finally, the information found about each of the rate limiting processes involved may lead to suggestions for improving the electrode performance, as discussed in a following section.

8.3. Recommendations for Further Studies

The recommendations for future investigations of LSM/YSZ composite cathodes can be divided into a scientific part and a technical part aiming at increasing the understanding of the oxygen reduction kinetics and other parameters affecting the electrode impedance and improving the performance, respectively. However, the two approaches are connected, as increased understanding may help to improve the performance and vice versa. The suggested approaches are listed in Table 8.1, and are discussed further in the following.

8.3.1. Scientific

From a scientific point of view it is important to investigate the nature of each of the five processes, which have been found to limit or affect the performance, and to analyse whether even more processes may contribute to the impedance. Impedance spectroscopy is the method of most benefit for this task. The impedance is sensitive to many different parameters. Some are beyond our control and others are irrelevant with

Table 8.1. Proposals for further studies of the oxygen reduction proceeding in LSM/YSZ composite cathodes. The properties of each of the arcs mentioned below are listed in Table 7.1.

Arc	Process type	Scientific / Theoretical	Technical / Practical
A+B	**Transport**	**Try to separate these processes more by testing at extreme conditions, by testing extreme microstructures (very dense or very porous) or by testing electrodes containing reaction products.**	**Keep sintering temperature low (long TPB).** **Ensure good percolation of LSM, YSZ and gas in the composite (long TPB, avoid contributions from nonactive LSM/YSZ contacts).**
C	**Reaction arc (oxygen reduction)**	**Investigate the effect of segregates at the TPB by addition of the relevant materials during fabrication.** **Investigate effect of oxygen partial pressure, gas composition, temperature and microstructure further.**	**Keep sintering temperature low (long TPB).** **Keep thickness proper (long TPB).** **Ensure good percolation of LSM and YSZ in the composite (long active TPB), and assure good oxygen supply.**
D	**Gas diffusion**		**Ensure that the air flow above the electrode surface is high.** **Test at conditions where the gas flow above the electrode surface resembles the conditions in a stack (contact to and channels in interconnect, gas flow).**
E	**Inductive process**	**Determine the effect of polarisation, temperature and oxygen partial pressure. Investigate which segregates that may form a passive layer at the TPB by addition of excessive amount of the relevant materials, which must first be defined.**	**Minimise the amount of harmful segregates at the TPB**

respect to oxygen reduction. Despite this, impedance spectroscopy is believed to be a very valuable method, which is recommendable, as discussed in Chapter 6.

For each of the processes found in the present work it is interesting to look in more detail at the dependence on temperature (activation energy) and oxygen partial pressure, as this may indicate which species are involved in each of the processes.

Changes in the composite microstructure may affect arcs A, B and C, as it alters the transportation routes for oxide ions and oxygen intermediates and the length of the TPB. Deliberate, extreme changes in the microstructure may, thus, reveal information about the processes, although the resulting microstructure may not be suitable for SOFC operation.

Arcs A, B, C and E may be sensitive to formation of reaction products between LSM and YSZ in the composite. With the purpose of investigating this in further detail electrodes sintered at high temperature or based on stoichiometric LSM may be investigated, as this may accentuate the properties of each of the mentioned arcs.

Several competitive elementary processes in the oxygen reduction process may contribute to Arc C. It is relevant to study, which of these processes dominates under which conditions. It is suggested to perform experiments where the measurement atmosphere is varied systematically, not just with respect to the oxygen partial pressure, but also by varying the composition of the inert part of the gas. Such experiments may indicate whether dissociative adsorption limits the performance under some conditions, as suggested in Chapter 7.

An alternative way of investigating arc C could be to use dense, pointed LSM electrodes in contact with YSZ. In such a test the effect of reaction products and other segregates at the TPB in addition to geometric effects are minimised. Thus, it should in principle be possible to gain uncontaminated information about process C. In practice some effect of geometry will most likely be obtained (Juhl et al., 1995), however, valuable information may still be gained.

Only very limited information about arc E is available. Important information about this arc may be gained by revealing when this arc is actually present, and investigate whether its appearance varies systematically with parameters such as oxygen partial pressure and temperature. In all the impedance measurements performed in the present work the frequency was varied from high to low frequency. By measuring in both directions with respect to frequency when arc E is present, it may be possible to determine whether this arc is a time dependent activation phenomenon (if the appearance of arc E changes with the direction of the measuring frequency), or if it must be ascribed to another so far unknown phenomenon. Finally, arc E could be characterised further by determining its response to current passage on both short term and long term.

As discussed in Chapter 5 the degradation rate of LSM/YSZ composite electrodes may depend on the current density. To reveal more information about the degradation mechanism of LSM/YSZ composite cathodes, it is suggested to perform long term experiments, where nominally identical composite electrodes are tested galvanostatically with different current densities. In practice this may be done by making a number of symmetrical two electrode cells with varying area, and connecting these in series with a current supply. In parallel another batch of electrodes could be stored at the test temperature in question in different atmospheres with oxygen partial pressures corresponding to the potentials obtained by passing current. This should reveal whether the potential difference or the passage of current is responsible for the microstructural changes observed in the durability study.

An important approach, which may reveal further information about the oxygen reduction process is to model the data using equivalent circuits. The model must include all the five observed processes. As discussed in Chapter 7 such a model will include a large number of parameters, and the work with data processing may seem enormous. Nevertheless, such a model can be used to test the hypothesis made about the oxygen

reduction process in Chapter 7, as the dependence of the different model parameters on temperature, overvoltage and oxygen partial pressure may reveal information about the nature of each of the processes. The present work provides a good basis for constructing a model, as the apparent number of processes, and suggestions for their nature are provided.

8.3.2. Technical

Optimisation of the performance of composite electrodes is not straightforward, as the performance is affected by both materials composition and processing parameters. This makes it difficult to optimise the individual parameters. For instance when investigating the effect of composition using a particular set of fabrication parameters, e.g. a pre-set sintering temperature, one optimum composition may be found. However, the optimum could be different if another sintering temperature was chosen. Further, changing the composition also changes the sintering behaviour, thus when using the same sintering temperature for different compositions, different microstructures are investigated for each composition. This means that the electrodes are essentially not comparable. Thus, when optimising the composition and the individual processing parameters it is relevant to make a matrix, where different compositions and processing parameters are combined. In such a test quite a large number of electrodes having a certain composition and certain processing parameters must be tested in order to determine the electrode performance (Chapter 6). However, if a systematic performance variation is observed as a function of a systematic change in composition or processing (as for instance with thickness and sintering temperature, Chapter 3 and 4), the trend may be trustworthy although only a few of each sample type are tested.

From a technological point of view it seems most important to optimise the microstructure in order to maximise the length of active TPB within the C-layer and at its interfaces. A long TPB is assumed to lower the contribution of arc C, which is often the

major contribution to the electrode impedance. Further, this may decrease the magnitude of arc A and B. This may be done by improving the percolation of all three phases (LSM, YSZ and pores) in the structure, lowering the sintering temperature, increasing the porosity and minimising the mean particle size.

Another promising approach is use of electrode structures which are graded in composition. Two examples of how this has been implemented in practice can be found in literature. Suzuki et al. (1994) made electrode structures where the YSZ eletrolyte was extended into the LSM electrode structure giving a long contact zone between the materials and thereby a long TPB. Grading of composition and microstructure through a number of layers having increasing LSM content when going away from the electrolyte surface has also been reported (Cassidy et al., 2000; Holtappels and Bagger, 2000b). This concept should minimise the thermal mismatch problem between the electrode and the electrolyte. The optimum number of layers, their composition, thickness and microstructure needs further investigation.

Based on the findings in Chapter 4 it is relevant to optimise the microstructure of the C-layer and the CCC-layers individually.

When an improved microstructure has been made it is important to investigate the stability of the structure during operation. In addition to kinetic demixing fatal sintering may occur due to ohmic heating (Chapter 5). Electrodes containing fine powder and sintered at low temperature are believed to be most exposed to structural changes during operation.

References

Adler, S.B., Lane, J.A. and Steele, B.C.H., *J. Electrochem. Soc.*, **143** (1996) 3554-3564.

Andersen, I.G.K., Andersen, E.K., Norby, P. and Skou, E., *J. Solid State Chem.*, **113** (1994) 320-326.

Appel, C.C., at 'Geological Survey of Greenland' and Denmark, Personal communication (2000).

Appel, C.C., Bonanos, N., Horsewell, A. and Linderoth, S., Sumitted to *J. Mat. Sci.* (2000).

Badwal, S.P.S. and Drennan, J., *J. Mat. Sci.*, **22** (1987) 3231-3239.

Badwal, S.P.S and Hughes, A.E., In *Proceedings of Second Int. Symp. on SOFC*, Greece, Editors F. Grosz, P. Zegers, S.C. Singhal, O. Yamamoto, Report EUR 135 64 EN (1991) 445-454.

Badwal, S.P.S., *Solid State Ionics*, **52** (1992) 23-32.

Badwal, S.P.S. and Foger, K., *Materials Forum*, **21** (1997) 187-224.

Bagger, C., Juhl, M., Hendriksen, P.V., Larsen, P.H., Mogensen, M., Larsen, J.G. and Pehrson, S., In *Proceedings of 2nd European SOFC Forum*, Norway, Editor B. Thorstensen (1996) 175-184.

Bagger, C., Kindl, B. and Mogensen, M., US Patent Number 5,591,537 (1997).

Baker, R., Guindet, J. and Kleitz, M., *J. Electrochem. Soc.*, **144** (1997) 2427-2432.

Bay, L. and Jacobsen, T., *Solid State Ionics*, **93** (1997a) 201-205.

Bay, L. and Jacobsen, T., In *Proceedings of 10th International Energy Agency (IEA) SOFC Workshop: Materials and Processes*, Switzerland (1997b) 142-145.

Berenov, A.V., MacManus-Driscoll, J.L. and Kilner, J.A., *Solid State Ionics*, **122** (1999) 41-49.

Bonanos, N., Steele, B.C.H., Butler, E.P., Johnson, W.B., Worrell, W.L., Macdonald, D.D. McKubre, M.C.H., In *Impedance Spectroscopy*, J.R. Mcdonald, Editor, John Wiley and

Sons, Inc. (1987) 191-316.

Boukamp, B.A., *Solid State Ionics*, **20** (1986) 31-44.

Cassidy, M., Bagger, C., Brandon, N. and Day, M.J., In *Proceedings of 4th European SOFC Forum*, Switzerland, Editor A.J. McEvoy (2000) 637-646.

Chick, L.A., Pederson, L.R., Maupin, G.D., Bates, J.L., Thomas, L.E. and Exarhos, G.J., *Materials Letters*, **10** (1990) 6-12.

Christiansen, N. and Gordes, P., In *Proceedings of Second Int. Symp. on SOFC*, Greece, Editors F. Grosz, P. Zegers, S.C. Singhal, O. Yamamoto, Report EUR 135 64 EN (1991) 495-506.

Ciacchi, F.T., Crane, K.M. and Badwal, S.P.S., *Solid State Ionics*, **73** (1994) 49-61.

Clausen, C., Bagger, C., Bilde-Sørensen, J.B. and Horsewell, A., *Solid State Ionics*, **70/71** (1994) 59-64.

Davy, H., *Nicholson's J. Nat. Phil.* (1802) p. 145.

Diethelm, R., Schmidt, M., Doggwiler, B., Gamper, T., Keller, M., Honegger, K. and Batawi, E., In *Proceedings of 3rd European SOFC Forum*, France, Editor P. Stevens (1998) 87-93.

Eguchi, K., Inoue, T., Ueda, M. Kamimae, J., Aral, H., In *Proceedings of Second Int. Symp. on SOFC*, Greece, Editors F. Grosz, P. Zegers, S.C. Singhal, O. Yamamoto, Report EUR 135 64 EN (1991) 697-704.

European Commission, 'A Ten Year Fuel Cell Strategy for Europe', Brussels, 5 December 1997.

Fabry, P., Kleitz, M. and Deportes, C., *J. Solid State Chem*. **5** (1972) 1-10.

Fabry, P., and Kleitz, M., *Electroanal. Chem. Interfac. Electrochem.*, **57** (1974) 165-177.

Gharbage, B., Pagnier, T., Hammou, A., *Solid State Ionics*, **72** (1994) 248-252.

Greef, R., Peat, R., Peter, L.M. and Pletcher, D., *Instrumental Methods in Electrochemistry*, Ellis Horwood Ltd, UK (1990).

Grove, W.R., *Phil. Mag.*, **14** (1839) p. 127.

de Haart, L.G.J., Kuipers, R.A., de Vries, K.J. and Burggraf, A.J., *J. Electrochem. Soc*., **138** (1991) 1970-1975.

Hammouche, A, Schouler, E.J.L. and Henault, M., *Solid State Ionics*, **28-30** (1988) 1205-1207.

Hammouche, A. Ph.D. thesis, Institute National Polytechnique de Grenoble (1989).

Hammouche, A., Siebert, E., Hammou, A., *Mat. Res. Bull.*, **24** (1989) 367-380.

Hammouche, A., Siebert, E., Hammou, A. and Kleitz, M., *J. Electrochem. Soc.*, **138** (1991) 1212-1216.

van Hassel, B.A., Boukamp, B.A., Burggraaf, A.J., *Solid State Ionics*, **53-56** (1992) 890-903.

Herbstritt, D., Weber, A., and Ivers-Tiffée, E., In *Proceedings of Sixth Int. Symp. on SOFC*, Hawaii, Editors S.C. Singhal and M. Dokiya, Electrochemical Society Proceedings Volume 99-19 (1999) 972-980.

van Heuveln, F.H., van Berkel, F.P.F. and Huijsmans, J.P.P., In *High Temperature Electrochemical Behaviour of Fast Ion and Mixed Conductors*, Risø National Laboratory, Denmark, Editors F.W. Poulsen, J.J. Bentzen, T. Jacobsen, E. Skou, M.J.L. Østergård (1993) 53-68.

van Heuveln, F., Bouwmeester, H.J.M. and van Berkel, F.P.F., *J. Electrochem. Soc.*, **144**, (1997a) 126-133.

van Heuveln, F.H.; Bouwmeester, H.J.M., *J. Electrochem. Soc.*, **144** (1997b) 134-140.

van Heuveln, F., *Ph.D. thesis*, Technical Univerisity of Twente, The Netherlands, (1997c).

Hohnke, D.K., In *Fast Ion Transport in Solids*, Elsevier/North-Holland, Amsterdam, Editors P. Vashishta, J.N. Mundy and G.K. Shenoy (1979) 669-677.

Holtappels, P., Jørgensen, M. J., Primdahl, S., Mogensen, M. and Bagger, C., In *Proceedings of 3rd European SOFC Forum*, France, Editor P. Stevens (1998) 311-320.

Holtappels, P., Jørgensen, M. J. and Mogensen, M., in preparation (2000a).

Holtappels, P. and Bagger, C., in preparation (2000b).

Hong, J.-O. and Yoo, H.-I., *Solid State Ionics*, **113-115** (1998) 265-270.

Horita, T., Yamaji, K., Sakai, N., Yokokawa, H., Kawada, T., Kato, T., *Solid State Ionics*, **127** (2000) 55-65.

Huang, K., Lee, H.Y. and Goodenough, J.B. *J. Electrochem. Soc.*, **145** (1998) 3220-3227.

Isaacs, H. and Olmer, L.J., *J. Electrochem. Soc.*, **129** (1982) 436-443.

Ishihara, T., Honda, M., Shibayama, T., Minami, H., Nishiguchi, H., Takita,Y., *J. Electrochem. Soc.*, **145** (1998) 3177-3183.

Ivers-Tiffée, E., Schieβl, M., Oel, H.J., Wersing, W., In *High Temperature Electrochemical Behaviour of Fast Ion and Mixed Conductors*, Risø National Laboratory, Denmark, Editors F.W. Poulsen, J.J. Bentzen, T. Jacobsen, E. Skou, M.J.L. Østergård (1993) 69-88.

Jacobsen, T., Zachau-Christiansen, B., West, K. and Skaarup, S., In *Proc. of 2nd Nordic Symp. on High Temp. Fuel Cells*, Norway (1994) 139-145.

Jacobsen, T., Zachau-Christiansen, B., Bay, L. and Skaarup, S., In *High temperature Electrochemistry: Ceramics and Metals*, Risø National Laboratory, Denmark, Editors F.W. Poulsen, N. Bonanos, S. Linderoth, M. Mogensen, B. Zachau-Christiansen (1996) 29-40.

Jiang, S.P. Love, J.G. Zhang, J.P. Hoang, M. Ramprakash, Y. Hughes, A.E. Badwal, S.P.S., *Solid State Ionics*, **121** (1999) 1-10.

Juhl, M., *Undersøgelse af SOFC-katodens kinetik (Investigation of the SOFC cathode kinetics)*, Master Thesis from the Technical University of Denmark, in Danish (1994).

Juhl, M., Mogensen, M., Jacobsen, T., Zachau-Christiansen, B., Thorup, N. and Skou, E., In *Proceedings of Fourth Int. Symp. on SOFC*, Japan, Editors M. Dokiya, O. Yamamoto, H.

Tagawa and S.C. Singhal, Electrochemical Society Proceedings Volume 95-1 (1995) 554-563.

Juhl, M., Primdahl, S., Manon, C. and Mogensen, M., *J. Power Sources*, **61** (1996a) 173-181.

Juhl, M., Primdahl, S. and Mogensen, M., In *High Temperature Electrochemistry: Ceramics and Metals*, Denmark, Editors F.W. Poulsen, N. Bonanos, S. Linderoth, M. Mogensen and B. Zachau-Christiansen (1996b) 295-300. Reproduced in Appendix A.

Jørgensen, M.J., Primdahl, S., Bagger, C. and Mogensen, M., Risø National Laboratory, Unpublished results (1996-2000).

Jørgensen, M.J., Primdahl, S. and Mogensen, M., *Electrochimica Acta*, **44** (1999) 4195-4201.

Jørgensen, M.J., Risø National Lab., Denmark, unpublished result (2000).

Jørgensen, M.J., Holtappels, P. and Appel, C.C., *J. Appl. Electrochem.*, **30** (2000a) 411-420.

Jørgensen, M.J., Primdahl, S., Bagger, C. and Mogensen, M., Submitted to *Solid State Ionics* (2000b).

Jørgensen, M.J. and Mogensen, M., Submitted to *J. Electrochemical Soc.* (2000c).

Kawada, T., Sakai, N., Yokokawa, H., Dokiya, M., *Solid State Ionics*, **50** (1992) 189-196.

Kendall, K. and Prica, M., In *Proceedings of First European SOFC Forum*, Switzerland, Editor U. Bossel (1994) 163-170.

Kenjo, T. and Nishiya, M., *Solid State Ionics*, **57** (1992) 295-302.

Kertesz, M., Riess, I., Tanhauser, D.S., Langpape, L. and Rohr, F. J., *J. Solid State Chemistry*, **42** (1982) 125-129.

Kleitz, M., Kloidt, T. and Dessemond, L., in *High temperature Electrochemical Behaviour of Fast Ion and Mixed Conductors*, Risø National Laboratory, Denmark, Editors F.W. Poulsen, J.J. Bentzen, T. Jacobsen, E. Skou, M.J.L. Østergård (1993) 89-116.

Kröger, F.A. and Vink, H.J., *Solid State Physics*, **3** (1956) 307-435.

Kuo, J.H. and Andersen, H.U., *J. Solid State Chem*., **83** (1989) 52-60.

Lane, J.A., Adler, S., Middleton, P.H. and Steele, B.C.H., In *Proceedings of Fourth Int. Symp. on SOFC*, Japan, Editors M. Dokiya, O. Yamamoto, H. Tagawa and S.C. Singhal, Electrochemical Society Proceedings Volume 95-1 (1995) 584-596.

Larsen, P.H., Hendriksen, P.V. and Mogensen, M., In *Proceedings of 3rd European SOFC Forum*, France, Editor P. Stevens (1998) 181-190.

Lasia, A., in *Modern Aspects of Electrochemistry No. 32*, Kluwer Academic/Plenum Publishers, New York, B.E. Conway, J.O'M. Bockris, and R.E. White, Editors (1999) 143-243.

Lauvstad, G. Ø., Tunold, R. and Sunde, S., In *Proc. of 7th IEA SOFC Workshop: Theory and Measurement of Microscale Processes in Solid Oxide Fuel Cells*, Norway (1995) 41-45.

Lee, H.Y., Cho, W.S. Oh, S.M., Wiemhöfer, H.-D., Göpel, W., *J. Electrochem. Soc.*, **142** (1995) 2659-2664.

Mackor, A., Koster, T.P.M., Kraaijkamp, J.G. and Gerretsen, J., In *Proceedings of Second Int. Symp. on SOFC*, Greece, Editors F. Grosz, P. Zegers, S.C. Singhal, O. Yamamoto, Report EUR 135 64 EN (1991) 463-471.

McEvoy, A.J., *In Proc. of 7th IEA SOFC Workshop: Theory and Measurement of Microscale Processes in Solid Oxide Fuel Cells*, Norway (1995) 127-132.

Minh, N.Q. and Takahashi, T., Science and technology of ceramic fuel cells, Elsevier Science B. V. (1995).

Mitchell, J.F., Argyriou, D.N., Potter, C.D., Hinks, D.G., Jorgensen, J.D. and Bader, S.D., *Phys. Rev. B*, **54** (1996) 6172-6183.

Mitterdorfer, A., Cantoni, M. and Gauckler, L.J., In *Proceedings of 2nd European SOFC Forum*, Norway, Editor B. Thorstensen (1996) 373-382.

Mitterdorfer, A. and Gauckler, L.J., *Solid State Ionics*, **111** (1998) 185-218.

Mizusaki, J., Tagawa, H., Tsuneyoshi, K., Mori, K. and Sawata, A., *Nippon Kagaku Kaishi* (1988) 1623-1629.

Mizusaki, J., Tagawa, H., Tsuneyoshi, K. and Sawata, A., *J. Electrochem. Soc.*, **138** (1991) 1867-1873.

Mogensen, M., in *High temperature Electrochemical Behaviour of Fast Ion and Mixed Conductors*, Risø National Laboratory, Denmark, Editors F.W. poulsen, J.J. Bentzen, T. Jacobsen, E. Skou, M.J.L. Østergård (1993) 117-135.

Mogensen, M., Primdahl, S. and Juhl, M., *In Proceedings of Fifth Int. Symp. on SOFC*, Germany, Editors U. Stimming, S.C. Singhal, H. Tagawa and W. Lehnert, The Electrochemical Society Proceedings Volume 97-40 (1997) 385-392.

Mogensen, M., Primdahl, S, Jørgensen, M.J. and Bagger, C., Accepted for publication in special issue of *J. Electrochemistry* (2000).

Monceau, D., Filal, M., Tebtoub, M., Petot, C. and Petot-Ervas, G., *Solid State Ionics* **73** (1994) 221-225.

Mori, M., Yamamoto, T., Itoh, H. and Abe, T., In *Proceedings of the Second Int. Fuel Cell Conference*, Japan (1996) p. 485-488.

Murray, E.P., Tsai, T, Barnett, S.A., *Solid State Ionics*, **110** (1998) 235-243.

Murray, E.P. and Barnett, S.A., In *Proceedings of Sixth Int. Symp. on SOFC*, Hawaii, Editors S.C. Singhal and M. Dokiya, Electrochemical Society Proceedings Volume 99-19 (1999) 369-378.

Møller, P., *Overfladeteknologi*, ("Surface technology", in Danish), Teknisk forlag A/S, København (1998).

Narita, H., Mizusaki, J. and Tagawa, H., *Denki Kagaku*, **61** (1993) 756-757.

Nernst, W., *Z. Electrochem.*, **6** (1899) p. 41.

Odgaard, M and Skou, E., *Solid State Ionics*, **86-88** (1996) 1217-1222.

Odgaard, M. and Skou, E., *Ionics*, **3** (1997) 75-82.

Onoda, G. Y. and Hench, L. L., *Ceramic processing before firing*, John Wiley & Sons, Inc. (1978).

Poulsen, F.W., van der Puil, N., *Solid State Ionics*, **53 - 56** (1992) 777-783.

Primdahl, S. and Hendriksen, P.V., In *High Temperature Electrochemistry: Ceramics and Metals*, Denmark, Editors F.W. Poulsen, N. Bonanos, S. Linderoth, M. Mogensen and B. Zachau-Christiansen (1996) 403-410.

Primdahl, S. and Jørgensen, M. J., *Journal of the Danish Ceramic Society*, **2** (1999a) 13-19 (in Danish).

Primdahl, S., Jørgensen, M. J., Bagger, C. and Kindl, B., In *Proceedings of Sixth Int. Symp. on SOFC, SOFC-VI*, Hawaii, Editors S.C. Singhal and M. Dokiya, Electrochemical Society Proceedings Volume 99-19 (1999b) 793-802.

Primdahl, S. and Mogensen, M., *J. Electrochemical Soc.*, **146** (1999c) 2827-2833.

Primdahl, S., Sørensen, B. F. and Mogensen, M., *J. Am. Cer. Soc.*, **83** (2000) 489-494.

van Roosmalen, J.A.M. and Cordfunke, E.H.P., *Solid State Ionics*, **52** (1992) 303-312.

van Roosmalen, J.A.M., van Vlaanderen, P. and Cordfunke, E.H.P., *J. Solid State Chem.*, **114** (1995) 516-523.

Sasaki, K., Wurth, J.P., Gödickemeier, M., Mitterdorfer, A. and Gauckler, L.J., In *Proceedings of Fourth Int. Symp. on SOFC*, Japan, Editors M. Dokiya, O. Yamamoto, H. Tagawa and S.C. Singhal, Electrochemical Society Proceedings Volume 95-1 (1995) 625-636.

Sasaki, K., Wurth, J.-P., Gschwend, R., Gödickemeier, M. and Gauckler, L.J., *J. Electrochem. Soc.*, **143** (1996) 530-543.

Sasaki, Y., Takeda, Y., Kato, A., Imanishi, N., Yamamoto, O., Hattori, M., Iio, M. and Esaki, Y., *Solid State Ionics*, **118** (1999) 187-194.

Schouler, E.J.L. and Kleitz, M., *J. Electrochem. Soc.*, **134** (1987) 1045-1050.

Scotti, C., Gharbage, B., Lauret, H., Levy, M. and Hammou, A., *Mat. Res. Bull.*, **28** (1993) 1215-1220.

Siebert, E., Hammouche, A. and Kleitz, M., *Electrochim. Acta*, **40** (1995) 1741-1753.

Singhal, S.C., *In Proceedings of Fifth Int. Symp. on SOFC*, Germany, Editors U. Stimming, S.C. Singhal, H. Tagawa and W. Lehnert, The Electrochemical Society Proceedings Volume 97-40 (1997) 39-51.

SOFC I, *Proceedings of First Int. Symp. on SOFC*, U.S.A., Editor: S. C. Singhal, The Electrochemical Society Proceedings Volume 89-11 (1989).

Solartron, Operating Manual, Solartron 1250 frequency response Analyser, Issue 6, Schlumberger Instruments, Victoria Road, Farnborough, England. Oct. (1985).

Srilomsak, S., Schilling, D.P. and Anderson, H.U., In *Proceedings of First Int. Symp. on SOFC*, U.S.A., Editor S.C. Singhal, The Electrochemical Society Proceedings Volume 89-11 (1989) 129-140.

Steele, B.C.H., *J. Power Sources*, **49** (1994a) 1-14.

Steele, B.C.H., In *Proceedings of First European SOFC Forum*, Switzerland, Editor U. Bossel (1994b) 375-393.

Stevenson, J.W., Hallman, P.F., Armstrong, T.R. and Chick, L.A., *J. Am. Ceram. Soc.*, **78** (1995) 507-512.

Stevenson, J.W., Armstrong, T.R., Carneim, R.D., Pederson, L.R. and Weber, W.J., *J. Electrochem. Soc.*, **143** (1996) 2722-2729.

Stochniol, G., Syskakis, E. and Naumidis, A., *J. Am. Ceram. Soc.*, **78** (1995) 929-932.

Sunde, S., *J. Electrochem. Soc.*, **143** (1996) 1930-1939.

Sunde, S., *Electrochim. Acta*, **42** (1997) 2637-2648.

Suzuki, M., Sasaki, H., Otoshi, S., Kajimura, A., Sugiura, N. and Ippommatsu, M., *J. Electrochem. Soc.*, **141** (1994) 1928-1931.

Sørensen, B. F. and Primdahl, S., *J. Mat. Sci.*, **33** (1998) 5291- 5300.

Tagawa, H., Mori, N., Takai, H., Yonemura, Y., Minamiue, H., Inaba, H., Mizusaki, J. and Hashimoto, T., In *Proceedings of Fifth Int. Symp. on SOFC*, Germany, Editors U. Stimming, S.C. Singhal, H. Tagawa and W. Lehnert, The Electrochemical Society Proceedings Volume 97-40 (1997) 785-794.

Tai, L.-W., Nasrallah, M.M., Anderson, H.U., Sparlin, D.M. and Sehlin, S.R., *Solid State Ionics*, **76** (1995) 259-271.

Takahashi, T., Iwahara, H. and Suzuki, Y., In *Proceedings of Third Int. Symp. on Fuel Cells*, Presses Academiques Europeennes, Bruxelles (1969) 113-119.

Takeda, Y., Kanno, R., Noda, M., Tomida, Y. and Yamamoto, O., *J. Electrochem. Soc.*, **134** (1987) 2656-2661.

Tietz, F., Dias, F.J. and Naoumidis, A., In *Proceedings of 3rd European SOFC Forum*, France, Editor P. Stevens (1998) 171-180.

Tricker, D.M. and Stobbs, W.M., in *High temperature Electrochemical Behaviour of Fast Ion and Mixed Conductors*, Risø National Laboratory, Denmark, Editors F.W. Poulsen, J.J. Bentzen, T. Jacobsen, E. Skou, M.J.L. Østergård (1993) 453-460.

Tsukuda, H. and Yamashita, A., In *Proceedings of First European SOFC Forum*, Switzerland, Editor U. Bossel (1994) 715-724.

Tsuneyoshi, K., Mori, K. and Sawata, A., *Solid State Ionics*, **35** (1989) 263-268.

Weber, A., Männer, R., Waser, R. and Ivers-Tiffée, E., *Denki Kagaku*, **64** (1996a) 582-589.

Weber, A., Männer, R., Jobst, B., Schiele, M., Cerva, H., Waser, R. and Ivers-Tiffée, E., In *High temperature Electrochemistry: Ceramics and Metals*, Editors F.W. Poulsen, N. Bonanos, S. Linderoth, M. Mogensen, B. Zachau-Christiansen, Risø National Laboratory, Denmark (1996b) 473-478.

Welty, J.R., Wicks, C.E. and Wilson, R.E. *Fundamentals of Momentum, Heat and Mass Transfer*, Third Edition, John Wiley and Sons Inc., New York (1984) 490-491.

Wiik, K., Schmidt, C.R., Faaland, S., Shamsili, S., Einarsrud, M.-A., Grande, T., *J. Am. Ceram. Soc.*, **82** (1999) 721-728.

Williams, M.C., In *Proceedings of 3rd European SOFC Forum*, France, Editor P. Stevens (1998) 27-41.

Winkler, J., Hendriksen, P.V., Bonanos, N. and Mogensen, M., *J. Electrochem. Soc.*, **145** (1998) 1184-1192.

Yamamoto, O., Takeda, Y., Kanno, R. and Noda, M., *Solid State Ionics*, **22** (1987) 241-246.

Yokokawa, H., Horita, T., Sakai, N., Kawada, T. and Dokiya, M., In *Proceedings of First European SOFC Forum*, Switzerland, Editor U. Bossel (1994) 425-434.

Yoo, H.-I. and Lee, K.-C., *J. Electrochem. Soc.*, **145** (1998) 4243-4247.

Youngblood, G.E., Rupaak, A.S., Pederson, L.R., Bates, J.L., In *Proceedings of Third Int. Symp. on SOFC*, Hawaii, Editors S.C. Singhal and H. Iwahara, The Electrochemical Society Proceedings Volume 93-4 (1993) 585-597.

Yurek, G.J. and Schmalzried, H., *Berichte der Bunsen-Gesellschaft Phys. Chem.* **79** (1975) 255-262.

Zachau-Christiansen, B., Jacobsen, T. and Skaarup, S., In *Proceedings of Fifth Int. Symp. on SOFC*, Germany, Editors U. Stimming, S.C. Singhal, H. Tagawa and W. Lehnert, The Electrochemical Society Proceedings Volume 97-40 (1997) 795-804.

Østergård, M.J.L and Mogensen, M., *Electrochimica Acta*, **38** (1993) 2015-2020.

Østergård, M.J.L., Clausen, C., Bagger, C. and Mogensen, M., *Electrochemica Acta*, **40** (1995) 1971-1981.

Appendix A

This appendix contains a reproduction of the paper: M. Juhl, S. Primdahl, and M. Mogensen, In *High Temperature Electrochemistry: Ceramics and Metals*, Denmark, Editors F.W. Poulsen, N. Bonanos, S. Linderoth, M. Mogensen and B. Zachau-Christiansen (1996b) 295-300.

CHARACTERISATION OF COMPOSITE SOFC CATHODES BY IMPEDANCE SPECTROSCOPY

M. Juhl, S. Primdahl and M. Mogensen

Materials Department, Risø National Laboratory,
DK-4000 Roskilde, Denmark

ABSTRACT

Composite cathodes of $(La_{0.75}Sr_{0.25})_{0.9}MnO_{3\pm\delta}$ and $Zr_{0.94}(Y_{0.06})O_{2-x}$ with varying thickness and structure were tested electrochemically in air by means of impedance spectroscopy at temperatures between 700 and 1000°C. The impedance spectra were fitted to an equivalent circuit containing a high and a low frequency (RQ)-element connected in series. At 700 and 850°C the high frequency resistance increased with the thickness of the composite cathode, while the low frequency resistance decreased. At 1000°C the trends were unclear. At all temperatures the ratio between the low frequency resistance and the high frequency resistance tends to decrease with increasing electrode thickness. The high frequency resistance is ascribed to an unknown transport mechanism related to the microstructure of the composite, while the low frequency resistance is ascribed to an elementary process in the oxygen reduction mechanism.

1. INTRODUCTION

One of the factors limiting the performance of Solid Oxide Fuel Cells (SOFCs) is the overvoltage related to the cathode process. Therefore, an extensive amount of work has been done to clarify the oxygen reduction reaction mechanism taking place on this electrode. The electrode kinetics are found to be influenced by factors such as electrode morphology, composition and preparation technique (Kenjo and Nishiya 1992; Østergård, Clausen, Bagger and Mogensen 1995; Juhl, Manon, Primdahl and Mogensen 1996). At present no single reaction mechanism is commonly accepted.

Composite SOFC cathodes made from a mixture of electrode and electrolyte material have shown good performance compared to electrodes without electrolyte material (Kenjo and

Nishiya 1992; Østergård et al. 1995) as the bulk of the composite electrode is to some extent active with respect to oxygen reduction. Composite electrodes might not be suitable for fundamental kinetic studies, due to the interaction between the microstructure and the kinetics. However, electrochemical studies of composite cathodes are useful for optimisation purposes, since they can lead to a better understanding of the limitations caused by the microstructure.

The cathodes investigated in this work are composites made from equal amounts of $(La_{0.75}Sr_{0.25})_{0.9}MnO_{3\pm\delta}$ and yttria stabilised zirconia (YSZ) with 3 mol% yttria. In a previous paper the correlation between the composite electrode thickness and the polarisation resistance was investigated in the thickness range 2-11 μm (Juhl et al. 1996). In the present work electrodes with thicknesses from 2 to 41 μm are investigated. As an attempt to increase the porosity of the composite electrode combustible carbon fibres are added to some samples as artificial pore formers. The electrodes are characterised by means of impedance spectroscopy.

2. EXPERIMENTAL

The electrodes are made by spray-painting a low viscous slurry on an electrolyte substrate made of YSZ with 8 mol% Y_2O_3 (TZ8Y, Tosoh Corporation). The electrode area is approximately 0.43 cm^2. The composite Cathode layer (C-layer) contains equal amounts by weight of $(La_{0.75}Sr_{0.25})_{0.9}MnO_{3\pm\delta}$ (nominal composition) and YSZ with 3 mol% Y_2O_3 (TZ3Y, Tosoh Corporation). The slurry preparation and the spraying is carried out as described for series 1 in (Juhl et al. 1996). The C-layer is sintered at 1300°C for 2 hours. To obtain an extra thick C-layer four samples are produced by spraying two layers of the slurry with intermediate sintering. On two of these samples the first layer is sintered at 1200°C for 2 hours, while the second layer is sintered at the usual 1300°C. On the other two samples both layers are sintered at 1300°C. Carbon fibres are used as artificial pore formers on two samples. Fibres having a diameter of 5 μm and a length of up to a few mm are added to the C-layer slurry prior to the spray-painting. Some samples have a layer of coarse YSZ particles (denoted P-layer) between the electrolyte and the C-layer.

A Cathode Current Collecting layer (CCC-layer) consisting of $(La_{0.75}Sr_{0.25})_{0.9}MnO_{3\pm\delta}$ (nominal composition) is applied on the sintered C-layer. The CCC-layer is produced by spray-painting two layers, which are both sintered at 1300°C for two hours. The CCC-layer thickness is approximately 40 μm after sintering.

The electrodes are tested electrochemically using a three electrode, four leads system. The tests are performed in air at 700, 850 and 1000°C. Impedance spectroscopy measurements are taken at open circuit voltage (OCV) after 15 minutes equilibration. Details about the electrochemical set-up and equipment and the measuring conditions are given elsewhere (Juhl et al. 1996).

The impedance spectra are fitted to the equivalent circuit $LR_s(R_{high}Q_{high})(R_{low}Q_{low})$ by the program EQUIVCRT (Boukamp 1986). L is the inductance due to the leads. R_s is the series resistance of the electrolyte. R_{high} and R_{low} are polarisation resistances referring to high and low frequency, respectively. Q_{high} and Q_{low} are constant phase elements defined as $Q = Y_0(j\omega)^n$ (Boukamp 1986). Inductive effects observed at low frequencies (positive imaginary part) are neglected during the fitting procedure. Often the first few data points

taken at high frequency are scattered due to electrical noise. These points were eliminated before fitting.

After the electrochemical tests the C-layer microstructure and thickness was determined by scanning electron microscopy (SEM) on polished cross sections.

3. RESULTS

Impedance spectra obtained at OCV on 16 samples are fitted to the equivalent circuit described in section 2. An example of an impedance plot is shown in Fig. 1 and the microstructure of an electrode is shown in Fig 2. At 700°C a majority of the measurements are not suitable for fitting due to high frequency phase error or noise. Six data set obtained at 700°C are fitted satisfactorily together with 15 data set obtained at 850°C and 16 data set measured at 1000°C. The quality of the fits is evaluated from frequency-error plots in EQUIVCRT (Boukamp 1986). The error is below approx. 1% for data obtained at 850 and 1000°C and around 2% for data measured at 700°C.

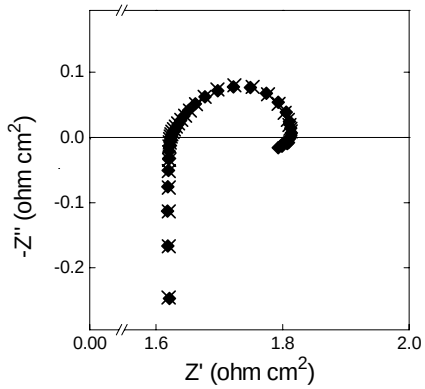

Fig. 1. Impedance spectra measured at OCV in air at 1000°C (◆). The experimental data are fitted to the equivalent circuit described in section 2 using EQUIVCRT (Boukamp 1986) (✕).

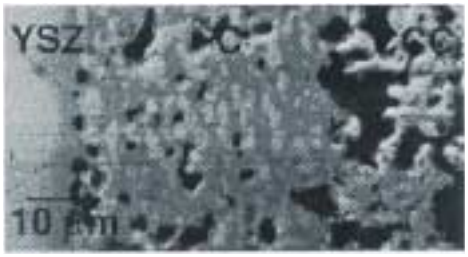

Fig. 2. SEM micrograph showing a cross section of a composite electrode. The manganite phase looks brighter than the zirconia phase, as the image is obtained with backscattered electrons.

Previous investigations have shown that the polarisation resistance decreases as the C-layer thickness increases from 2 to 11 µm at temperatures between 700 and 1000°C (Juhl et al. 1996). The observed increase in the electrode efficiency with increasing thickness suggests that there is some activity with respect to oxygen reduction in the bulk of the electrode. The samples with an extra thick C-layer tested in this work have thicknesses between 21 and 41 µm. At 700 and 850°C the overall polarisation resistance, $R_p = R_{high} + R_{low}$, asymptotically approaches a constant value for thick samples. At 1000°C the picture is more scattered, but R_p seems to be constant for thicknesses above approximately 15 µm.

The resistances R_{high} and R_{low} related to the high and the low frequency arc, respectively, are both dependent on thickness and temperature. At 700 and 850°C R_{high} increases with increasing thickness, while R_{low} decreases, as illustrated at 850°C in Fig. 3. At 1000°C the trends are less distinct. Both R_{high} and R_{low} seems to be constant for thicknesses above approximately 15 μm, and both resistance-thickness graphs are scattered for lower thicknesses.

The ratio R_{low}/R_{high} decreases with increasing thickness, as shown in Fig. 4. At 850°C and 1000°C the ratio seems to approach a constant value for thicknesses exceeding 25 μm, although some scatter is observed. At 1000°C two samples having a C-layer thickness of approx. 6 μm have rather low R_{low}/R_{high} ratios compared with the other samples (Fig. 3). There is no obvious explanation for this. At both 850 and 1000°C the samples made with a P-layer do not follow the trend, as the ratio R_{low}/R_{high} is lower than for other samples with similar thickness (Fig. 4). This is assumed to be due to the samples with a P-layer having different C-layer structure than the other electrodes (Juhl et al. 1996).

The n-values obtained from the fitting procedure are around 0.9 for the low frequency arc at all temperatures. The n-values of the high frequency arc vary and no clear trends are found.

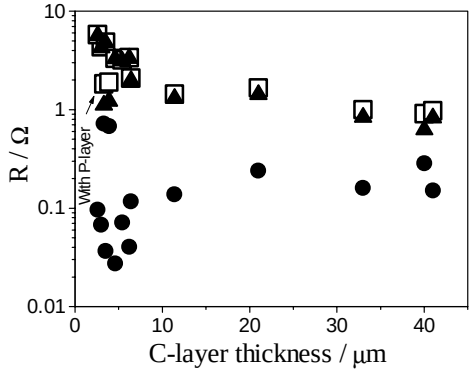

Fig. 3. R_p (□), R_{high} (●) and R_{low} (▲) plotted as a function of the C-layer thickness. Experimental conditions: 850°C, air, OCV.

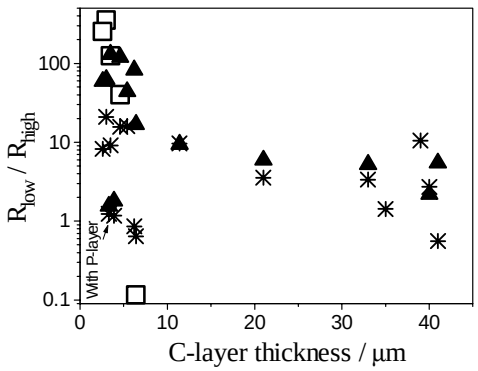

Fig. 4. R_{low}/R_{high} measured at 700°C (□), 850°C (▲) and 1000°C (✳) plotted as a function of the C-layer thickness. Experi-mental conditions: air, OCV.

The frequency, f_{max}, corresponding to the maximum imaginary part of an arc is calculated from $f_{max} = 1/(RQ)^{(1/n)}$. f_{max} of the low frequency arc, $f_{max,low}$, increases with increasing temperature. With increasing thickness $f_{max,low}$ appears to be constant or only slightly increasing. $f_{max,high}$ does not show any clear trends.

To determine the apparent activation energies of the resistances R_{high} and R_{low} Arrhenius plots are made for the samples which are fitted at three temperatures. The apparent activation energy of the low frequency arc varies with temperature, as the Arrhenius plots are not straight lines. For the low frequency arc the Arrhenius plots deviates less from a straight line. The apparent activation energy of R_{low} is close to 2 eV. This is in agreement with the activation energy of the electrode reaction on $La_{1-x}Sr_xMnO_3$ reported in literature (Kleitz, Kloidt and Dessemond 1993).

4. DISCUSSION

The decrease of the low frequency resistance, $R_{low,}$ with increasing C-layer thickness is interpreted as an increase in the number of active reaction sites per nominal electrode area rather than an increase in the reaction rate of the elementary process limiting the oxygen reduction rate. This is supported by the magnitude of the apparent activation energy, which is close to the literature value given for the electrode reaction on $La_{1-x}Sr_xMnO_3$ (Kleitz, Kloidt and Dessemond 1993). $f_{max,low}$ was found to be roughly independent of electrode thickness. This is in agreement with the assumption that the same elementary process limits the reaction rate for all thicknesses.

The increase of the high frequency resistance, R_{high}, with increasing C-layer thickness suggests that it is related to transport phenomena in the C-layer rather than an elementary process in the overall oxygen reduction mechanism. The nature of the transport resistance cannot be determined with the present experimental results, but several possibilities can be pointed out.

a) The further away the active sites are from the bulk electrolyte the higher the ionic resistance.

b) R_{high} might be related to contacts between electrode and electrolyte particles for which at least one of the phases is not connected to its corresponding bulk phase. Sunde (1996) has simulated the polarisation resistance of composite electrodes using random resistor networks. The above-described type of contacts were found to influence the polarisation resistance (Sunde 1996). SEM micrographs of the samples studied in the present work confirm the potential existence of these electrode/electrolyte contacts in the C-layer structure (see Fig. 2).

c) As the thickness increases or the structure becomes more complex electrons and intermediate oxygen species will have to pass an increasing number of LSM-LSM or YSZ-YSZ grain boundaries, respectively, on their way to or from the active reaction sites. Thus, the resistance due to interparticular and intraparticular conduction is expected to increase with thickness.

d) The resistance related to surface and grain boundary conduction of intermediate oxygen species within the electrode structure might also change with the electrode thickness and structure.

e) During sintering of composite electrodes zirconates are likely to form at the interface between LSM and YSZ grains (Mitterdorfer, Cantoni and Gauckler 1996). The consequence of formation of zirconates might be that oxygen species or electrons have to cross a layer with very low ionic and electronic conductivity (Mitterdorfer and Gauckler 1996), leading to an increase in the interface resistance between LSM and YSZ. The effect of a zirconate layer on the polarisation resistance might vary with the electrode structure.

The thickness dependence of R_{high} and R_{low} is less distinct at 1000°C compared with the resistances at 700 and 850°C. This is in correspondence with the previously observed insensitivity to structural changes at 1000°C (Juhl et al. 1996). The reason for this might be that the active electrode thickness is likely to decrease with temperature. In addition to this the activation energies of the various mechanisms included in R_{high} might be different, as the apparent activation energy of R_{high} varies with temperature.

Comparing samples of similar thickness, the samples with a P-layer have the lowest R_{low} and the highest R_{high} (Fig. 3). The low R_{low} can be explained by the formation of additional active sites due to an opening of the C-layer structure (Juhl et al. 1996). The structural changes might, however, have deteriorated the routes of transportation of various species through the C-layer leading to an increase in R_{high}.

The results in Fig. 4 suggest that the ratio R_{low}/R_{high} is the lowest when the polarisation resistance is low. At 1000°C the thickness dependence of this ratio is more distinct than for the individual resistances. This suggests that the two resistances are closely related to each other. Further investigations are needed in order to clarify the nature of the two resistances and the relation between them.

5. CONCLUSIONS

The polarisation resistance of composite cathodes of $(La_{0.75}Sr_{0.25})_{0.9}MnO_{3\pm\delta}$ and $Zr_{0.94}(Y_{0.06})O_{2-x}$ with varying thickness and structure was determined at open circuit voltage at 700, 850 and 1000°C in air by impedance spectroscopy. The impedance spectra are divided into a high and a low frequency (RQ)-element connected in series. At 700 and 850°C the high frequency resistance increases with electrode thickness while the low frequency resistance decreases. At 1000°C both resistances are less dependent on the electrode thickness. The ratio between the low frequency resistance and the high frequency resistance tends to decrease with increasing electrode thickness at the temperatures investigated. The high frequency resistance is assumed to be related to a transport mechanism determined by the electrode thickness and structure, while the low frequency resistance is believed to be a chemical elementary process in the oxygen reduction mechanism.

Impedance spectroscopy has proved to be a useful tool for the characterisation of composite cathodes. The results can be used directly for optimisation purposes, and for understanding the relations between structure and chemistry in the polarisation resistance of composite cathodes.

ACKNOWLEDGEMENTS

This work was carried out as a part of the Joule Thermie Project: “Improving Durability of SOFC Stacks”, contract JOE3-CT95-0005. The authors would like to thank C. Manon for carrying out the SEM investigations.

REFERENCES

Boukamp, B.A. (1986). A Nonlinear Least Squares Fit Procedure for Analysis of Immitance Data of Electrochemical Systems. Solid State Ionics 20, 31-44.

Juhl, M., Primdahl, S., Manon, C. and Mogensen, M. (1996). Performance/Structure Correlation for Composite SOFC Cathodes. J. Power Sources (In press).

Kenjo, T. and Nishiya, M. (1992). $LaMnO_3$ Air Cathodes Containing ZrO_2 Electrolyte for High Temperature Solid Oxide Fuel Cells. Solid State Ionics 57, 295-302.

Kleitz, M., Kloidt, T. and Dessemond, L. (1993). Conventional Oxygen Electrode Reaction: Facts and Models. In: Proceedings of 14th Risø Int. Symp. on Mat. Sci., Roskilde, Denmark. Edited by F.W. Poulsen, J.J. Bentzen, T. Jacobsen, E. Skou and M.J.L. Østergård 89-116.

Mitterdorfer, A., Cantoni, M., and Gauckler, L.J. (1996). Interphase Formation Between Yttria-Stabilized Zirconia and Porous $La_{0.85}Sr_{0.15}Mn_yO_3$ During Firing at Intermediate Temperatures. In: Proceedings of 2nd European SOFC Forum, Oslo, Norway. Editor. B. Thorstensen 373-382.

Mitterdorfer, A. and Gauckler, L.J. (1996). Oxygen Reduction at the $La_{0.85}Sr_{0.15}Mn_{0.98}O_3$/YSZ Interface. In: These proceedings.

Sunde, S. (1996). Monte Carlo Simulations of Polarization Resistance of Composite Electrodes for Solid Oxide Fuel Cells. J. Electrochem. Soc. 143, 1930-1939.

Østergård, M.J.L., Clausen, C., Bagger, C. and Mogensen, M. (1995). Manganite-Zirconia Composite Cathodes for SOFC: Influence of Structure and Composition. Electrochimica Acta 40, 1971-1981.

Bibliographic Data Sheet **Risø-R-1242(EN)**

Title and authors

Lanthanum Manganate Based Cathodes for Solid Oxide Fuel Cells

Mette Juhl Jørgensen

ISBN	ISSN
87-550-2827-6 87-550-2828-4 (internet)	0106-2840

Department or group	Date
Materials Research Department	July 2001

Groups own reg. number(s)	Project/contract No(s)

Sponsorship

Pages	Tables	Illustrations	References
181	8	57	146

Abstract

Composite cathodes for solid oxide fuel cells were investigated using electrochemical impedance spectroscopy and scanning electron microscopy. The aim was to study the oxygen reduction process in the electrode in order to minimise the voltage drop in the cathode. The electrodes contained a composite layer made from lanthanum strontium manganate (LSM) and yttria stabilised zirconia (YSZ) and a layer of pure LSM aimed for current collection. The performance of the composite electrodes was sensitive to microstructure and thickness. Further, the interface between the composite and the current collecting layer proved to affect the performance. In a durability study severe degradation of the composite electrodes was found when passing current through the electrode for 2000 hours at 1000°C. This was ascribed to pore formation along the composite interfaces and densification of the composite and current collector microstructure. An evaluation of the measurement approach indicated that impedance spectroscopy is a very sensitive method. This affects the reproducibility, as small undesirable variations in for instance the microstructure from electrode to electrode may change the impedance. At least five processes were found to affect the impedance of LSM/YSZ composite electrodes. Two high frequency processes were ascribed to transport of oxide ions/oxygen intermediates across LSM/YSZ interfaces and through YSZ in the composite. Several competitive elementary reaction steps, which appear as one medium frequency process in the impedance spectra, were observed. A low frequency arc related to gas diffusion limitation in a stagnant gas layer above the composite structure was detected. Finally, an inductive process, assumed to be connected to an activation process involving segregates at the triple phase boundary between electrode, electrolyte and gas phase, was found.

Descriptors INIS/EDB

Cathodes; Composite Materials; Electric Impedance; Electrochemistry; Scanning Electron Microscopy; Solid Electrolyte Fuel Cells.

Available on request from Information Service Department, Risø National Laboratory,
(Afdelingen for Informationsservice, Forskningscenter Risø), P.O.Box 49, DK-4000 Roskilde, Denmark.
Telephone +45 4677 4004, Telefax +45 4677 4013